SÃO PAULO STATE UNIVERSITY
FACULTY OF ENGINEERING OF BAURU
MECHANICAL ENGINEERING POST-GRADUATION PROGRAM

ON SATURATION PHENOMENON IN ENERGY HARVESTING BASED ON NONLINEAR PIEZOELECTRIC MATERIALS COUPLED TO A PORTAL FRAME FOUNDATION WITH IDEAL AND NON-IDEAL EXCITATIONS

Author: Rodrigo Tumolin Rocha
Advisor: Full Professor José Manoel Balthazar

Bauru, 2016
SP, Brazil

SÃO PAULO STATE UNIVERSITY
FACULTY OF ENGINEERING OF BAURU
MECHANICAL ENGINEERING POST-GRADUATION PROGRAM

ON SATURATION PHENOMENON IN ENERGY HARVESTING BASED ON NONLINEAR PIEZOELECTRIC MATERIALS COUPLED TO A PORTAL FRAME FOUNDATION WITH IDEAL AND NON-IDEAL EXCITATIONS

Author: Rodrigo Tumolin Rocha
Advisor: Full Professor José Manoel Balthazar

Course: Mechanical Engineering
Area of concentration: Mechanical Project

Ph.D. Dissertation to be presented to the Program of Post-Graduation in Mechanical Engineering of the Faculty of Engineering of Bauru - São Paulo State University, as one of the requirements for the degree of the Doctor of Philosophy in Mechanical Engineering.

Bauru, 2016
SP, Brazil

Rocha, Rodrigo Tumolin.
On saturation phenomenon in energy harvesting based on nonlinear piezoelectric materials coupled to a portal frame foundation with ideal and non-ideal excitations / Rodrigo Tumolin Rocha, 2016
129 f. : il.

Orientador: José Manoel Balthazar

Tese (Doutorado – Universidade Estadual Paulista. Faculdade de Ciências, Bauru, 2016

1. Energy Harvesting. 2. Nonlinear Dynamics. 3. Portal frame structure. 4. Saturation Phenomenon I. Universidade Estadual Paulista. Faculdade de Engenharia de Bauru.

UNIVERSIDADE ESTADUAL PAULISTA

Câmpus de Bauru

ATA DA DEFESA PÚBLICA DA TESE DE DOUTORADO DE RODRIGO TUMOLIN ROCHA, DISCENTE DO PROGRAMA DE PÓS-GRADUAÇÃO EM ENGENHARIA MECÂNICA, DA FACULDADE DE ENGENHARIA.

Aos 04 dias do mês de agosto do ano de 2016, às 08:00 horas, no(a) Anfiteatro da Pós-Graduação, reuniu-se a Comissão Examinadora da Defesa Pública, composta pelos seguintes membros: Prof. Dr. JOSE MANOEL BALTHAZAR - Orientador(a) do(a) Departamento de Estatística, Matemática Aplicada e Computação / Instituto de Geociências e Ciências Exatas - UNESP Rio Claro, Prof. Dr. AIRTON NABARRETE do(a) Departamento de Engenharia Aeroespacial e Aeronáutica / Instituto Tecnológico de Aeronáutica, Prof. Dr. ANGELO MARCELO TUSSET do(a) Departamento de Eletrônica / Universidade Tecnológica Federal do Paraná, Prof. Dr. VINICIUS PICCIRILLO do(a) Departamento de Matemática/Universidade Tecnológica Federal do Paraná, Prof. Dr. ATILA MADUREIRA BUENO do(a) Departamento de Engenharia de Controle e Automação / Instituto de Ciência e Tecnologia/UNESP/Sorocaba, sob a presidência do primeiro, a fim de proceder a arguição pública da TESE DE DOUTORADO de RODRIGO TUMOLIN ROCHA, intitulada **ON SATURATION PHENOMENON IN ENERGY HARVESTING BASED ON NONLINEAR PIEZOELECTRIC MATERIALS COUPLED TO A PORTAL FRAME FOUNDATION WITH IDEAL AND NON-IDEAL EXCITATIONS**. Após a exposição, o discente foi arguido oralmente pelos membros da Comissão Examinadora, tendo recebido o conceito final: APROVADO. Nada mais havendo, foi lavrada a presente ata, que após lida e aprovada, foi assinada pelos membros da Comissão Examinadora.

Prof. Dr. JOSE MANOEL BALTHAZAR

Prof. Dr. AIRTON NABARRETE

Prof. Dr. ANGELO MARCELO TUSSET

Prof. Dr. VINICIUS PICCIRILLO

Prof. Dr. ATILA MADUREIRA BUENO

Dedicated to
My parents Carlos and Silvia
My girlfriend Fernanda
All my family
My unforgettable friends
My supervisors

Acknowledgments

Firtly, I thank God for the opportunity to reach this achievement, when several difficulties were left behind and always showing the right ways of the life.

I would like to thank very much my great friend and amazing advisor, Professor José Manoel Balthazar, for giving me the opportunity to work with him and his research group, trusting and believing in me in each past moment preparing works, showing me new research subjects, and the most important, in the professional means., guiding me until the end of this work. Even in the most difficult times, he never forgot what was the best for me. I have been working with him since 2010, and I intend to ever follow him because he is an example as an advisor and as a person to me.

I would also like to really thank Professors Ângelo Marcelo Tusset and Vinicius Piccirillo for each help, discussions, take my doubts, for all the support the whole time in the post-graduation, always improving my knowledge about my research. Of course, without them, it would not be the same.

My grateful thanks to Professor Osvaldo Luís Manzoli for his teachings when he was my supervisor in the teaching internship. It was very important to my learning as a post-graduation student.

My sincerely thanks to all my friends of the Faculty of the Engineering of Bauru for the moments we spent together, playing soccer, pizza and fun during the past years. In special, Julio, Pedro, my companion of laboratory Guilherme and Jaime, the Ph.D foreigners Bruno Agostinho and Michael. My big brothers of our same ship Carlao and Hassan for every spent moment studying and having fun, and also my friends Alexandre Alves and Daniel Daltin for the few and great past moments. My friends of my hometown for we always be together sharing their knowledge, their companionship and the best moments of my life.

My deep thanks to my girlfriend Fernanda Dias for always be my partner, advising and encouraging me, and thinking about the well of my future.

My best and sincerely thanks to my parents Carlos Rocha and Silvia Tumolin for all the encouragement, assistance and belief in my will in this time travel since I was a young boy. I know if It was not you, I never would get where I am today.

Resumo

Rocha, R. T., SOBRE FENÔMENO DE SATURAÇÃO EM COLETA DE ENERGIA BASEADA EM MATERIAIS PIEZOELÉTRICOS NÃO-LINEARES ACOPLADOS A UMA FUNDAÇÃO APORTICADA COM EXCITAÇÕES IDEAL E NÃO-IDEAL, Bauru, Faculdade de Engenharia, UNESP – Universidade Estadual Paulista, 2016, 129 p., Tese de Doutorado.

Recentemente, o interesse e a pesquisa de coleta de energia têm aumentado substancialmente no meio técnico-científico. Com a grande demanda mundial por energia elétrica, muitos pesquisadores, no Brasil e no Mundo, têm concentrado seus esforços na busca de novas fontes de energia. Além disso, com os avanços da tecnologia, é possível utilizar dispositivos de baixo consumo de energia, que são, na maioria das vezes, alimentados por uma bateria, que são fontes de energia finita havendo a necessidade da recarga ou troca periodicamente, das mesmas. No processo de coleta de energia, a energia elétrica é obtida através da conversão de energia mecânica criada por uma fonte de vibração do meio ambiente através de um transdutor. Entre os mais comuns meios de transdução de energia, o uso de materiais piezoelétricos vêm sendo de grande interesse em meio a coleta de energia devido sua facilidade de aplicação e seu uso para coleta de energia em um amplo intervalo de frequências. Fontes de vibração do meio ambiente podem ser causadas em estruturas através do movimento de veículos, um trêm, ondas do mar e até o deslocamento de pessoas. Com isso, este trabalho tem como objetivo estudar a coleta de energia utilizando uma plataforma aporticada não-linear de dois graus de liberdade contendo um material piezoelétrico não-linear acoplado a uma de suas colunas e excitado externamente em sua base. A plataforma não-linear possui ressonância interna 2:1 entre seus modos de vibrar. A não-linearidade do material é considerada através de uma relação matemática não-linear. Além disso, este trabalho será separado em duas partes para a análise das excitações externas. Em sua primeira parte, considera-se uma força harmonica excitando sua base. Na segunda parte, será considerando um vibrador eletrodinâmico com saída harmônica. A metologia empregada para a realização das análises deste trabalho foram: utilizar o método de múltiplas escalas para buscar as melhores configurações dos parâmetros e encontrar fenômenos devido à ressonancia interna 2:1; em seguida foram realizadas excessivas simulações numéricas utilizando o método de Runge-Kutta de quarta e quinta ordem com passo variável buscando otimizar a coleta de energia através da variação de parâmetros, diagramas de bifurcação, expoente de lyapunov, FFTs e históricos no tempo e outros tipos de simulações. Em geral serão feitas duas comparações muito importantes. A influência da não-linearidade do material piezoelétrico e do uso da força harmonica e do vibrador eletrodinâmico na coleta de energia. Os resultados mostraram grande influência da não-linearidade do material piezoelétrico, e utilizando o vibrador foi possível ter um ganho considerável na estabilidade do sistema.

Palavras-chave: Coleta de energia, Dinâmica Não-Linear, Estrutura Aporticada, Fenômeno de Saturação

Abstract

Rocha, R. T., ON SATURATION PHENOMENON IN ENERGY HARVESTING BASED ON NONLINEAR PIEZOELECTRIC MATERIALS COUPLED TO A PORTAL FRAME FOUNDATION WITH IDEAL AND NON-IDEAL EXCITATIONS, Bauru, Faculty of Engineering, São Paulo State University, 2016, 129 p., Ph.D. Dissertation.

Recently, the interest and research about energy harvesting has been increasing substantially in the technical-scientific community. With the great world demand for electrical energy, many researchers, in Brazil and in the World, have concentrated their efforts to seek new energy sources. In addition, with the technological advances is possible to use low-power consumption devices, that are, most of time, powered by a battery, which are limited energy sources having the necessity of recharging or substituting them periodically. In the energy harvesting process, the electrical energy is obtained through the conversion of mechanical energy created by a vibrating source in the environment using a transducer. Among the most common energy transduction mean, the use of piezoelectric materials has been of great interest in the energy harvesting matter due to its ease of application and its use to harvest energy in a wide range of frequencies. Vibration sources in the environment may occur in structures by vehicle traffics, a train movement, sea waves and even people. With that, the objective of this work is to study the energy harvesting using a nonlinear two-degrees-of-freedom portal frame platform with a nonlinear piezoelectric material coupled to one of its columns and externally base-excited. The nonlinear platform possesses two-to-one internal resonance between its two vibration modes. The nonlinearities of the piezoelectric material is considered as a nonlinear mathematical relation. Moreover, this work is separated in two parts to the analysis of the external excitations. In the first part, a harmonic force base-exciting the system is considered. In the second part is considered an electro-dynamical shaker with harmonic output. The employed methodology to carry out the analysis of this work was: the application of the method of multiple scales to find the best configuration of the parameters, and to find some kind of phenomena due to the two-to-one internal resonance; in the following were carried out several numerical simulations using the method of Runge-Kutta of 4th and 5th order with variable step seeking to optimize the energy harvesting through parametrical variations, bifurcation diagrams, FFTs, time histories and other typos of simulations. In general, it will be done two much important comparisons: the influence of the nonlinearity of the piezoelectric material and the use of the harmonic force and the shaker to the energy harvesting. The results showed great influence of the nonlinearity of the material, and using the electro-dynamical device it was possible to have a considerably gain in the system stability.

Keywords: Energy Harvesting, Nonlinear Dynamics, Portal Frame Structure, Saturation Phenomenon

List of Figures

1.1 **Illustration of the energy harvesting processes in the environment (Fujitsu, 2010).** 2

2.1 **Operating mode of a piezoelectric transducer; D is the applied force and V is the generated electric voltage (adapted from Priya and Inman (2009)** 9
2.2 **(a) Picture of a thin film piezoelectric, (b) Illustrative scheme of the thin film piezoelectric (adapted from Pique (2013))** 10
2.3 **(a) Conceptual model of a piezoelectric generator, (b) Equivalent circuit of a piezoelectric generator (adapted from Cottone (2007))** 10
2.4 **Operating modes of a piezoelectric transducer; D is the applied force and V is the generated electrical voltage (adapted from Priya and Inman (2009)** 11
2.5 **Set of figures of nonlinearity by hysteresis, (a) magnetic, (b) piezoelectric, (c) shape-memory alloy** 12
2.6 **Dependence of d_{31} on the induced voltage. The experimental curve as represented by Crawley and Anderson (1990)** 13
2.7 **Electro-dynamical shaker's mechanical and electrical representation** 17

3.1 **Schematic model of a simple portal frame with a piezoelectric material coupled to one of its column, (a) non-deformed, (b) deformed** 20

4.1 **Energy percentage of the motion in horizontal direction (in red), vertical (in black), and the electric energy of the piezoelectric (in blue), (a) $\omega_n = 100 rad/s$ and $\theta = 0$, (b) $\omega_n = 148 rad/s$ and $\theta = 0$, (c) $\omega_n = 148 rad/s$ and $\theta = 0.3$** 29
4.2 **Time histories of the displacements of horizontal (in gray) and vertical (in black) motions. (a) $\omega_n = 100 rad/s$ and $\theta = 0$, (b) $\omega_n = 148 rad/s$ and $\theta = 0$, (c) $\omega_n = 148 rad/s$ and $\theta = 0.3$; (d) time history of the harvested power with $\omega_n = 148 rad/s$ and $\theta = 0.3$** . . . 30

4.3 **Phase plane (in black) and Poincaré map (gray dot) with $\omega_n = 148rad/s$ and $\theta = 0.3$, (a) Horizontal, (b) Vertical** 31
4.4 **FFT with $\omega_n = 148rad/s$ and $\theta = 0.3$** 31
4.5 **Parametrical analysis of the frequency related to the average power to (a) ω_n (dimensional), (b) Ω (dimensionless)** 33
4.6 **Bifurcation diagram of the dimensionless frequency Ω related to the (a) horizontal, (b) vertical coordinates** 33
4.7 **(a) Surface (b) Contour; of the excitation frequency ω_n related to the excitation amplitude $F_0[N]$ and the maximum displacement of the structure** 34
4.8 **Parametrical variation of the linear piezoelectric coefficient θ related to the average harvested power** 36
4.9 **Bifurcation diagram of the linear piezoelectric coefficient θ related to the (a) horizontal, (b) vertical coordinates** 36
4.10 **Parametrical variation of the linear piezoelectric coefficient θ related to the average harvested power** 37
4.11 **Bifurcation diagram of the linear piezoelectric coefficient θ related to the (a) horizontal, (b) vertical coordinates** 38
4.12 **Surface of the maximum horizontal displacement related to the amplitude of the external excitation and initial conditions (a) x_{01}, (b) x'_{01}, (c) x_{02}, (d) x'_{02}** 40
4.13 **Contour of the maximum displacement of the structure related to the amplitude E_0 versus (a) x_{01}, (b) x'_{01}** 41
4.14 **Parametrical variation of the amplitude of the external force E_0 related to the average harvested power with $x_{01} = 0.3$** 41
4.15 **Piezoelectric linear case $\Theta = 0$ and initial condition $x_{01} = 0.001$ (a) Contour of the maximum displacement of the structure related to the amplitude E_0 versus θ; (b) surface of the harvested power related to the amplitude E_0 versus θ; (c) coloured contour of the harvested power related to the amplitude E_0 versus θ** 43
4.16 **Piezoelectric linear case $\Theta = 0$ and initial condition $x_{01} = 0.3$ (a) Contour of the maximum displacement of the structure related to the amplitude E_0 versus θ; (b) surface of the harvested power related to the amplitude E_0 versus θ; (c) coloured contour of the harvested power related to the amplitude E_0 versus θ** 44

4.17 **Piezoelectric nonlinear case $\Theta = 1$ to surfaces (a) and (c), Contour (b) and (d), of the maximum horizontal displacement of the structure related to the amplitude *versus* initial conditions x_{01} and x'_{01}** 46
4.18 **Piezoelectric nonlinear case $\Theta = 1$ and initial condition $x_{01} = 0.001$ (a) Contour of the maximum displacement of the structure related to the amplitude E_0 versus θ; (b) surface of the harvested power related to the amplitude E_0 versus θ; (c) coloured contour of the harvested power related to the amplitude E_0 versus θ** 47
4.19 **Piezoelectric nonlinear case $\Theta = 1$, and initial condition $x_{01} = 0.3$ (a) Contour of the maximum displacement of the structure related to the amplitude E_0 versus θ; (b) surface of the harvested power related to the amplitude E_0 versus θ; (c) coloured contour of the harvested power related to the amplitude E_0 versus θ** 48

5.1 **Schematic model of a simple portal frame with a piezoelectric material coupled to one of its column and an electro-dynamical shaker coupled to its base, (a) non-deformed, (b) deformed** 51

6.1 **Energy percentage of the motion, considering the shaker, in horizontal direction (in red), vertical (in black), and the electric energy of the piezoelectric (in blue), (a) $\omega_n = 100 rad/s$ and $\theta = 0$, (b) $\omega_n = 148 rad/s$ and $\theta = 0$, (c) $\omega_n = 148 rad/s$ and $\theta = 0.3$** 58
6.2 **Time histories of the displacements, considering the shaker, of horizontal (in gray) and vertical (in black) motions. (a) $\omega_n = 100 rad/s$ and $\theta = 0$, (b) $\omega_n = 148 rad/s$ and $\theta = 0$, (c) $\omega_n = 148 rad/s$ and $\theta = 0.3$; (d) time history of the harvested power with $\omega_n = 148 rad/s$ and $\theta = 0.3$** 59
6.3 **Full portal frame phase plane (in black) and Poincaré map (gray dot) with $\omega_n = 148 rad/s$ and $\theta = 0.3$, (a) Horizontal, (b) Vertical** . . 60
6.4 **FFT with $\omega_n = 148 rad/s$ and $\theta = 0.3$** 60
6.5 **Parametrical analysis of the shaker's frequency related to the average power to (a) ω_n (dimensional), (b) Ω (dimensionless)** . . . 61
6.6 **Bifurcation diagram of the dimensionless shaker's frequency Ω related to the (a) horizontal, (b) vertical coordinates** 62
6.7 **(a) Surface (b) Contour; of the shaker's frequency $\omega_n[rad/s]$ related to the shaker's amplitude $e_0[V]$ and the maximum displacement of the structure** 63

6.8 **Parametrical variation of the linear piezoelectric coefficient θ related to the average harvested power, considering the shaker** . . . 65
6.9 **Bifurcation diagram, considering the shaker, of the linear piezoelectric coefficient θ related to the (a) horizontal, (b) vertical coordinates** 65
6.10 **Parametrical variation of the linear piezoelectric coefficient θ related to the average harvested power, considering shaker and $\Theta = 1$** 66
6.11 **Bifurcation diagram, considering shaker and $\Theta = 1$, of the linear piezoelectric coefficient θ related to the (a) horizontal, (b) vertical coordinates** 66
6.12 **Surface of the maximum horizontal displacement related to the shaker's amplitude of the external excitation and initial conditions (a) x_{01}, (b) x'_{01}, (c) x_{02}, (d) x'_{02}** 68
6.13 **Contour of the maximum displacement of the structure related to the shaker's amplitude E_0 versus (a) x_{01}, (b) x'_{01}** 68
6.14 **Parametrical variation of the shaker's amplitude $e_0[V]$ related to the average harvested power with $x'_{01} = 0.3015$** 69
6.15 **Bifurcation diagrams of the electro-dynamical shaker's amplitude $e_0[V]$ with $x'_{01} = 0.3015$** 70
6.16 **(a) FFT (b) Phane plane (in black) and Poincare Map (in gray) of the horizontal displacement of the portal frame (c) Phane plane (in black) and Poincare Map (in gray) of the vertical displacement of the portal frame; with $e_0 = 233V$ ($E_0 = 1199$), $x'_{01} = 0.3015$** 71
6.17 **Piezoelectric linear case $\Theta = 0$ and initial condition $x_{01} = 0.001$ (a) Contour of the maximum displacement of the structure related to the amplitude E_0 versus θ; (b) surface of the harvested power related to the amplitude E_0 versus θ; (c) coloured contour of the harvested power related to the amplitude E_0 versus θ** 73
6.18 **Piezoelectric linear case $\Theta = 0$ and initial condition $x'_{01} = 0.3015$ (a) Contour of the maximum displacement of the structure related to the amplitude E_0 versus θ; (b) surface of the harvested power related to the amplitude E_0 versus θ; (c) coloured contour of the harvested power related to the amplitude E_0 versus θ** 74

6.19 **Piezoelectric nonlinear linear case $\Theta = 1$ and initial condition $x'_{01} = 0.001$ (a) Contour of the maximum displacement of the structure related to the amplitude E_0 versus θ; (b) surface of the harvested power related to the amplitude E_0 versus θ; (c) coloured contour of the harvested power related to the amplitude E_0 versus θ** 76

6.20 **Piezoelectric nonlinear linear case $\Theta = 1$ and initial condition $x'_{01} = 0.3015$ (a) Contour of the maximum displacement of the structure related to the amplitude E_0 versus θ; (b) surface of the harvested power related to the amplitude E_0 versus θ; (c) coloured contour of the harvested power related to the amplitude E_0 versus θ** 78

A.1 **Simple two-degrees-of-freedom portal frame foundation, (a) without NES, (b) With NES in vertical mode, (c) With NES in horizontal mode, (d) NES in both vertical and horizontal mode** 93

A.2 **Time histories of (a) displacements, (b) harvested power; and Phase planes (in black) and Poincaré Maps (red dot) of (a) horizontal displacement, (b) vertical displacement** 97

A.3 **Parametrical analysis of the control parameter "e" related to the average harvested power to the NES in vertical mode** 98

A.4 **Bifurcation diagrams of the control parameter "e", to the NES in vertical mode, related to (a) horizontal movement, (b) vertical movement, (c) NES movement** 99

A.5 **Parametrical analysis of the control parameter "e" related to the average harvested power to the NES in horizontal motion** 100

A.6 **Bifurcation diagrams of the control parameter "e", to the NES in horizontal movement, related to (a) horizontal movement, (b) vertical movement, (c) NES movement** 101

A.7 **Parametrical analysis of the control parameter "e" related to the average harvested power to the NES in both vertical and horizontal modes** 102

A.8 **Bifurcation diagrams of the control parameter "e", to NES in both vertical and horizontal directions, related to (a) horizontal movement, (b) vertical movement, (c) NES in horizontal movement, (d) NES in vertical movement** 103

List of Tables

4.1 **Parameters of the Portal Frame Harmonically Base-Excited** 27
4.2 **Studied regions of Fig. 4.7b** 34
4.3 **Summary of Sec. 4.2** 35
4.4 **Numerical results to the linear piezoelectric coupling** 36
4.5 **Numerical results to the linear piezoelectric coupling, considering the nonlinear contribution** 38
4.6 **Numerical results of the initial displacement condition x_{01} variation related to the amplitude of the external force** 42
4.7 **Summary of Subsec. 4.4.1** 45
4.8 **Summary of Subsec. 4.4.2 in comparison to Subsec. 4.4.1** 49

6.1 **Parameters of the Full Portal Frame Foundation** 57
6.2 **Studied regions of Fig. 6.7b** 62
6.3 **Summary of Sec. 6.2** 63
6.4 **Numerical results to the linear piezoelectric coupling** 64
6.5 **Numerical results to the linear piezoelectric coefficient considering its nonlinearity and the electro-dynamical shaker** 67
6.6 **Numerical results of the initial displacement condition x'_{01} variation related to the amplitude of the electro-dynamical shaker** . . . 71
6.7 **Summary of Subsec. 6.4.1** 75
6.8 **Summary of Subsec. 6.4.1 in comparison to Subsec. 6.4.2** 79

7.1 **Summary of the comparison between the frequencies of Sec. 4.2 and 6.2** 81
7.2 **Summary of the nonlinear piezoelectric material contribution with ideal and non-ideal excitations** 82

A.1 **Parameters of the Portal Frame coupled to the NES** 96
A.2 **Summary of the Energy Harvesting VS. Control Parameter** 104
A.3 **Regions of the Behaviours** 104

Contents

Resumo vi

Abstract vii

List of Figures viii

List of Tables xii

Nomenclature xvii

1 Introduction 1

1.1 Motivation . . . 2
1.2 Objectives . . . 3
1.3 Contributions of the Work . . . 3
1.4 Materials and Method . . . 3
1.5 Layout of the Dissertation . . . 4

2 Basic Concepts 6

2.1 Piezoelectric Materials . . . 6
2.1.1 Energy Harvesting from the Environment . . . 7
2.1.2 Piezoelectricity . . . 7
2.1.3 Constitutive Relations of the Piezoelectric Material . . . 8
2.1.4 Piezoelectric Energy Harvesting Devices . . . 9
2.1.5 Operating Modes of a Piezoelectric Transducer . . . 11
2.1.6 Piezoelectric's Nonlinearity . . . 11
2.2 Saturation Phenomenon . . . 13
2.3 Energy Harvesting Systems . . . 16
2.4 Electro-Dynamical Shaker . . . 17

PART I - Global Analysis of the System with Harmonic Base Excitation 19

3 Portal Frame Foundation under Harmonic base excitation Mathematical Model **20**

3.1 Mathematical Modelling of the Dynamical System with Harmonic Excitation 22

3.2 Dimensionless Process of the Governing Equations of Motion 24

4 Numerical Simulations of the System Harmonically Base-Excited and Discussions **26**

4.1 Energy Transfer and Saturation Phenomenon 27

4.2 Influence of the External Frequency ω_n 32

4.3 Influence of the Piezoelectric Material 35

4.3.1 Case of the sole linear piezoelectric coupling $\Theta = 0$ 35

4.3.2 Case of the nonlinear piezoelectric coupling $\Theta \neq 0$ 37

4.4 Influence of the Amplitude of External Frequency *versus* Initial Conditions 39

4.4.1 Amplitude *versus* Sole Linear Piezoelectric Coefficient Case 42

4.4.2 Amplitude *versus* Nonlinear Piezoelectric Coefficient Case 45

PART II - Global Analysis of the System with Electro-dynamical Shaker **50**

5 Full Portal Frame Foundation Mathematical Model **51**

5.1 Mathematical Modelling of the Full Portal Frame 52

5.2 Dimensionless Process of the Governing Equations of Motion of the Full System 54

6 Numerical Simulations of the Full Portal Frame System **56**

6.1 Energy transfer and saturation phenomenon 57

6.2 Influence of the frequency of the shaker 61

6.3 Influence of the piezoelectric material 64

6.3.1 Case of the sole linear piezoelectric material $\Theta = 0$ 64

6.3.2 Case of the nonlinear piezoelectric material $\Theta = 1$ 65

6.4 Influence of the Shaker's Amplitude *versus* Initial Conditions 67

6.4.1 Electro-Dynamical Shaker‘s Amplitude *versus* Sole Linear Piezoelectric Coefficient Case 72

6.4.2 Electro-Dynamical Shaker‘s Amplitude *versus* NONLINEAR Piezoelectric Case 75

7 Conclusions **80**

8 Future Works **84**

Bibliography **85**

A Improvement of the Energy Harvesting using a Nonlinear Energy Sink 92
A.1 The Structural Problem 92
A.2 Numerical Simulations and Results 95
A.2.1 Case 1 - Dynamical analysis of the simple portal frame foundation . 96
A.2.2 Case 2 - Influence of the NES in vertical mode 98
A.2.3 Case 3 - Influence of the NES in horizontal mode 100
A.2.4 Case 4 - Influence of the NES in both vertical and horizontal modes 102
A.3 Short Conclusion of Appendix 103

Vita 105

Nomenclature

Latin Letter

Symbols	Description
A	Constant dependent on h
B_0	Magnetic field of the electro-dynamical shaker
B	Constant dependent on L
c_0	Damping of the base
c_1	Column damping
c_2	Beam damping
C_p	Piezoelectric's capacitance
d_{31}	Piezoelectric constant with electric field perpendicular to the poling direction
d_{33}	Piezoelectric constant with electric field parallel to the poling direction
$d(q_1)$	Piezoelectric coupling in the portal frame foundation
D	Piezoelectric's electric displacement given in charge power unit area
e_0	Output amplitude of the electro-dynamical shaker
E	Electric field of the piezoelectric material
E_{x_1}	Energy index of the vertical coordinate
E_{x_2}	Energy index of the horizontal coordinate
E_{V_p}	Energy index of the piezoelectric coordinate
$E_{\%x_1}$	Percentage of energy index of the vertical coordinate
$E_{\%x_2}$	Percentage of energy index of the horizontal coordinate
$E_{\%V_p}$	Percentage of energy index of the piezoelectric coordinate

E_{total}	Total energy index of the coordinates
E_0	Dimensionless amplitude of the electro-dynamical shaker
EI	Linear flexural stiffness of the portal frame foundation
F_0	Amplitude of the external force
F_{em}	Electromotive force of the electro-dynamical shaker
F_{ext}	Harmonic force function of base excitation
g	Gravity acceleration
G_0	Dimensionless constant of gravity acceleration
G_1	Dimensionless constant of gravity acceleration
h	Length of a portal frame foundation's column
i_0	Free parameter for dimensionless process
I_0	Electric current of the electro-dynamical shaker
k_0	Stiffness of the base
k_c	Linear stiffness of the columns
k_b	Linear stiffness of the beam
K	Electromagnetic force of the electro-dynamical shaker
L_0	Electric inductance of the electro-dynamical shaker
L	Length of the portal frame foundation's supported beam
m_0	Base mass
m	Column mass
M	Beam mass
P_{avg}	Average dimensionless power
$P_{dimensional}$	Dimensional power
$P_{dimensionless}$	Dimensionless power
q_i	Dimensional general coordinates of the dynamical system
$\dot{q}_i$	Dimensional velocity of the coordinates of the dynamical system
$\ddot{q}_i$	Dimensional acceleration of the coordinates of the dynamical system
Q_0	Free parameter for dimensionless process
Q_{s0}	Electric charge of the electro-dynamical shaker circuit

Q_p	Produced charge of the piezoelectric material
R_0	Electric resistance of the electro-dynamical shaker
R_L	Resistive charge of the piezoelectric material
R_p	Resistance of the internal piezoelectric element
R_{p_0}	Dimensionless constant of the harvested power relations
s^E	Inverse of Young's modulus (compliance)
S_0	Electro-dynamical shaker's displacement of base excitation
S	Piezoelectric's mechanical tension/deformation
t	Dimensional time
T	Stress of the piezoelectric material
T_p	Length of the vector harvested power
u	Form function of the columns
u_i	Nodal horizontal displacement of the portal frame foundation
U	Dimensionless electric current of the electro-dynamical shaker
U'	Dimensionless electric flux of the electro-dynamical shaker
v	Form function of the beam
v_i	Nodal vertical displacement of the portal frame foundation
V_{piezo}	Electric voltage produced by the piezoceramic
V_p	Dimensionless electric charge of the piezoelectric material
V_p'	Dimensionless electric current of the piezoelectric material
x	Coordinate of support axis of the portal frame
x_i	Dimensionless displacements of the general coordinates of the dynamical system
x_{0i}	Dimensionless initial conditions
x_i'	Dimensionless velocity of the general coordinates of the dynamical system
x_i''	Dimensionless acceleration of the general coordinates of the dynamical system
x_{df}	Representative deformation to the nonlinear piezoelectric explanation

Y	Dimensionless displacement of the base
Y'	Dimensionless velocity of the base
Y''	Dimensionless acceleration of the base

Greek Letter

Symbol	**Description**
α_1	Dimensionless quadratic nonlinear constant of the horizontal motion
α_2	Dimensionless quadratic nonlinear constant of the vertical motion
β_i	Dimensionless constants related to the base motion
γ_i	Dimensionless constants related to electric circuit of the electro-dynamical shaker
δ_i	Dimensionless constants related to piezoelectric charge
θ	Linear piezoelectric coefficient
Θ	Nonlinear piezoelectric coefficient
μ_0	Dimensionless damping of the base
μ_1	Dimensionless damping of the column
μ_2	Dimensionless damping of the beam
τ	Dimensionless time
ω_1	Dimensional natural frequency of the horizontal motion
ω_2	Dimensionaless natural frequency of the vertical motion
ω_n	Dimensional frequency of external excitation
Ω	Dimensionless frequency of external excitation
ε^T	Piezoelectric material's dielectric constant (Permittivity)

Abbreviation

Symbol	**Description**
NES	Nonlinear Energy Sink
NIS	Non-Ideal System
PZT	Lead Zirconate Titanate
$PVDF$	Polyvinulidene Fluoride

Chapter 1

Introduction

Nowadays, there is a great demand for electrical energy due to the increasing of the World population. With that, the interest and research about new energy sources has been increased substantially in the technical-scientific community. There are many different types of energy sources available for energy harvesting, for example, provided by nuclear reactors, fossil fuels provided by oil, mineral coal and natural gas, hydroelectric, among others.

However, with the technological advances, smaller devices were developed and they are low-power consumption. These kind of devices, most of time, are powered by a battery, which is a limited energy source, because the necessity of its recharge or replaced. With that, it was developed some devices capable of transforming energy of the environment. Among them, there are the micro-generators that are capable to harvest electrical energy of the vibrations of a railway, a runway, a roadway, for example. Photovoltaic plates that transform energy through the solar light. In addition, there are thermoelectric generators that collect energy of heat. Moreover, the Rectenna that are antennas used to convert microwaves into DC power, i.e., they convert electromagnetic waves into electrical energy. These kind of energy harvesting are illustrated in Fig. 1.1.

One of the newest and most promising means of energy harvesting is from the kinetic energy, which is one of the energy sources that is most abundantly available. The kinetic energy is found in the environment's vibration, whose may be generated by: the winds, vehicle traffic, people displacement, among others. Therefore, there is a great interest in the concept of harvest energy from the operating environment of mechanical systems. Among the possible energy harvesting devices, the use of piezoelectric material as a means of energy transduction has been widely studied, because they are capable to transform the kinetic energy of the vibrations into electrical energy. Furthermore, these materials are of easy application, and they can be used in a wide range of frequencies.

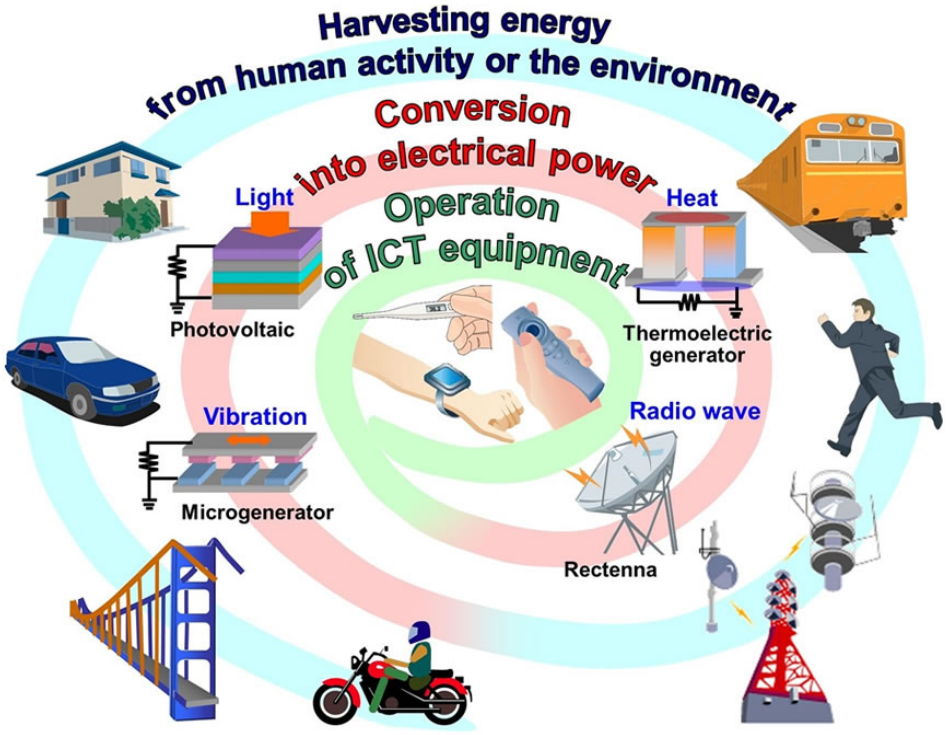

Figure 1.1: Illustration of the energy harvesting processes in the environment (Fujitsu, 2010).

1.1 Motivation

The study of energy harvesting has increased substantially, and it has been applied in several nonlinear structures in order to harvested energy from environment's vibration. Nowadays, there is a great number of vibrational energy sources in the environment, mainly in the daily life, that could be used to this kind of application. The piezoelectric material is one of the most studied energy harvesting devices, because of its ease of application. The study of its influence as a means of energy transduction becomes to be very important because it is a possible renewable low power energy source and it has a great potential to future purposes.

Other important question to be pointed out is the study of the saturation phenomenon. Some kind of structures such as bridges, cranes, or structures that possess internal resonances relations can be of great contribution to the energy harvesting subject. This kind of phenomenon, depending on the structure, may provoke damages, that is, fractures/breaks/softening from small to big important structures.

As the piezoelectric can be used as transducers, coupled in theses structures may avoid these kind of damage, and at the same time, harvest energy from the excessive vibrations. Moreover, saturation phenomenon may be of great contribution when known its conditions

and applied in interested dynamical systems.

1.2 Objectives

With all the knowledge presented in the introduction, the importance of the energy harvesting theme in nonlinear structures, and considering the study of a continuous portal frame foundation discretized in two-degrees-of-freedom with concentrated parameters, the coupling of the nonlinear piezoelectric material, and the external excitation through the electro-dynamical shaker, the main objectives are:

• carry out the mathematical modelling of the electro-mechanical system, obtaining dimensionless equations of motion,

• verify the vibration energy transfer and the existence of the saturation phenomenon through numerical simulations,

• study the behaviour of the system with parametrical variations,

• through saturation phenomenon, analyse the energy harvesting in periodic regions with the piezoelectric material, considering its linear and nonlinear contribution.

1.3 Contributions of the Work

Aiming to conclude the pointed objectives of this work, the contributions of this work to the energy harvesting and nonlinear dynamics theme were:

• a fully state of the art,

• carry out the study of energy harvesting taking the advantage of the saturation phenomenon using a nonlinear piezoelectric material,

• use an electro-dynamic shaker to excite the base of a two-degrees-of-freedom structure, where saturation phenomenon continued to exist,

• compare the difference between a harmonic external excitation to the electro-dynamical shaker's excitation.

1.4 Materials and Method

To this work, it will be presented numerical simulations performed using the method of Runge-Kutta of 4th and 5th order. To the analysis of the phenomena and behaviour of the system in this work, the following numerical tools will be used:

• time histories of displacement, generally used as first steps to characterize the system's motion,

• phase planes to geometric representation of the dynamical system's trajectory in the plane,

• FFT (Fast-Fourier Transform), which is an algorithm to calculate the Discrete Fourier Transform (DFT) and its inverse. It converts time (or space) in frequencies,

• Poincare maps, which is a point sequence in which the flow intercepts a transversal section, in a way to show the periodicity of the system,

• bifurcation diagrams, which shows a qualitative change in the response of the dynamic system due to control parameter variation. They occur when there is a qualitative change in the topology of the phase plane in a determined point, named bifurcation point, that is, a bifurcation is the lost of structural stability,

1.5 Layout of the Dissertation

This work is divided in two major parts, which consist in the analysis of the energy harvesting based on nonlinear piezoelectric materials using the saturation phenomenon considering two kinds of excitation. The PART I consists of the analysis of the dynamical system excited by a harmonic force. The PART II shows the analysis of the dynamical excited by the electro-dynamical shaker.

Therefore, to achieve the indicated objectives, this work was organized by the following.

In Chapter 1 is presented the introduction about this work followed by the motivation to carry out this research, objectives, contributions and the materials and method used to perform such analysis.

Chapter 2 presents the basic concepts about the structure to be analyzed, the piezoelectric material used as a means of energy transduction, the electro-dynamical shaker as a base exciter device and the role of the nonlinear phenomena present in the whole dynamical system.

Followed by Chapter 2, the PART I begins focusing on the study of the harmonic force as a means of external excitation.

PART I begins in Chapter 3 which presents the dynamical system excited by the harmonic force, its composition, couplings, coordinates, etc. Moreover, the mathematical modelling was carried out using the energy method of Lagrange's function, where the kinetic, potential, Rayleigh dissipation energies and the external excitation function were defined. In addition, a dimensionless process was carried out giving the dimensionless governing equations of motion. At the end, the relations of dimensional and dimensionless harvested power were defined.

Chapter 4 shows the numerical simulations of the dimensionless governing equations of motion of Chap. 3. The results were presented using time histories, FFT's, surfaces,

parametrical variations, bifurcation diagrams, Poincare maps, and etc. However, in this Chapter was studied many important parameters related to the energy harvesting and the change of the behaviour of the dynamical system.

Next, PART II focuses on the study of the portal frame excited by an electro-dynamical shaker.

This PART II begins in Chapter 5 which presents the portal frame foundation of two-degrees-of-freedom base-excited by an electro-dynamical shaker, whose compositions, couplings, coordinates and etc. Furthermore, the mathematical modelling is carried out presenting the dimensional and dimensionless governing equations of motion of the dynamical system.

Chapter 6 shows the same numerical simulations carried out in Chap. 4, however considering the dimensionless governing equations of motion of Chap. 5, which considers the electro-dynamical shaker to excites the base.

Finally, Chapter 7 shows the conclusions of this work. The importance of PART I and PART II is compared each other in the end of this work to observe the influence and importance of the electro-dynamical shaker. These comparisons were discussed in the conclusions.

To go further of the results of this work, in Chap. 8 is shown the purposed future works from the results of this one.

Chapter 2

Basic Concepts

In this chapter, the basics concepts to develop the purposed objectives are detailed here.

The energy harvesting is based on a nonlinear piezoelectric material, which will be widely discussed in this chapter. Moreover, the saturation phenomenon which is the most important phenomenon to improve the energy harvesting is explained and discussed. Furthermore, the electro-dynamical shaker is defined to be possible its usage in the mathematical model.

2.1 Piezoelectric Materials

According to the exposed above, the use of piezoelectric material to harvest energy of some mechanical structures becomes to a be a real fact. These materials are commonly called smart materials or multi-functional because of their significantly response for stimulus of different physicists natures. They are usually used as transducers, sensors, actuators, fibers and also they can control or being responsible for their operating environment, as for example, form shaping, modelling of precision control, damage detection and even softening of dynamical response (Preumont, 2006).

The application of the piezoelectric material as a transducer to harvest energy associated to vibrations/deformations, which are induced by displacements or operation of systems and equipments, enables it to work as an energy harvesting device, making possible the use of barely used energy sources. Recently, a great number of works are found in development as in the energy harvesting from renewable energy sources theme as in the usage of vibrating energy sources provided by human activity, like natural motions or induced motions by the own system and equipments condition of operation. The technique of harvesting and storage of energy is know in the literature as Energy Harvesting, described by many authors (Preumont, 2006; Erturk, 2009; Erturk et al., 2009; Erturk and Inman,

2011; Anton and Sodano, 2007; Litak et al., 2012, 2015; Syta et al., 2015; Priya and Inman, 2009; Stephen, 2006; Jalili, 2010; DuToit and Wardle, 2007; Twiefel et al., 2008), among others.

2.1.1 Energy Harvesting from the Environment

Energy harvesting is described as a process which converts environment's energy into electrical energy. The interest of the technique-scientific community to energy sources to futures conceptions of electronic devices has grown considerably, according to Priya and Inman (2009).

Taking by convention that electricity is provided by a power plant, or a battery, it is required an electrical wiring and consequently its substitution. In last past years, the idea of the environment's energy usage in the light, heat, vibrations, sea waves forms and etc, became often more attractive and many methods to produce electrical energy from these different kinds of energy source have been developed. With that, the needs of substitute the batteries, and also its feed cables could be eliminated with the usage of the energy harvesting devices.

Among the possible energy sources available in the environment, it is known that kinetic energy is one of the most readily available. The principle of harvesting these kind of energy is the motion of deformation of a structure, coupled to the transducer. This vibration, or deformation, can be converted into electrical energy by three methods that are: piezoelectricity, electrostatics or magnetic induction, being that the piezoelectricity is the most efficient between the three methods (Cottone, 2007).

2.1.2 Piezoelectricity

Piezoelectricity is a kind of coupling between the mechanical and electrical behaviour of certain materials that exhibit this effect. They are called piezoelectric materials, whose effect is divided in two parts: direct effect and inverse effect (Heywang et al., 2008).

When the piezoelectric material is comprised, i.e., deformed, an electrical charge is caught by the electrodes located in its surface. This is called direct piezoelectric effect, and it was showed for the first time by the Currie brothers in 1880. If the material is submitted to a voltage drop, i.e., an electrical potential difference applied to its electrodes, a mechanical deformation occurs. This is the inverse piezoelectric effect, and it was mathematically deduced (after the discovery of the direct effect) from the fundamental principles of the thermodynamic by Gabriel Lippmann in 1881 and, in the following, experimentally confirmed by Currie brothers in the same year (Jalili, 2010; Heywang et al., 2008).

It is important to note that the two effects normally coexist in the same piezoelectric material. Therefore, in an application where the direct effect is of particular interesting, which is the energy harvesting case, neglecting the presence of the inverse effect would be thermodynamically inconsistent, according to Erturk (2009).

According to Cottone (2007), the materials that shows piezoelectricity are widely available in many forms, it can be naturally or artificially developed, as for example: quartz crystals, sugar cane and Rochelle salt (whose scientific name is potassium sodium tartrate).

Other materials that show piezoelectricity are the piezoceramics, as for example, lead zirconate titanate (PZT) whose formula is $PbTiO_3$, composites as $BaTiO_3$, and polymers such as polyvinulidene fluoride (PVDF) (Preumont, 2006).

A complete description about the piezoelectric materials properties can be found in many works of Priya and Inman (2009); Jalili (2010); Preumont (2006); Heywang et al. (2008); Erturk and Inman (2011), among others.

2.1.3 Constitutive Relations of the Piezoelectric Material

In a general form, the piezoelectric effect can be defined as the transformation of mechanical energy into electrical energy (direct piezoelectric effect) or electrical energy into mechanical energy (inverse piezoelectric effect). Thus, a piezoelectric system is constituted by two physical coupled systems, the mechanical and electrical. Hence, this effect can be denoted in a simplified form neglecting the symmetry of the material by the constitutive relations, given by Eq. (2.1).

$$\begin{aligned} D &= \varepsilon^T E + d_{33} T \\ S &= d_{33} E + s^E T \end{aligned} \tag{2.1}$$

The given relation of Eq. (2.1) are the Onsager relations, where D is the electric displacement given in charge per unit area, expressed in $[C/m^2]$. The electric field E is expressed in $[V/m]$. The stress T is given in $[N/m]$. The mechanical tension/deformation S given in $[N/m^2]$. The material's dielectric constant is denoted by ε^T (Permittivity) under constant stress. The compliance when the electric field is constant is s^E (inverse of the Young's modulus). The piezoelectric constant d_{33} is expressed in $[m/V$ or $C/N]$. The reason for the subscript 33 is that, by convention, the index 3 is always aligned with the poling direction of the material and it is assumed that the electric field is parallel to the poling direction, as illustrated in Fig. 2.1 (Preumont, 2006; Heywang et al., 2008; Priya and Inman, 2009).

It is highlighted that, the absence of a center of symmetry is a necessary condition to

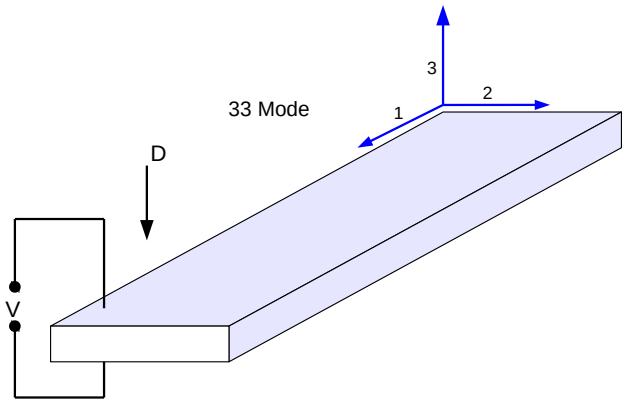

Figure 2.1: Operating mode of a piezoelectric transducer; *D* is the applied force and *V* is the generated electric voltage (adapted from Priya and Inman (2009)

the material can present the piezoelectricity phenomenon, duo to that, all the piezoelectric materials are anisotropic. To describe the properties of all anisotropic material classes there are 18 (eighteen piezoelectric), 21 (twenty-one) elastics coefficients and 6 (six) independent dielectric coefficients (Preumont, 2006).

Two sets of electric coefficients are resulted between the electrical and mechanical system, from the piezoelectric interactions: $\varepsilon^T S$ or $\varepsilon^T T$; and two sets of elastics coefficients: $c^E E$, $S^E E$ or $c^E D$, $S^E D$, where $c^E = 1/S^E$. In addition are defined, depending on the conditions where the measurements are carried out, the mechanical tension T, the mechanical deformation S, the electric field E and the electric displacement vector D are constants. Depending on the symmetry which the material presents, the number of non-zero coefficients can decrease, i.e., higher the symmetry lesser will be the number of non-zero coefficients (Anton and Sodano, 2007).

2.1.4 Piezoelectric Energy Harvesting Devices

A cantilever beam is one of the most used structures to kinetic energy conversion into electrical energy. In this process, the beam has one or two both surfaces covered by a thin piezoelectric film, illustrated by Figs. 2.2.

Figures 2.3a shows the scheme of a piezoelectric generator. The structure is planned to be deflected with the environment's vibration, the thin film will be compressed and the conversion of energy occurs.

The highest output power occurs when the structure vibrates on its resonance frequency, that is, when it vibrates on its natural frequency, that explains the chosen of a cantilever beam structure since it can be easily determined which its natural frequency is. In the

representation showed by Cottone (2007), as showed in Fig. 2.3b, the voltage source represents the developed electric voltage due to the change excess in the surface of the crystal. The series capacitor C_p represents the capacitance in the piezoelectric layer which is proportional to the film permittivity and area that is inversely proportional to the film thickness. The resistance of the internal piezoelectric element is represented by R_p, and R_L is a purely resistive charge. This configuration is called "bimorph", and it is one of the most studied in the actual literature. A detailed analysis about the piezoelectric energy harvesting devices can be found in the works of, among others, Priya and Inman (2009); Jalili (2010); Heywang et al. (2008); Erturk (2009); Erturk and Inman (2011).

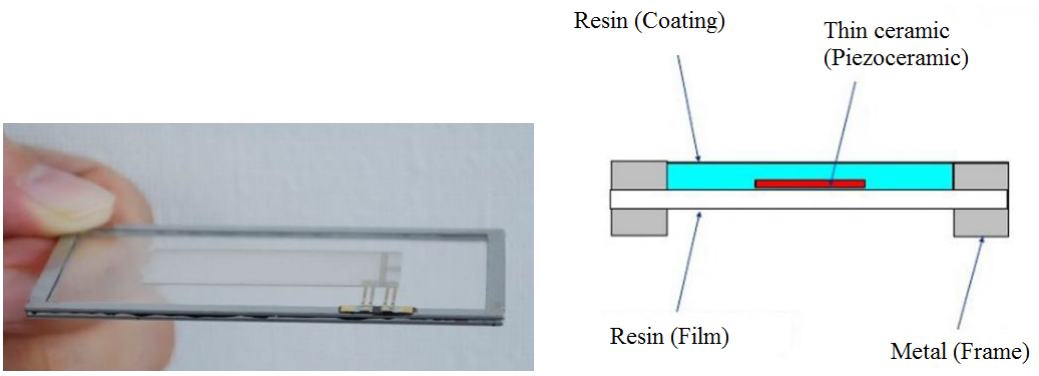

Figure 2.2: (a) Picture of a thin film piezoelectric, (b) Illustrative scheme of the thin film piezoelectric (adapted from Pique (2013))

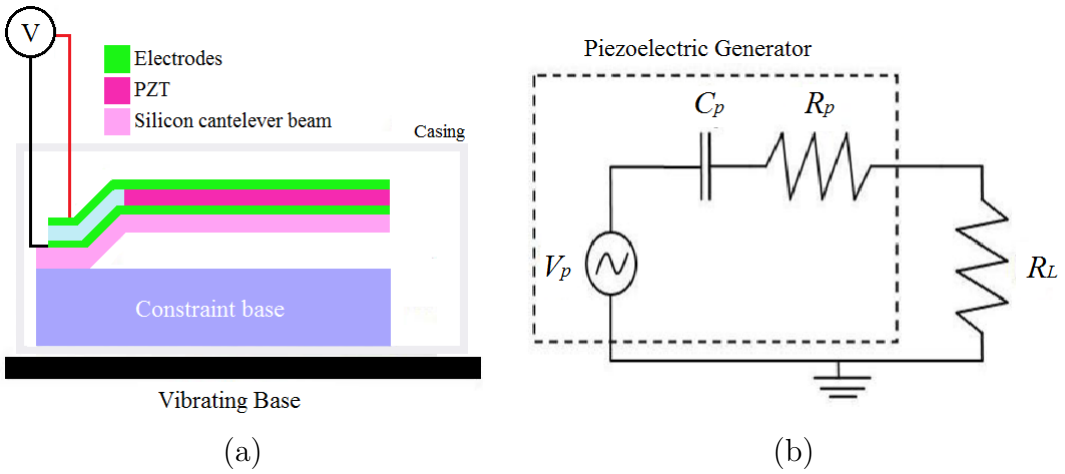

Figure 2.3: (a) Conceptual model of a piezoelectric generator, (b) Equivalent circuit of a piezoelectric generator (adapted from Cottone (2007))

2.1.5 Operating Modes of a Piezoelectric Transducer

The operating mode of a piezoelectric transducer is defined as the way of usage to energy harvesting. There are two most common used operating modes to energy harvesting, which are d_{33} and d_{31}. The d_{33} mode is used in stack actuators of piezoelectric elements, and the d_{31} mode are commonly used in conception of devices based on cantilever beams. When the piezoelectric element is coupled in both cantilever beam sides, i.e., applied in two layers, it has the configuration called "bimorph". In d_{33} mode, the direction of the applied stress (D) and the generated electric voltage (V) is the same. However, in d_{31} mode, the stress is applied in axial direction while the voltage is obtained from the perpendicular direction as shown in Fig. 2.4 (Priya and Inman, 2009).

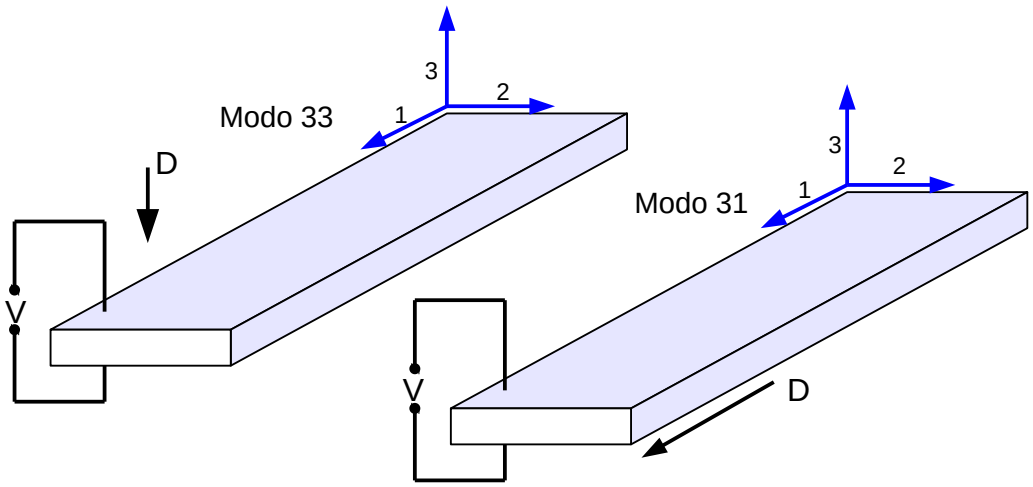

Figure 2.4: Operating modes of a piezoelectric transducer; D is the applied force and V is the generated electrical voltage (adapted from Priya and Inman (2009)

2.1.6 Piezoelectric's Nonlinearity

The piezoelectric materials exhibits a nonlinear characteristic that can be identified in practice and including the most important nonlinearity, which is the hysteresis (Jalili, 2010). In different areas of science the phenomenon hysteresis are found, and the piezoelectric materials are included on it. This phenomenon is found in materials and system that includes alloys with shape memory, viscous-elastic materials, electro-active polymers, magnetic materials, electro/magneto-rheological fluids, and etc. Typical examples of nonlinearities by hysteresis is illustrated in Figs. 2.5, in three different materials., that are the magnetic materials, as in Fig. 2.5a, the piezoelectric materials, illustrated in Fig.

2.5b, and the shape memory alloy materials, as it is shown in Fig. 2.5c. This phenomenon still is a subject of many research and investigations in different fields due to, mainly, its oblique and complex structure (Jalili, 2010).

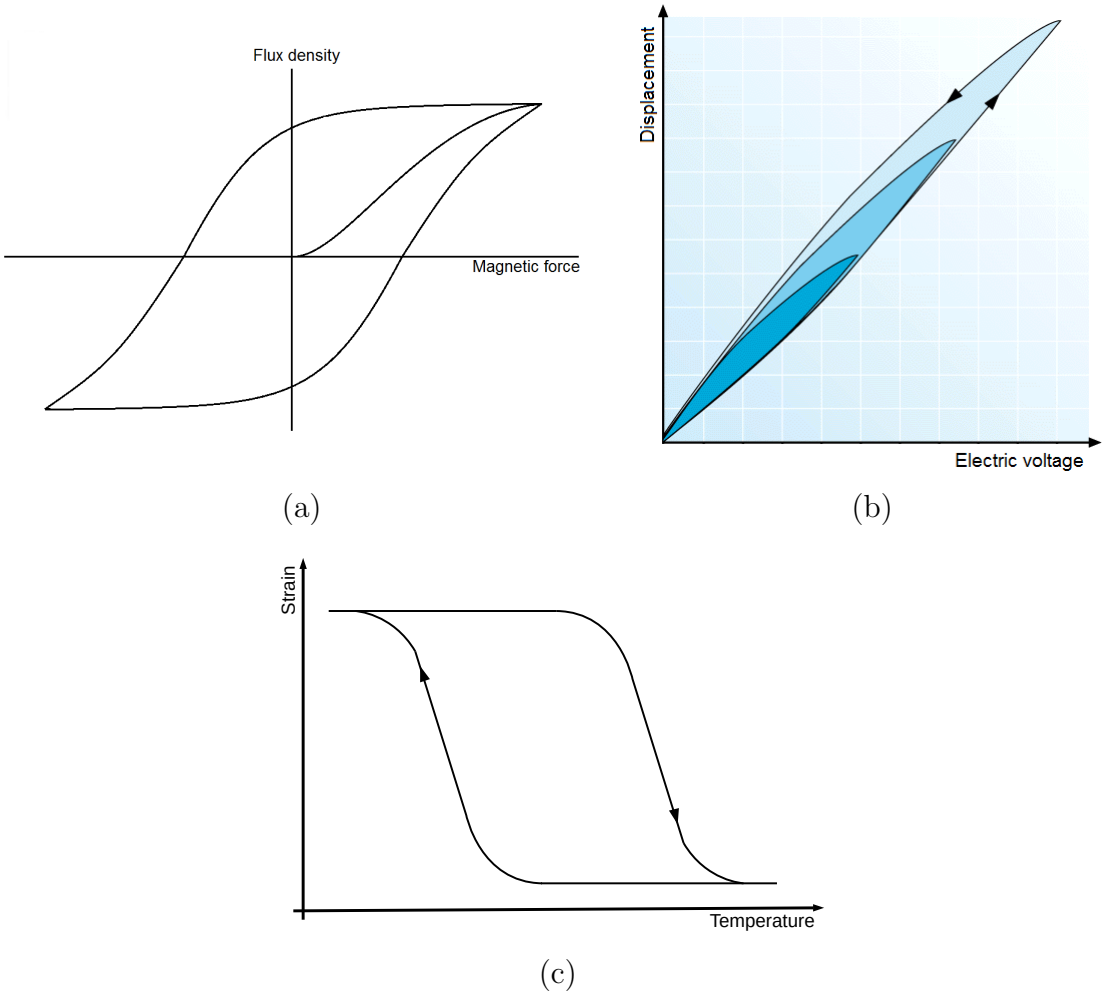

Figure 2.5: Set of figures of nonlinearity by hysteresis, (a) magnetic, (b) piezoelectric, (c) shape-memory alloy

Many works considered the study of hysteresis in piezoelectric materials, as in the work of Von Wagner and Hagedorn (2002), which was identified the effects of the phenomenon by a cantilever beam model with piezoelectric coupling, excited by a high voltage in d_{31} mode.

However, there is a certain nonlinearity in the material, also to the d_{31} mode coefficient, specifically, a nonlinear relation between the applied deformation and the electric field (DuToit and Wardle, 2007; Twiefel et al., 2008). This nonlinearity was experimentally demonstrated by Crawley and Anderson (1990), who exhibited a significantly dependency in the induced deformation of the material, as shown in Fig. 2.5. Based on this curve of Fig. 2.6, it was possible to perform an approximation of the coefficient to an analytical expression that depends on this small deformation of the material, defined by Triplett and

Quinn (2009), given by Eq. (2.2), where x_{df} is the deformation, θ is the linear piezoelectric coefficient, and Θ is the nonlinear piezoelectric coefficient.

$$d(x_{df}) = \theta(1 + \Theta|x_{df}|) \tag{2.2}$$

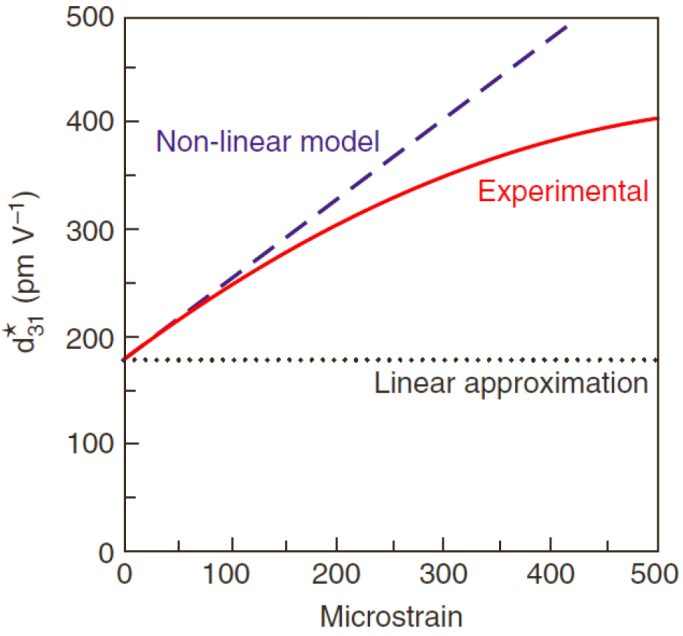

Figure 2.6: Dependence of d_{31} on the induced voltage. The experimental curve as represented by Crawley and Anderson (1990)

Recently, an overview of the nonlinearities of the piezoelectric material was carried out by Daqaq et al. (2014), which shows the actuality of the described theme above. As the nonlinearities became an important feature to the use of the piezoceramics, many authors introduced the nonlinear piezoelectric coupling on their works and showed that the energy harvesting can be more or less efficient. In special it is mentioned the works of Iliuk et al. (2013a,b, 2014); Balthazar et al. (2014a).

2.2 Saturation Phenomenon

Structures such as bridges, cranes or structures supported by support columns (called portal frames), may possess some kind of nonlinearities in its motion, may occur phenomena where almost all the vibration induced in the supported beam, i.e., where there are traffic of cars, trains, or even people, may be transferred to the columns, which are the sustenance of the structure, making possible to damage it. This is a phenomenon called saturation described by many authors, for example, in special Nayfeh et al. (1973); Nayfeh (2000);

Nayfeh and Mook (2008); Nayfeh and Balachandran (2008); Haddow et al. (1984); Mook et al. (1985); Mankala and Quinn (2004); Quinn (2007); Brasil (1990); Felix (2002).

For a system having quadratic nonlineatiries under some conditions an external resonance, which might involve one or more modes, exists in a system that has an 2:1 internal resonance, i.e., $\omega_2 = 2\omega_1$, saturation phenomenon exists when $\Omega \approx \omega_2$. Moreover, when the amplitude of excitation k is small, only the second mode with frequency ω_2 is excited. As k reaches a critical value k_c, which depends on the damping coefficient of the two modes and the detuning factors, the excited mode becomes saturated and the energy "spills over" into the other mode, i.e., the other mode of vibration begins to vibrate. As k increases further, all the additional energy goes into the other mode due to the internal resonance. These results were detailed commented by Nayfeh and Mook (2008).

Specifically, the suggested equations by Nayfeh and Mook (2008), which are Eqs. (2.3) and (2.4), show the quadratic nonlinearity coupling and a possible usage of the 2:1 internal resonance.

$$\ddot{u}_1 + 2\mu_1\dot{u}_1 + \omega_1^2 u_1 = u_1 u_2 \tag{2.3}$$

$$\ddot{u}_2 + 2\mu_2\dot{u}_2 + \omega_2^2 u_2 = u_1^2 + f\cos(\Omega t) \tag{2.4}$$

where μ_1 and μ_2 are damping factors of the system, as the natural frequencies are given by ω_1 and ω_2. The displacements are denoted by u_1 and u_2. In addition, an external harmonic force is applied with amplitude f and exciting frequency Ω, and time t.

The possible internal resonance is one of the conditions to the appearance of the saturation phenomena, i.e., natural frequency (ω_2) of u_2 must be twice the natural frequency (ω_1) of u_1, that is, $\omega_2 = 2\omega_1 + \sigma_1$, where $\sigma_1 << 1$ is a detuning factor. In addition, another condition is the external resonance between u_2 and the external excitation, that is $\omega_2 = \Omega + \sigma_2$, where $\sigma_2 << 1$ is also a detuning factor. In addition, the amplitude of excitation has to be strong enough to the excited mode of vibration becomes saturated, this value will depend on damping's value, which will depend on the parameters of the considered system.

Using the method of multiple scales, which is a method that seek an approximated solution to nonlinear equations, Eqs. (2.5) and (2.6) are the approximated solutions to the Eqs. (2.3) and (2.4), carried out by Nayfeh and Mook (2008).

$$u_1 \approx a_1\cos\left(\frac{1}{2}\Omega t + \sigma_1\right) \tag{2.5}$$

$$u_2 \approx a_2\cos(\Omega t + \sigma_2) \tag{2.6}$$

Substituting Eqs. (2.5) and (2.6) in the quadratic nonlinearities of Eqs. (2.3) and (2.4), the relations (2.7) and (2.8) are obtained, which can be verified, analytically, the energy transfer between the displacements, and the occurrence of saturation phenomenon. It is due to de fact that the internal and external resonance interactions. It is possible to observe in Eq. (2.7) that there is a relation between the natural frequency of the first coordinate (ω_1) with the excitating frequency (Ω), and in the Eq. (2.8), the relation between the natural frequency of the first coordinate (ω_1) to the second coordinate (ω_2).

$$u_1 u_2 \approx a_1 a_2 \cos\left(\frac{1}{2}\Omega t + \sigma_1\right) + ... \qquad where \quad \frac{1}{2}\Omega t = \omega_1 t \tag{2.7}$$

$$u_1^2 \approx a_1^2 \cos(\omega_1 t + \sigma_2) + ... \qquad where \quad 2\omega_1 t = \omega_2 t \tag{2.8}$$

In the last past years, the interest in researches about saturation phenomenon has increased significantly in the control and vibration areas.

One of the first occurrence of the saturation phenomenon was in a problem of a ship motion because of its nonlinear coupling of pitch and roll modes (Nayfeh et al., 1973). Some investigations of a nonlinear control method based on saturation phenomenon in coupled system with quadratic nonlinearities, was treated in more details in Nayfeh and Mook (2008); Mook et al. (1985); Nayfeh (2000); Mankala and Quinn (2004); Quinn (2007). In addition, the implementation of an active saturation control was proposed by Golnaraghi (1991); Oueini et al. (1997); Oueini (1999), which is an active control type that uses the existence of an 2:1 internal resonance between the modes of vibration, i.e., therefore, the existence of a quadratic nonlinearity that uses the saturation phenomenon to suppress vibration at steady state (Felix et al., 2005). The study of the saturation control was performed, in special, in Pai et al. (1998); Pai and Schulz (2000); Balthazar et al. (2003); Shoeybi and Ghorashi (2005); Felix et al. (2005); Warminski et al. (2013); Felix et al. (2014); Tusset et al. (2015).

Moreover, the usage of the nonlinear saturation control method for a nonlinear problem requires an adaptative frequency-tuning mechanism, because the frequency of the nonlinear system changes with the amplitude of motion. Thus, the controller will become out of tune with the system to be controlled (Pratt et al., 1999; Hall et al., 2001; Ashour and Nayfeh, 2002; Balthazar et al., 2003).

A model of a two-degrees-of-freedom simple portal frame was studied by Brasil (1990); Felix (2002), that considered the vertical and horizontal motions of the structure, and could be found the existence of saturation phenomenon in the studied portal frame. Experimentally, the portal frame was studied and also verified the saturation presence in Balthazar et al. (2004). The usage of two-degrees-of-freedom portal frame structures was

also studied by de Paula et al. (2013); Felix et al. (2013).

2.3 Energy Harvesting Systems

In general, many works of vibration-based energy harvesting based on nonlinear piezoelectric materials were performed in the last decade.

A model of an energy harvester based on a simple portal frame structure of single-degree-of-freedom was presented in Iliuk et al. (2013a,b). The system was considered a non-ideal system (NIS), due to full interaction of the structure motion with the energy source, a DC motor with limited power supply. The nonlinearities presented in the piezoelectric material were considered in the piezoelectric coupling mathematical model. In addition, the system was found to be a bi-stable Duffing oscillator presenting chaotic behaviour. The works performed the control of the chaos by a passive control strategy, which are a Nonlinear Energy Sink (NES) and a simple Pendulum.

The NES device is a simple mass-spring-damper device, whose term is named energy pumping that refers to the fast and irreversible energy transfer from a vibrating mechanical system to an energy sink totally dependent on the nonlinear cubic stiffness. This phenomenon corresponds to the controlled canalization of unique direction of vibrational energy to a passive nonlinear structure, where it is located, and decreases along the time because of the damping sink. Advances studies of passive control using a NES device can be found in the works of Jiang et al. (2003); Musienko et al. (2006); Gourdon et al. (2007); Manevitch et al. (2007); Malatkar and Nayfeh (2007); Vakakis (2008); Luongo and Zulli (2012); Tusset et al. (2012); Luongo and Zulli (2013); Zulli and Luongo (2015).

The simple linear Pendulum is another passive control strategy that is also able to drastically modify the global dynamic of a system. It can be used in certain necessary conditions in order to obtain practical benefits of this process, such as to modify a chaotic system to a periodic orbit. The mechanism was studied in many works, among others, in Xu et al. (2005); Kecik (2013); Arbex et al. (2015); Rocha et al. (2015).

The obtained results with the passive controllers was the improvement of the energy harvesting, because the system was forced into a periodic orbit.

However, there are some works that studied energy harvesting considering the saturation phenomenon in a two-degrees-of-freedom structure. In the works of Rocha et al. (2014); Rocha (2014); Rocha et al. (2015); Balthazar et al. (2014b,a); Iliuk et al. (2014), among others, was considered a portal frame foundation of two-degrees-of-freedom structure with a nonlinear piezoelectric coupling. The structure possesses a 2:1 internal resonance between its two modes of vibration, and it is externally base-excited by an harmonic force.

These works showed the amount of harvested power, using the linear and nonlinear

piezoelectric coupling, due to saturation phenomenon. With the nonlinear contribution, there were diverse contributions, since periodic behaviours until quasiperiodic orbits, making possible to harvest low and high amount of power.

2.4 Electro-Dynamical Shaker

Looking for a future experiment, some kind of electromechanical systems are capable to perform an external excitation in a main system. One of them, very important and studied by many authors is the electro-dynamical shaker, illustrated in Fig. 2.7. The excitation performed by the shaker has been used by several authors as, in special, in Xu et al. (2005, 2007); Lenci et al. (2008); Lee et al. (2008); de Paula et al. (2013); Lenci and Rega (2011); Lenci et al. (2012); Wang and Jing (2004); Yokoi and Hikihara (2011); Litak et al. (2010); Alevras et al. (2014); Avanço et al. (2015).

The device is used taking into a dependent variable the electric current, and the electromotive force as $F_{em} = KI_0$, where $K = 2\pi r_{coil} N B_0$, and the equation of motion of the electrical part is given in Eq. (2.9).

$$L_0 \dot{I}_0 + R_0 I_0 + E_{backfem} = E_0 \tag{2.9}$$

where the input voltage of the vibrator is of the form $E_0 = e_0 \cos \omega_n t$, the inductance of the coil is defined by L_0, the resistance is given by R_0, the back electromotive force is $E_{backfem}$, the radius of the coil is denoted by r_{coil}, the number of the coil windings is defined by N, and the produced magnetic field is B_0.

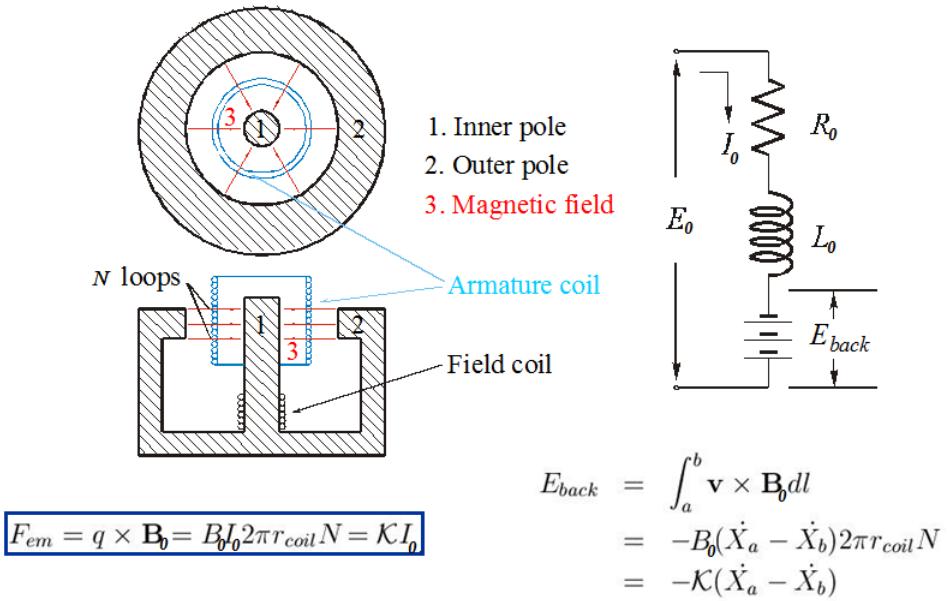

Figure 2.7: Electro-dynamical shaker's mechanical and electrical representation

With all the basic concepts discussed, this work was divided into two parts to the analysis of different excitations. In PART I will be considered a harmonic force as a base-exciter. In PART II will be considered the electro-dynamical shaker as the external base-exciter. In the end, these two parts will be compared defining some differences, advantages and disadvantages of using each other.

Therefore, in the following, the PART I of the work is presented.

PART I

Global Analysis of the System with Harmonic Base Excitation

Chapter 3

Portal Frame Foundation under Harmonic base excitation Mathematical Model

It is known that in the current literature, the development of energy conversion techniques using piezoelectric materials in structure of a single-degree-of-freedom, as metallics cantilever beam, has deserved a special attention of many researchers, in particular, traditionally it has been used a free clamped cantilever beam model coupled to a piezoelectric material to harvest energy from the vibration.

Particularly, in this work will be studied the energy harvesting in a two-degrees-of-freedom structure (a simple portal frame) from the column vibration, considering the energy transfer and saturation phenomena.

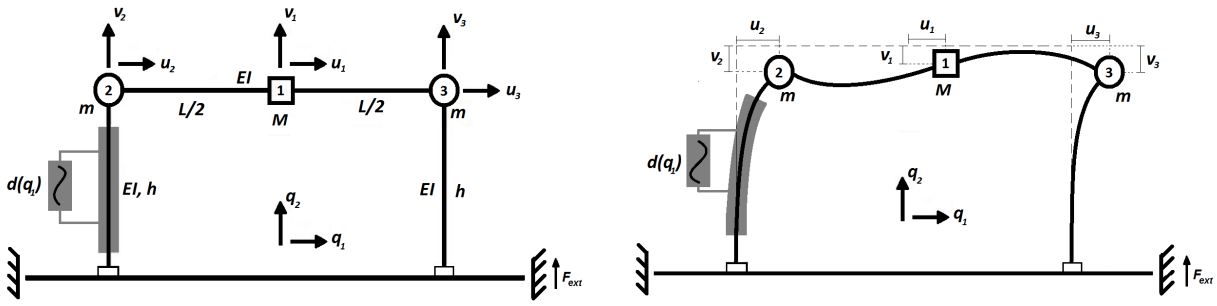

(a) (b)

Figure 3.1: Schematic model of a simple portal frame with a piezoelectric material coupled to one of its column, (a) non-deformed, (b) deformed

The continuous system discretized in two-degrees-of-freedom with concentrated parameters, illustrated in Figs. 3.1, was based on the works of Brasil (1990); Felix (2002); Balthazar et al. (2014b, 2003), whose Fig. 3.1a represents the non-deformed schematic model of the simple portal frame, and Fig. 3.1b represents the deformed schematic model.

This system is constituted by:

- two columns clamped in their bases with length h,
- horizontal beam pinned to the columns at both ends with length L,
- both columns and beam have flexural stiffness EI, where E is the Young's modulus and I is the are momentum of inertia of beam and columns,
- the mass at mid-span of the beam is M,
- the masses of each columns is represented by m,
- piezoelectric coupling given by $d(q_1)$,
- base-excitation by an harmonic force of cosine kind represented by F_{ext}

The main structure is modelled as a lumped mass system with two-degrees-of-freedom. The coordinate q_1 is related to the horizontal displacement (sway mode), with natural frequency ω_1, and the coordinate q_2 is related to the vertical displacement (symmetric mode) with natural frequency ω_2. The generalized coordinates q_i are the displacement of the mass at the mid-span of the beam M, that are given by the nodal displacements of Eq. (3.1).

$$q_1 = u_1 \qquad\qquad q_2 = v_1 \tag{3.1}$$

where u_1 is the horizontal displacement of the mid-span of the beam, and v_1 is the vertical displacement. Considering the two first vibration modes of the portal frame, the ways of the vibration of the columns and beam can be approximated by mathematical functions, nominated shape functions purposed by (Brasil, 1990; Felix, 2002). An approximation to the shape functions of the columns and beam are given by the Eqs. (3.2) and (3.3).

$$u = \frac{3}{h^3}\left(\frac{hx^2}{2} - \frac{x^3}{6}\right), \qquad 0 \leq x \leq h \tag{3.2}$$

$$v = \frac{12}{L^3}\left(\frac{x^3}{3} - \frac{L^2 x}{4}\right), \qquad 0 \leq x \leq \frac{L}{2} \tag{3.3}$$

where u and v describes, respectively, the static deformations that a cantilever beam clamps in a boundary with concentrated mass on its free boundary, and a simple supported beam with concentrated mass on its central point, with x being the coordinate of the support axis.

The linear stiffness of the columns and the beam can be evaluated by a Rayleigh-Ritz procedure using cubic trial functions, obtaining the relations of Eq. (3.4).

$$k_c = \frac{3EI}{h^3} \qquad\qquad k_b = \frac{48EI}{L^3} \tag{3.4}$$

Geometric nonlinearity is introduced by considering the shortening due to bending of the columns and of the beam, neglecting terms of order superior to two, given by Eqs. (3.5).

$$\begin{aligned} u_2 &= u_1 + \frac{B}{4}v_1^2 & u_3 &= u_1 - \frac{B}{4}v_1^2 \\ v_2 &= -\frac{A}{2}u_1^2 & v_3 &= -\frac{A}{2}u_1^2 \end{aligned} \tag{3.5}$$

where $A = 6/5h$ and $B = 24/5L$.

The nonlinear piezoelectric material is coupled to the column as an electric RC circuit, which is excited by an internal voltage (back-emf) proportional to the mechanical velocity, in order to harvest energy from the vibration of the column. This circuit consists of a resistor R_p, a produced charge Q_p, and a capacitance C_p of the capacitor. The nonlinear contribution of the material to the energy harvesting, i.e., the piezoelectric coupling coefficient in dimensionless form is given by $d(q_1)$, that is, given by the relation of Eq. (2.2), where θ is the dimensionless linear piezoelectric coefficient and Θ is the dimensionless nonlinear piezoelectric coefficient. Given that the columns suffer such deformations in both coordinates, it is observed that there is contribution in both vibration modes, vertical and horizontal. Hence, the piezoceramic produce an electric voltage denoted by Eq. (3.6).

$$V_{piezo} = -\frac{d(q_1)}{C_p}(u_2 + v_2) + \frac{Q_p}{C_p} \tag{3.6}$$

In the following section 3.1, the mathematical modelling of the system neglecting the use of the electro-dynamical shaker was considered. The performance of the equations of motion was used the energy method of the Langrage's function and the equations of Euler-Lagrange.

3.1 Mathematical Modelling of the Dynamical System with Harmonic Excitation

The mathematical modelling of the purposed system in this part of this work, it will be used the Lagrange's function given by Eq. (3.7), and the equations of Euler-Lagrange denoted by Eq. (3.8).

$$L = T - V \tag{3.7}$$

$$\frac{d}{dt}\left(\frac{\partial L}{\partial \dot{q}_i}\right) - \left(\frac{\partial L}{\partial q_i}\right) + \left(\frac{\partial D}{\partial \dot{q}_i}\right) = F_{ext} \tag{3.8}$$

where the subscript i represents the number of degrees-of-freedom, the Rayleigh dissipation function D and the function of the external force denoted by F_{ext}.

The kinetic energy of the system is given by the movement of the masses of the beam M and columns m, defined by Eq. (3.9).

$$T = \frac{1}{2}M(\dot{u}_1^2 + \dot{v}_1^2) + \frac{1}{2}m(\dot{u}_2^2 + \dot{u}_3^2 + \dot{v}_2^2 + \dot{v}_3^2) \tag{3.9}$$

Substituting the nodal displacements of Eq. (3.1) and (3.5) in (3.9), the kinetic energy is given in relation to the generalized coordinates q_1 and q_2, obtaining the Eq. (3.10).

$$T = \frac{1}{2}M(\dot{q}_1^2 + \dot{q}_2^2) + \frac{1}{2}m(2\dot{q}_1^2) \tag{3.10}$$

The total potential energy of the system is given by the stiffness of the columns and beam, the gravitational potential energy of the column masses and beam mass, the piezoelectric's electrical potential energy, in which is denoted by Eq. (3.11).

$$\begin{aligned} V = \frac{1}{2}k_c(u_2^2 + u_3^2) + \frac{1}{2}k_b\left(v_1 - \frac{v_2 + v_3}{2}\right)^2 + mg(v_2 + v_3) + Mgv_1 ... \\ - \frac{d(q_1)}{C_p}Q_p(u_2 + v_2) + \frac{1}{2}\frac{Q_p^2}{C_p} \end{aligned} \tag{3.11}$$

Substituting Eq. (3.1) and (3.5) in (3.11), it is obtained the total potential energy in relation of the generalized coordinates q_1, q_2 and Q_p in Eq. (3.12).

$$V = (k_c - mgA)q_1^2 + \frac{1}{2}k_b(q_2^2 + Aq_2q_1^2) + Mgq_2 - \frac{d(q_1)}{C_p}Q\left(q_1 + \frac{B}{4}q_2^2\right) + \frac{1}{2}\frac{Q_p^2}{C_p} \tag{3.12}$$

The Rayleigh dissipation energy function is obtained by the method of Rayleigh-Ritz, whose terms to be considered are duo to the damping of the columns c_1 and beam c_2. In addition, there is a contribution of the piezoelectric material with the electric resistance R_p. Hence, the dissipation function is given by Eq. (3.13).

$$D = \frac{1}{2}c_1\dot{q}_1^2 + \frac{1}{2}c_2\dot{q}_2^2 + \frac{1}{2}R_p\dot{Q}_p^2 \tag{3.13}$$

Lastly, the external force is applied directly on the base, in the vertical direction, given by a displacement of harmonic characteristic denoted by Eq. (3.14).

$$F_{ext} = F_0 \cos \omega_n t \tag{3.14}$$

As energy functions are defined, the Lagrange function and Euler-Lagrange equations are used to obtain the governing equations of motion of the system, illustrated in Fig. 3.1,

presented by Eqs. (3.15), (3.16) and (3.17).

$$(2m+M)\ddot{q}_1 + 2(k_c - mgA)q_1 + k_bAq_1q_2 + c_1\dot{q}_1 = \frac{d(q_1)}{C_p}Q_p \tag{3.15}$$

$$M\ddot{q}_2 + k_bq_2 + c_2\dot{q}_2 + Mg + \frac{Ak_b}{2}q_1^2 = F_0 cos\omega_n t + \frac{d(q_1)}{C_p}\frac{B}{2}Q_pq_2 \tag{3.16}$$

$$R_p\dot{Q}_p - \frac{d(q_1)}{C_p}\left(q_1 + \frac{B}{4}q_2^2\right) + \frac{Q_p}{C_p} = 0 \tag{3.17}$$

In the following, a dimensionless process was carried out.

3.2 Dimensionless Process of the Governing Equations of Motion

In order to carry out a dimensionless process of the governing equations of motion of the dynamical system, making possible to generalize the obtained results, dimensionless variables are chosen, such as in Eq. (3.18).

$$\begin{aligned} &x_1 = \frac{q_1}{h} \qquad x_2 = \frac{q_2}{L} \qquad V_p = \frac{Q_p}{Q_0} \\ &\tau = \omega_1 t \qquad \omega_1 = \sqrt{\frac{2(k_c - mgA)}{(2m+M)}} \qquad \hat{d}(x_1) = \frac{h}{Q_0}d(q_1) \end{aligned} \tag{3.18}$$

Substituting the dimensionless variables of Eq. (3.18) in the equations of motion (3.15), (3.16) and (3.17), it is obtained the dimensionless governing equations of motion given by the Eqs. (3.19), (3.20) and (3.21).

$$x_1'' + \mu_1 x_1' + x_1 + \alpha_1 x_1 x_2 = \theta(1 + \Theta|x_1|)\delta_1 V_p \tag{3.19}$$

$$x_2'' + \mu_2 x_2' + \omega_2^2 x_2 + \alpha_2 x_1^2 + G_0 = E_0 cos\Omega\tau + \theta(1 + \Theta|x_1|)\delta_2 V_p x_2 \tag{3.20}$$

$$V_p' - \theta(1 + \Theta|x_1|)(\delta_3 x_1 + \delta_4 x_2^2) + \delta_3 V_p = 0 \tag{3.21}$$

where the dimensionless parameters are given in Eq. (3.22).

$$\begin{aligned}
&\mu_1 = \frac{c_1}{(2m+M)\omega_1}, \quad \mu_2 = \frac{c_2}{M\omega_1}, \quad \omega_2 = \frac{1}{\omega_1}\sqrt{\frac{k_b}{M}}, \quad \alpha_1 = \frac{Ak_bL}{(2m+M)\omega_1^2} \\
&\alpha_2 = \frac{Ak_bh^2}{2M\omega_1^2L}, \quad G_0 = \frac{g}{\omega_1^2L}, \quad \delta_1 = \frac{Q_0^2}{\omega_1^2h^2(2m+M)C_p}, \quad \delta_2 = \frac{BQ_0^2}{2M\omega_1^2hC_p} \\
&\delta_3 = \frac{1}{R_pC_p\omega_1}, \quad \delta_4 = \frac{BL^2}{4R_pC_p\omega_1h}, \quad E_0 = \frac{F_0}{M\omega_1^2L}, \quad \Omega = \frac{\omega_n}{\omega_1}
\end{aligned} \tag{3.22}$$

The harvested power by the piezoelectric material can be mathematically defined by Eq. (3.23), whose relation is the dimensional power. Substituting the dimensionless variables, the dimensionless harvested power becomes to the Eq. (3.24). Moreover, the average harvested power can be calculated by Eq. (3.25).

$$P_{dimensional} = R_p\dot{Q}_p^2 \tag{3.23}$$

$$P_{dimensionless} = R_{p_0}V_p'^2 \tag{3.24}$$

$$P_{avg} = \frac{1}{T_p}\int_0^{T_p} P(\tau)d\tau \tag{3.25}$$

where $R_{p_0} = R_p\omega_1^2Q_0^2$, and T_p is the length of the vector power. It is highlighted that only the dimensionless power will be analyzed.

In the next chapter will be performed numerical simulations of the dimensionless system with several analysis of the behaviour of the system and energy harvesting.

Chapter 4

Numerical Simulations of the System Harmonically Base-Excited and Discussions

In this first chapter of numerical simulations, will be exposed the results obtained of the system harmonically base-excited considering its mathematical modelling described in Chapter 3.

The parameters which are used to the numerical simulations are in Tab. 4.1, whose portal frame parameters' values were took out and adjusted from Felix (2002), because they were adjusted to obtain 2:1 internal resonance with the objective of saturation phenomenon occurs. The values of the electric part of the piezoelectric material were adjusted to an operating range of stability of the system, in which, physically, they are correctly represented.

In general, all the parameters of Tab. 4.1 are considered as default to the next simulations. However, some of them will be varied in order to analyse its influence on the dynamic and energy harvesting of the system. Hence, these parameters are to a first analysis. Along the work, the piezoelectric coefficients, the amplitude of excitation and frequency will be highly varied.

It is important to note that the system presents 2:1 internal resonance, i.e., $\omega_2 = 2\omega_1$, that is, $\omega_2 = 147.8 rad/s$ and $\omega_1 = 74 rad/s$, also external resonance, $\omega_2 \approx \omega_n$. With that, the system may present saturation phenomenon, in which will be presented analytically and numerically.

In addition, one of the parameters which has a foremost importance to the energy harvesting is the amplitude of the external excitation F_0 (E_0), because higher the amplitude higher will be the energy harvesting, it will be shown in Section 4.4. However, it will depend on the value of the other parameters. Because of that, every analysis will include

a parametrical analysis of the amplitude in function of the parameter to be analyzed, with the interval of $1 \leq F_0 \leq 700[N]$ ($0 \leq E_0 \leq 0.1229$).

Moreover, an initial condition $x_{01} = 0.001$ will be considered. All the other are considered as 0 (zero).

Table 4.1: Parameters of the Portal Frame Harmonically Base-Excited

Parameters	Values	Means
$g[m/s^2]$	9.81	Gravity acceleration
$M[kg]$	2.00	Beam mass
$m[kg]$	0.50	Column mass
$c_1[Ns/m]$	1.55	Column damping
$c_2[Ns/m]$	3.14	Beam damping
$EI[nm^2]$	128	Linear flexural stiffness
$L[m]$	0.52	Beam length
$h[m]$	0.36	Column length
$F_0[N]$	40	Amplitude of the external force
$\omega_n[rad/s]$	148	Frequency of the external force
$R_p[k\Omega]$	100	Electric resistance of the piezoelectric
$C_p[\mu F]$	1	Capacitance of the piezoelectric
θ	0.3	Linear piezoelectric coefficient
Θ	0	Nonlinear piezoelectric coefficient

4.1 Energy Transfer and Saturation Phenomenon

The energy transfer and saturation phenomenon are an important question in this work, because without them, it would not be possible to carry out the energy harvesting from the vibration of the structure's column.

As in Chap. 2 and according to Nayfeh and Mook (2008), there is some interactions between the modes of vibration when there is the 2:1 internal resonance and external resonance that are the energy transfer and saturation phenomenon. Thus, in this section will be presented numerical results that show the energy transfer and saturation. For that, it is necessary some considerations.

The total vibrating energy (energy index) of horizontal motion, vertical motion and the electrical part of the piezoelectric material is given, respectively, by Eqs. (4.1), (4.2) and (4.3).

$$E_{x_1} = \frac{1}{2}x_1^2 + \frac{1}{2}x_1'^2 \tag{4.1}$$

$$E_{x_2} = \frac{1}{2}x_2^2 + \frac{1}{2}x_2'^2 \tag{4.2}$$

$$E_{V_p} = V_p x_1 \tag{4.3}$$

where the total energy is given by the electro-mechanical system, i.e., the energy of the horizontal motion, vertical motion and piezoelectric, which is denoted by $E_{total} = E_{x_1} + E_{x_2} + E_{V_p}$.

To analyse the energy transfer between the two coordinates of the structure and the energy harvesting by the piezoelectric material, percentage algebraic relations of energy are considered and defined by the given relations in Eq. (4.4), (4.5) and (4.6).

$$E_{\%x_1} = \frac{E_{x_1}}{E_{total}} \tag{4.4}$$

$$E_{\%x_2} = \frac{E_{x_2}}{E_{total}} \tag{4.5}$$

$$E_{\%V_p} = \frac{E_{V_p}}{E_{total}} \tag{4.6}$$

Using the parameters of Tab. 4.1, the results of the percentage of the energy transfer are shown in three stages: neglecting the use of the piezoelectric material and external resonance, disregarding just the material, and then considering the resonance and the piezoceramic. Figures 4.1a, 4.1b and 4.1c show the analysis of the energy transfer between the three coordinates.

Firstly, the system is adopted out of external resonance, and assuming that $\omega_n = 100 rad/s$, i.e., frequency of external excitation out of resonance. Figure 4.1a presents the time history of the percentage of energy index assuming $\omega_n = 100 rad/s$, and it is observed that there is not energy transfer between the horizontal and vertical coordinates, consequently, there is no saturation phenomenon.

In the following, assuming that there is resonance between the vertical coordinate and the external force, with $\omega_n = 148 rad/s$, and still neglecting the presence of the piezoelectric coupling, Fig. 4.1b presents the time history of the percentage of energy index considering this condition. It is possible to observe that there is almost the total energy transfer between the horizontal and vertical coordinates, and in the steady state, it is possible to observe saturation phenomenon. Unlike in Fig. 4.1a, which the vertical motion keeps almost 100% while the horizontal tends to zero, the energy of the horizontal coordinate goes from zero, initially, to almost 100% of vibrating energy, while the energy in vertical motion, which presented 100% of energy due to the external excitation, decays to almost zero.

In Figs. 4.1a and 4.1b, there was not a curve that represents the harvested electric energy of the piezoelectric material because its contribution was disregarded. However, Fig. 4.1c shows the time history of the energy index in the resonance with the addition of the piezoelectric coupling. In this case, the variation of the energy between the vertical

and horizontal coordinates becomes a little smaller, while there is energy variation of the piezoelectric material due to the fact of the energy harvesting, that is, the piezoceramic is actuating on harvesting some energy from the vibration.

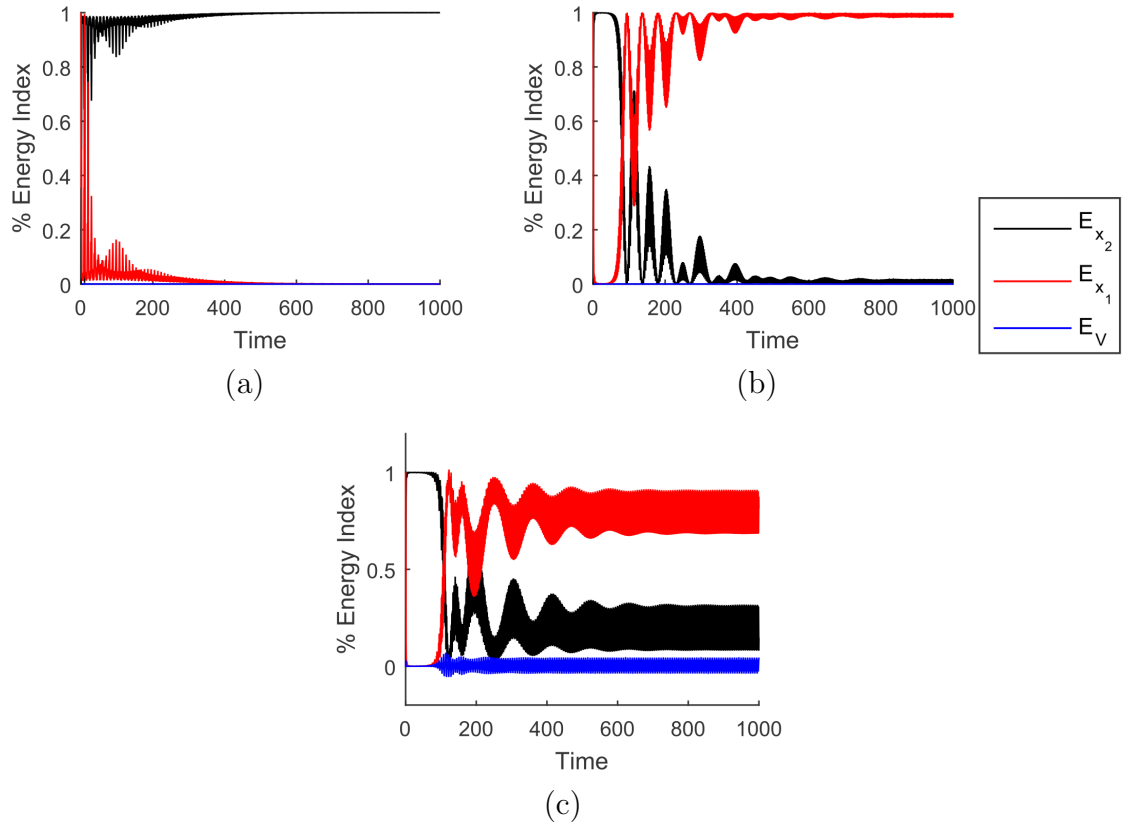

Figure 4.1: Energy percentage of the motion in horizontal direction (in red), vertical (in black), and the electric energy of the piezoelectric (in blue), (a) $\omega_n = 100 rad/s$ **and** $\theta = 0$**, (b)** $\omega_n = 148 rad/s$ **and** $\theta = 0$**, (c)** $\omega_n = 148 rad/s$ **and** $\theta = 0.3$

Other way to observe the energy transfer and saturation phenomenon is through time histories of the displacement. Figures 4.2a, 4.2b, and 4.2c are directly related with Figs. 4.1.

Figure 4.2a shows the time history of the vertical and horizontal motions out of resonance and without the piezoelectric coupling. It is possible to observe that there was no saturation phenomenon because the amplitude of the horizontal displacement tends to zero, while the vertical keeps in constant motion.

However, in Fig. 4.2b. which shows the time history just in resonance, the amplitude of the horizontal displacement becomes much higher than the vertical one. The amplitude of vertical motion becomes higher enough becoming saturated and "spills over" into the horizontal motion decreasing its amplitude and increasing the horizontal amplitude, i.e., transferred part of vibrational energy from the vertical direction to the horizontal direction.

With the coupling of the piezoelectric material, Fig. 4.2c shows a little decrease of the horizontal displacement amplitude. Even with saturation phenomenon occuring, it is due to the fact of transferring vibration energy to the piezoelectric. With the energy transfer, it is observed, in Fig. 4.2d, the harvested power through the piezoelectric material, that is, in average, 31.37 amount of power, approximately.

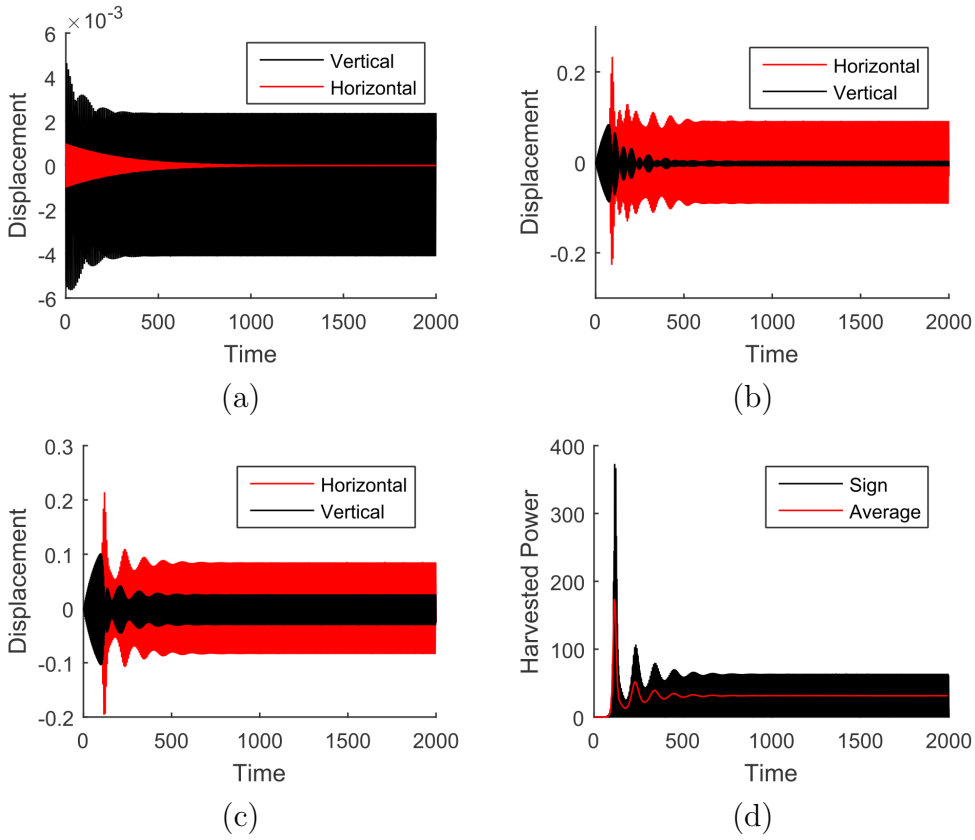

Figure 4.2: Time histories of the displacements of horizontal (in gray) and vertical (in black) motions. (a) $\omega_n = 100 rad/s$ and $\theta = 0$, (b) $\omega_n = 148 rad/s$ and $\theta = 0$, (c) $\omega_n = 148 rad/s$ and $\theta = 0.3$; (d) time history of the harvested power with $\omega_n = 148 rad/s$ and $\theta = 0.3$

In addition, it is observed, in external resonance and considering the piezoelectric coupling, that is $\omega_n = 148 rad/s$ and $\theta = 0.3$, the system presents stable and periodic behaviour, whose behaviour is essential to the maintain of energy harvesting, as showed in Figs. 4.3a and Figs. 4.3b.

Figures 4.3a and Figs. 4.3b show the phase plane (in black) with the Poincaré maps (gray dots). The system is periodic in both coordinates with periodicity 2 in the horizontal motion and periodicity 1 in the vertical motion.

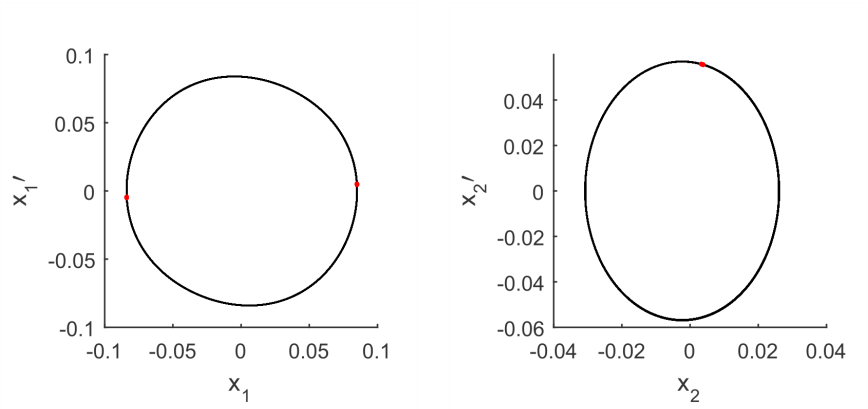

(a) (b)

Figure 4.3: Phase plane (in black) and Poincaré map (gray dot) with $\omega_n = 148 rad/s$ and $\theta = 0.3$, (a) Horizontal, (b) Vertical

Therefore, it is possible to numerically show the existence of the 2:1 internal resonance through the Fast-Fourier Transform (FFT) illustrated by Fig. 4.4. There are two frequencies actuating in the system, that are $\omega_2 = 2\omega_1 = \omega_n$. The amplitude of ω_1 is much higher than in ω_2, as predict in Figs. 4.2 and 4.3. Hence, numerically, the existence of the 2:1 internal resonance is verified.

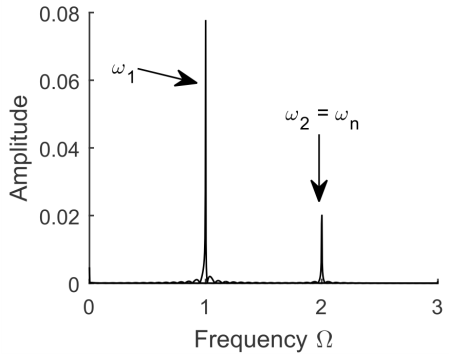

Figure 4.4: FFT with $\omega_n = 148 rad/s$ and $\theta = 0.3$

Considering that the external excitation frequency is a factor of utmost importance to the performance of the saturation phenomenon, the following section will discuss the analysis of the frequency variation related to the behaviour of the system and energy harvesting.

4.2 Influence of the External Frequency ω_n

From the governing equations of motion, is possible to observe several parameters that are a great influence to the behaviour of the system. In addition, it is possible to observe a limited number of these parameters to be studied. Therefore, the study of the influence of these parameters in the system is one of the greatest characteristic involved in this work.

The frequency of external excitation is one of the most important parameters, because with it is possible to obtain the phenomenon to be studied in this work. With the involvement of the internal and external resonances, there is the saturation phenomenon. Nevertheless, this parameter has a certain operating range which also can decrease and increase the energy harvesting.

Firstly, the frequency of excitation is varied in an interval between $140 \leq \omega_n \leq 155[rad/s]$, related to the harvested power of the system. In the following, bifurcation diagrams are constructed in order to analyze the behaviour of the system in the same interval of frequency. Hence, the obtained results are shown in the following graphics.

Figure 4.5 shows the parametrical analysis of the dimensional excitation frequency, in Fig. 4.5a, and dimensionless excitation frequency, in Fig. 4.5b. The frequency near $\omega_n \approx \omega_2$, i.e., $\Omega = \omega_2$, is where the energy harvesting has its high performance due to the saturation phenomenon. In addition, it is possible to observe that there is a small interval of frequency which the saturation phenomenon occurs, in which to the dimensional analysis is $144 \leq \omega_n \leq 151.2[rad/s]$, and to a dimensionless analysis is $1.948 \leq \Omega \leq 2.042$. The harvested amount of power in this interval is, in average, of $26.56 \leq P_{avg} \leq 38.97$.

Figures 4.6 show the bifurcation diagrams of the frequency Ω related to the horizontal and vertical displacements, illustrated in Fig. 4.6a and 4.6b, respectively. In the same dimensionless interval of frequency in Fig. 4.5, that is $1.948 \leq \Omega \leq 2.042$, the system presents stable and period-2 in both coordinates.

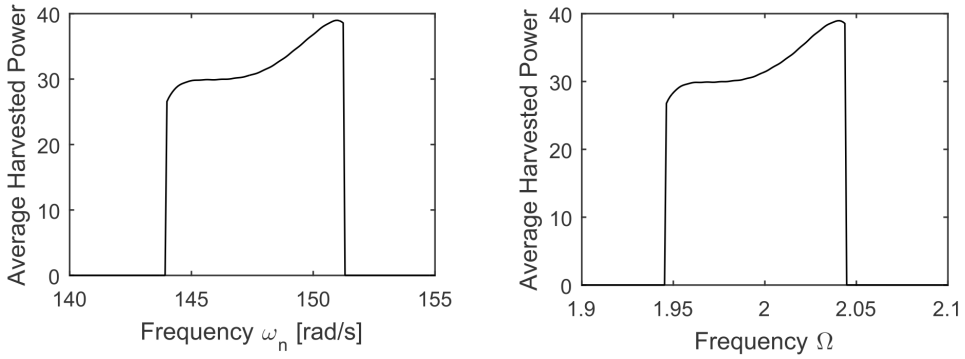

Figure 4.5: Parametrical analysis of the frequency related to the average power to (a) ω_n (dimensional), (b) Ω (dimensionless)

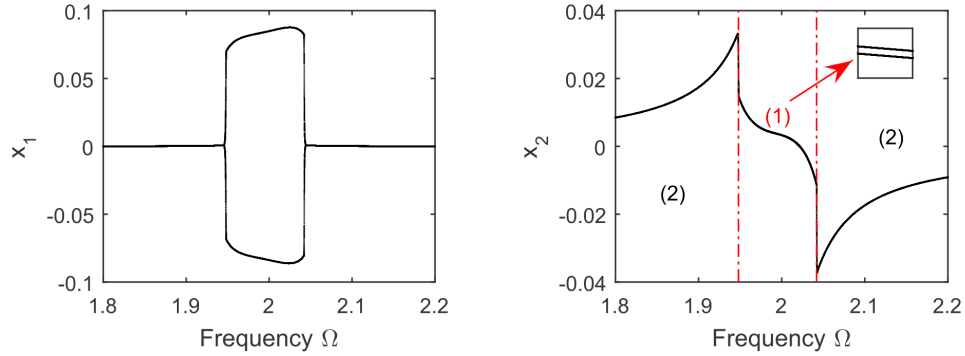

Figure 4.6: Bifurcation diagram of the dimensionless frequency Ω related to the (a) horizontal, (b) vertical coordinates

A deep analysis of instability of the system can be observed in Fig. 4.7. It shows a surface and contour of the surface in Fig. 4.7a and 4.7b, respectively, of the analysis of the external frequency related to the increase of the external amplitude and the maximum displacement induced in the structure. The peaks in the surface show when the displacement tends to be infinite, i.e., the structure can be damaged because of the high level of the amplitude of the displacement induced on it, that is the stability of the system, most of time called by safe behaviour of the system. The fulfilled areas in the contour means the higher amplitudes of the surface, i.e., the system is unstable in these areas, i.e., the unsafe behaviour of the system.

In the case of the frequency, the contour was separated in 3 (three) regions to be studied in Tab. 4.2.

In region 3, the system is out of resonance, consequently out of saturation. Higher the external amplitude, no effect is given to the columns. Hence, the column displacement is

almost zero.

When the system is approximating to resonance with the symmetric mode, saturation phenomenon begins to occur, and the column displacements increases, that is, part of the symmetric vibratory energy is transferred to the sway mode that is what region 1 shows in Fig. 4.7b. The column displacements are not zero anymore, growing significantly to keep the system stable. It is the best area to harvest energy, as showed in Figs. 4.5.

However, there is a limit which the amplitude of the external excitation has stable behaviour, that is approximately $F_0 = 121.2[N]$. It is shown by region 2 that the column displacements is higher than 5 (five) in several locations. Therefore, it is possible to see that, with saturation, the system presents a significantly sensibility in some parameters, in special, one of them, the frequency of the external excitation, because of the conditions of saturation occurs.

Table 4.2: Studied regions of Fig. 4.7b

Regions	Color	Frequency $\omega_n[rad/s]$	Amplitude F_0 [N]
1	Blue	$130 \leq \omega_n \leq 163$	$1 \leq F_0 \leq 121.2$
2	Red	$130 \leq \omega_n \leq 163$	$121.2 \leq F_0 \leq 500$
3	Black	$\omega_n < 130$ and $\omega_n > 163$	$1 \leq F_0 \leq 500$

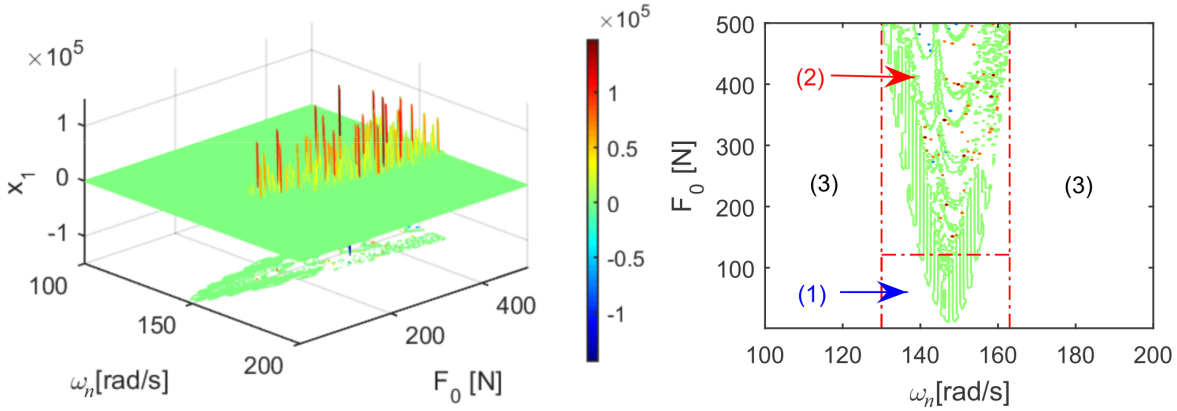

(a) (b)

Figure 4.7: (a) Surface (b) Contour; of the excitation frequency ω_n related to the excitation amplitude $F_0[N]$ and the maximum displacement of the structure

The frequency of the external force showed to be very important because it has some values of condition to saturation phenomenon occurs. It has a great influence in the stability and energy harvesting of the system, mainly in the region where saturation occurs, that is in Region 1, summarized in Tab. 4.3. The following section will be shown the analysis of the piezoelectric material and the influence of the nonlinear piezoelectric coefficient the the energy harvesting and the behaviour of the system.

Table 4.3: Summary of Sec. 4.2

Frequency	Behaviour		Average Power
	Horizontal	Vertical	
$144rad/s \leq \omega_n \leq 151.2rad/s$ (Dimensional)	Periódic - 2	Periódic - 2	$26.56 \leq P_{avg} \leq 38.97$
$1.948 \leq \Omega \leq 2.042$ (Dimensionless)			

4.3 Influence of the Piezoelectric Material

One of the main purposes of this work is the energy harvesting from the environment's vibration using a piezoelectric material as a means of energy transduction. However, as cited previously, the material possesses a certain nonlinearity through the hysteresis, and here, its influence will be analyzed considering linear and nonlinear cases. Thus, this section is divided in two subsections, firstly analyzing the case of the sole linear piezoelectric coupling, and then considering both linear and nonlinear coupling.

4.3.1 Case of the sole linear piezoelectric coupling $\Theta = 0$

The first analysis of the piezoelectric material is with the case of the sole linear coefficient in order to compare with the nonlinear case, showing the influence of the nonlinear coefficient.

Therefore, firstly, considering the parameters of Tab. 4.1, a parametrical analysis of the linear piezoelectric coefficient θ related to the average harvested power is carried out, where the results are shown in Fig. 4.8.

Figure 4.8 shows the analysis of the linear piezoelectric coefficient θ, in the interval $0 \leq \theta \leq 0.5$, related to the average harvested power separated in two regions. In region 1, the energy harvesting is efficient until the linear coefficient of maximum power $P_{max} = 50.81$, that is $0 \leq \theta \leq 0.423$. However, in region 2 with interval $0.423 < \theta \leq 0.456$, the energy harvesting tends to zero fastly.

Figures 4.9 shows the bifurcation diagram of the analysis of the linear coefficient related to the horizontal and vertical movements. The behaviour of the system when the energy harvesting is increasing is periodic, with periodicity 2 to both coordinates. However, after the linear coefficient of maximum power $0.423 < \theta \leq 0.456$, the energy harvesting tends to zero because the system tends to be unstable as the bifurcations shown. Therefore, there are two ranges of coefficient values to be considered, that is in Tab. 4.4.

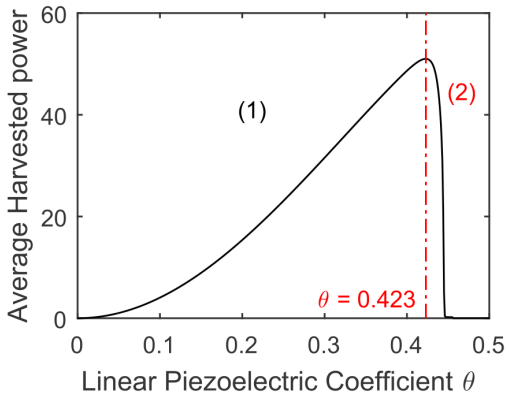

Figure 4.8: Parametrical variation of the linear piezoelectric coefficient θ related to the average harvested power

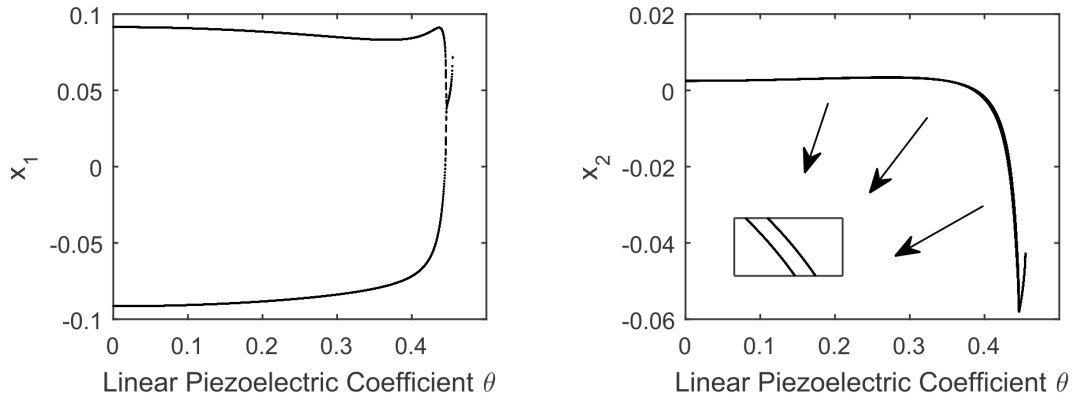

Figure 4.9: Bifurcation diagram of the linear piezoelectric coefficient θ related to the (a) horizontal, (b) vertical coordinates

Table 4.4: Numerical results to the linear piezoelectric coupling

Linear Piezoelectric Coefficient θ	General Behaviour	Average Power	Conclusion
$0 \leq \theta \leq 0.423$	Periodic-2 (Stable)	$0 \leq P_{avg} \leq 50.81$	Gain of Energy
$0.423 < \theta \leq 0.456$	- (Unstable)	P_{avg} tends to zero	Loss of Energy

In the next subsection, the same analysis of energy harvesting and behaviour of the system will be carried out, however, considering the NONLINEAR piezoelectric coefficient.

4.3.2 Case of the nonlinear piezoelectric coupling $\Theta \neq 0$

It is known that the piezoelectric material is defined by Eq. (2.2), where the piezoelectric coefficients θ e Θ are linear and nonlinear, respectively. The nonlinear coefficient is the one that perform the adjust of the experimental curve of the linear model, as seen in Sec. 2.1.6, i.e., it is the angular coefficient of the curve. Hence, in this subsection, the nonlinear coefficient will be considered as the value $\Theta = 1$ to the total possible adjust of the linear curve to the experimental curve, making possible to simulate results near the "real".

As in Subsec. 4.3.1, the same analysis of the linear piezoelectric coefficient will be carried out to further comparisons.

Figure 4.10 shows the analysis of the linear piezoelectric coefficient in the interval $0 \leq \theta \leq 0.5$ related to the average power, considering the nonlinear contribution, also separated in two regions. In this case, the range of the values of region 1 is smaller than in the linear case, which is $0 \leq \theta \leq 0.399$, with average power $0 \leq P_{avg} \leq 52.22$, approximately. Consequently, in region 2, the system tends to totally stop the energy harvesting more fastly than in the linear case, that is, the average power tends to zero, again, when $\theta \approx 0.420$.

Next, Figs. 4.11a and 4.11b show the bifurcation diagram of the same linear coefficient variation related to the horizontal and vertical coordinates, respectively. When the system tend to zero amount of power, in this case it becomes unstable faster than the sole linear case, so that the system did not become period-1 before the instability. Table 4.5 shows a summary of the results of this subsection.

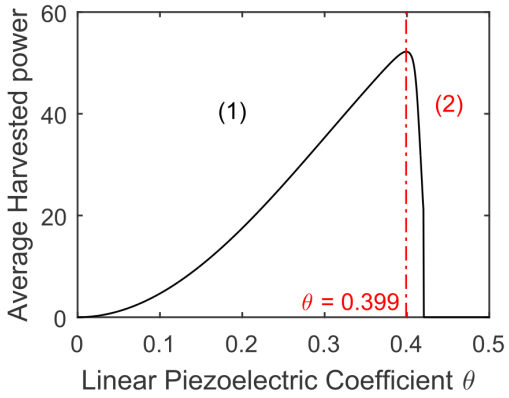

Figure 4.10: Parametrical variation of the linear piezoelectric coefficient θ related to the average harvested power

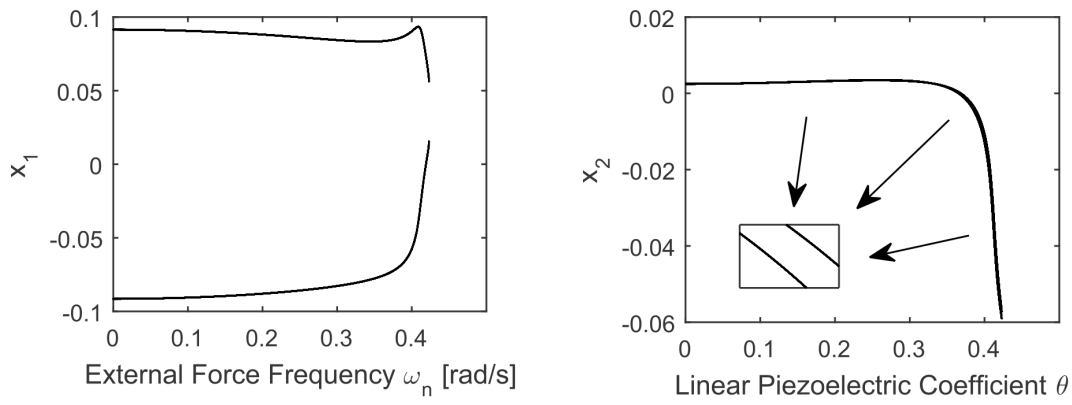

(a) (b)

Figure 4.11: Bifurcation diagram of the linear piezoelectric coefficient θ related to the (a) horizontal, (b) vertical coordinates

Table 4.5: Numerical results to the linear piezoelectric coupling, considering the nonlinear contribution

Linear Piezoelectric Coefficient θ	General Behaviour	Average Power	Conclusions
$0 \leq \theta \leq 0.399$	Period-2 (Stable)	$0 \leq P_{avg} \leq 52.22$	Gain of Power
$0.399 < \theta \leq 0.420$	- (Unstable)	P_{avg} tends to zero	Loss of Power

Until this part of this work, the system presented unstable by many times. However, this unstable behaviour may become stable with a different initial condition, that will be shown in the next section.

4.4 Influence of the Amplitude of External Frequency *versus* Initial Conditions

Duo to the small size of the considered structure in this work, the system presents with a great sensibility of its parameters, letting them limited to small ranges related to its variations. One of the most sensible parameter to a small range of values to be studied, and very important to the energy harvesting is the amplitude of the external excitation F_0, because higher the amplitude higher will be the energy harvesting. It will be shown in this Section.

The small range of these parameters, with the variation of the external amplitude, may become the system unstable faster. However, depending on they start, the system can present a faster stability with a higher range of the parameters to be varied. Thus, initial conditions of the structure of the system will be studied because it can change the stability of the system in certain value of the parameter. Even the initial conditions can induce this changes in the behaviour of the system, there is a certain difficulty to set it in an experimental model, for example, to set an initial velocity condition is much more complicated than the initial displacement condition. Then, it is important to take care which initial condition choose.

Thus, considering just the linear piezoelectric coupling, $\theta = 0.3$ and $\Theta = 0$, and the parameters of Tab. 4.1, the analysis of the range of the external force amplitude, $1 \leq F_0 \leq 500[N]$ ($0 \leq E_0 \leq 0.0878$), related to the value of the initial condition, $0 \leq x_{0i} \leq 0.3$, given to the system is performed, because higher the value of the amplitude, higher will be the energy harvesting.

Figures 4.12 show a surface of the maximum displacement of the horizontal coordinate of the structure related to the amplitude and the initial conditions of the portal frame. The initial conditions considered were the horizontal displacement (x_{01}), horizontal velocity (x'_{01}), vertical displacement (x_{02}), and vertical velocity (x'_{02}), in Figs. 4.12a, 4.12b, 4.12c and 4.12d, respectively. The peaks are considered as the instability of the system, when the displacement tends do infinite and the planes are the stable behaviour. The most influential initial conditions are from the horizontal motion, because they have the highest plane areas, i.e., of stable behaviour.

Note that the amplitude to the initial horizontal displacement (x_{01}) is $1 \leq F_0 \leq 700[N]$ ($0 \leq E_0 \leq 0.1229$). It was necessary to reach the unstable area.

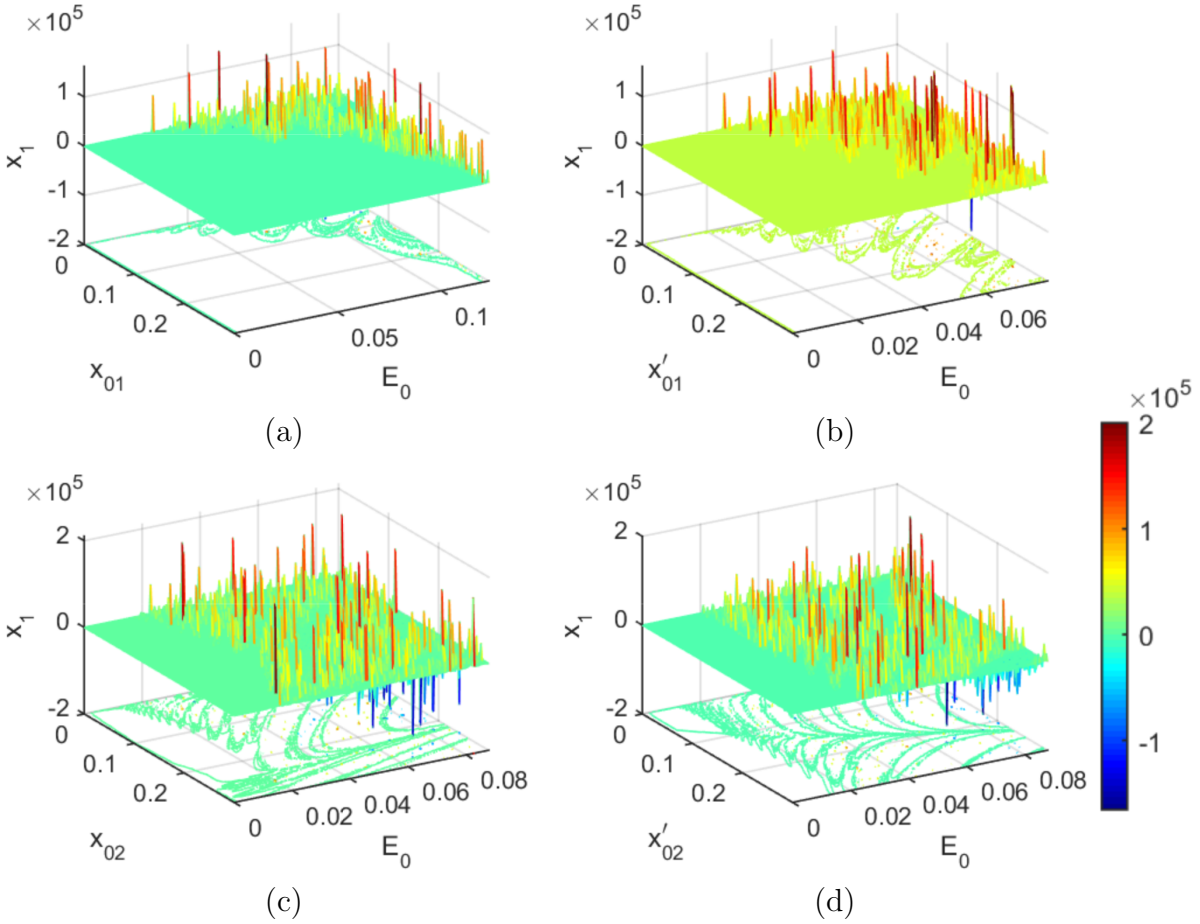

Figure 4.12: Surface of the maximum horizontal displacement related to the amplitude of the external excitation and initial conditions (a) x_{01}, (b) x'_{01}, (c) x_{02}, (d) x'_{02}

A deep analysis of the surfaces of Figs. 4.12a and 4.12b is shown in Figs. 4.13. The best value of the initial condition is to the initial horizontal displacement $x_{01} = 0.3$, because it varies the amplitude in $1 \leq F_0 \leq 688[N]$ $(0 \leq E_0 \leq 0.1208)$, approximately.

The best initial velocity condition of Fig. 4.12b is $x'_{01} = 0.2276$, however, the amplitude varies in the interval of $1 \leq F_0 \leq 408[N]$ $(0 \leq E_0 \leq 0.0716)$, approximately. It is a very small range of amplitude and, consequently, will be much smaller energy harvesting related to the initial displacement condition case.

Using the new initial condition $x_{01} = 0.3$, the variation of the amplitude F_0 is carried out in the interval of $1 \leq F_0 \leq 700[N]$ $(0 \leq E_0 \leq 0.1229)$, related to the energy harvesting, as illustrated by Fig. 4.14. Therefore, it is possible to observe that the average harvested power has a great increase of $0 \leq P_{avg} \leq 630.79$, and the amplitude range is $1 \leq F_0 \leq 688[N]$ $(0 \leq E_0 \leq 0.1208)$, approximately.

As said before, higher the amplitude higher the harvested power. In addition, the analysis of stability shows a change related to the quantity of the parameter to be used.

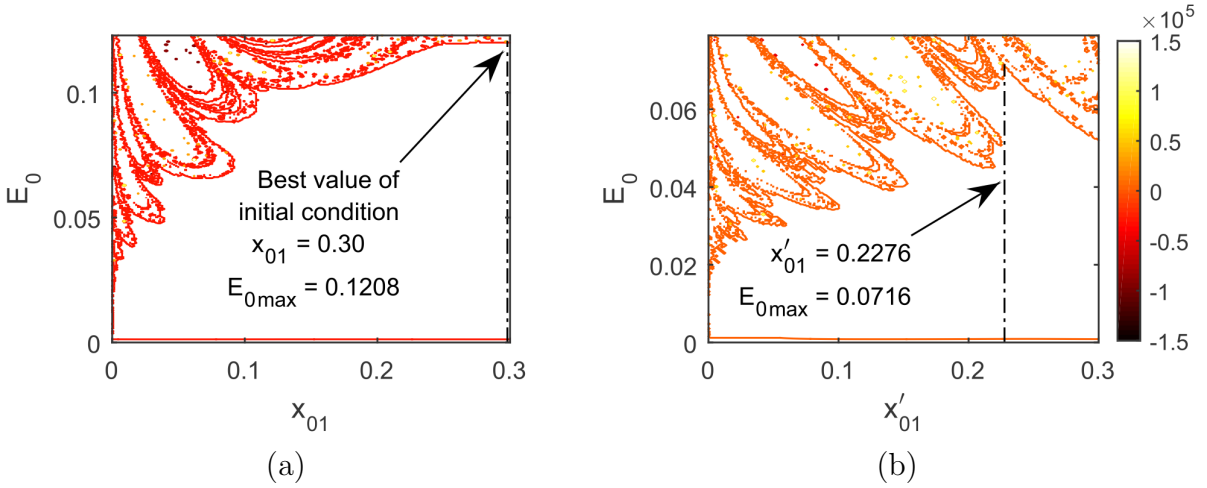

Figure 4.13: Contour of the maximum displacement of the structure related to the amplitude E_0 versus (a) x_{01}, (b) x'_{01}

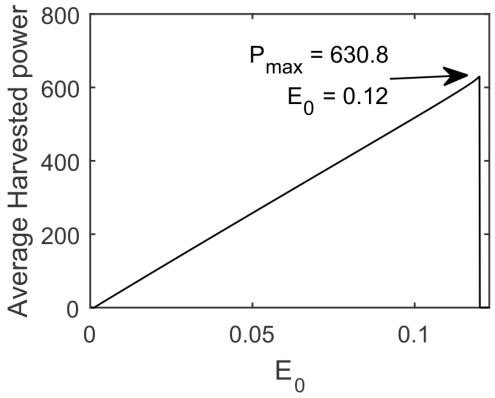

Figure 4.14: Parametrical variation of the amplitude of the external force E_0 related to the average harvested power with $x_{01} = 0.3$

This affects the way of parameter usage because with a different initial condition, it is possible to variate the parameters safely without the risk of damage the structure. Sometimes, a real system cannot support higher amplitudes and, consequently, possesses a small range of amplitude to work. Thus, with a new initial condition will be possible to obtain a higher acceptable range of amplitude with a safely work.

Therefore, a summary of the results obtained in this section is in Tab. 4.6. The table shows a comparison between the system the initial initial condition $x_{01} = 0.001$ and the new one $x_{01} = 0.3$.

Table 4.6: Numerical results of the initial displacement condition x_{01} variation related to the amplitude of the external force

Dimensional Amplitude of the External Force $F_0[N]$	Dimensionless Amplitude of the External Force E_0	Initial Displacement Condition x_{01}	Average Harvested Power	Stability
40	0.007	0.001	31.37	Stable
120	0.0211	0.001	105.87	Stable
240	0.0421	0.001	-	Unstable
		0.300	216.58	Stable
688	0.1208	0.001	-	Unstable
		0.300	630.79	Stable

As the amplitude and the new initial conditions showed to be very important, it is worth to study different combination of parameters with the previous ones. One of them is the piezoelectric coupling because of its directly influence on the energy harvesting. Therefore, an overview of combinations among the amplitude *versus* initial condition *versus* piezoelectric parameters related the harvested power will be carry out in the next Subsection.

4.4.1 Amplitude *versus* Sole Linear Piezoelectric Coefficient Case

In this subsection will be studied the general contribution of the initial condition to the energy harvesting. Thus, the use of the new found initial condition which possesses the highest range of amplitude will be considered, and compared to the case of the first initial condition. In addition, knowing the effect of the nonlinear piezoelectric coupling, here, the case of the sole linear coupling will be considered to further comparisons.

The interesting to combine these parameters is that both are strongly linked to the energy harvesting.

Firstly, a parametrical analysis of the linear piezoelectric coefficient of $0 \leq \theta \leq 0.5$ related to the amplitude of the external force $0 \leq F_0 \leq 300[N]$ ($0 \leq E_0 \leq 0.0527$), and to the average harvested power is carried out in Fig. 4.15.

Figure 4.15a shows the contour of the maximum displacement related to the variation of the amplitude E_0 *versus* the linear piezoelectric coefficient θ. The system presents two well defined areas of stable and unstable behaviour, whose stable area is delimited by the interval of $0 \leq F_0 \leq 141.7[N]$ ($0 \leq E_0 \leq 0.0249$) and $0 \leq \theta \leq 0.3266$.

Figures 4.15b and 4.15c show a surface and a coloured contour, respectively, of the average harvested power related to the variation of the amplitude E_0 *versus* the linear piezoelectric coefficient θ. The amount of power increases along the variation of the parameters until reach the maximum stable point, which is $F_0 = 141.7$ ($E_0 = 0.0249$) and $\theta \leq 0.3266$ with 148.24 amount of power. However, there are other stable point in the

unstable delimited area. These points are not considered because they are isolated cases in a big role of unstable points. These points can reach near 300 amount of harvested power.

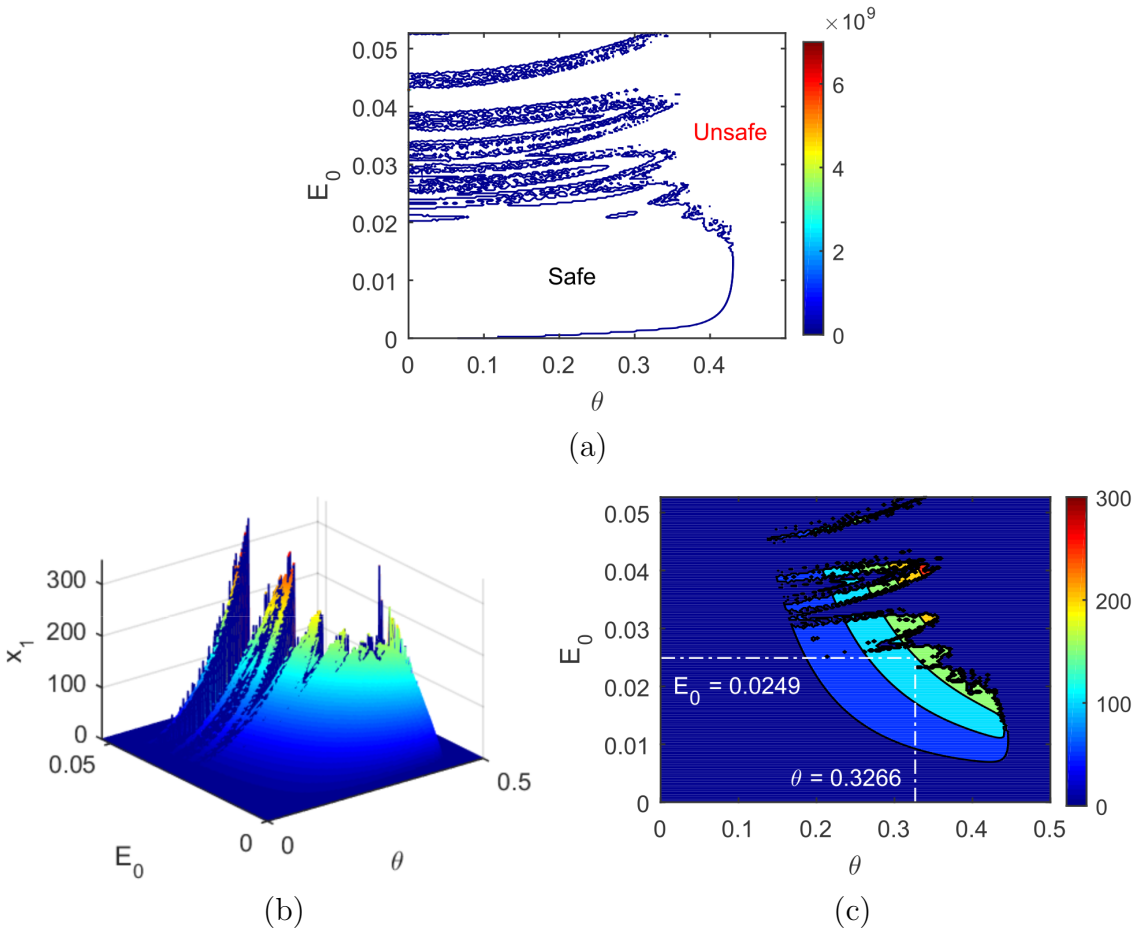

Figure 4.15: Piezoelectric linear case $\Theta = 0$ and initial condition $x_{01} = 0.001$ (a) Contour of the maximum displacement of the structure related to the amplitude E_0 versus θ; (b) surface of the harvested power related to the amplitude E_0 versus θ; (c) coloured contour of the harvested power related to the amplitude E_0 versus θ

Next, the same analysis of Fig. 4.15 is carried out with the new initial condition $x_{01} = 0.30$. Thus, the results are shown in Fig. 4.16.

Figure 4.16a shows the contour of the maximum displacement related to the variation of the amplitude E_0 *versus* the linear piezoelectric coefficient θ with $x_{01} = 0.3$. The stable are is very well delimited than in the case of the first initial condition. In addition, the amplitude's range overpass $F_0 = 700N$ ($E_0 = 0.1229$) with stable behaviour, unlike the previous situation that the amplitude has its maximum in $F_0 = 141.7N$ ($E_0 = 0.0249$). The unstable behaviour is presented when the piezoelectric coefficient has a higher value, i.e., when it is, theoretically, harvesting a high amount of vibration energy.

Figures 4.16b and 4.16c show a surface and a coloured contour, respectively, of the

average harvested power related to the variation of the amplitude E_0 *versus* the linear piezoelectric coefficient θ. In this case, the energy harvesting grows up along the increase of the amplitude and the value of the linear piezoelectric coefficient. The whole coloured area has a stable behaviour, and the highest amount of power is obtained when $F_0 = 566.75N$ ($E_0 = 0.0995$) and $\theta = 0.3291$ whose value is 645.00 amount of power, approximately.

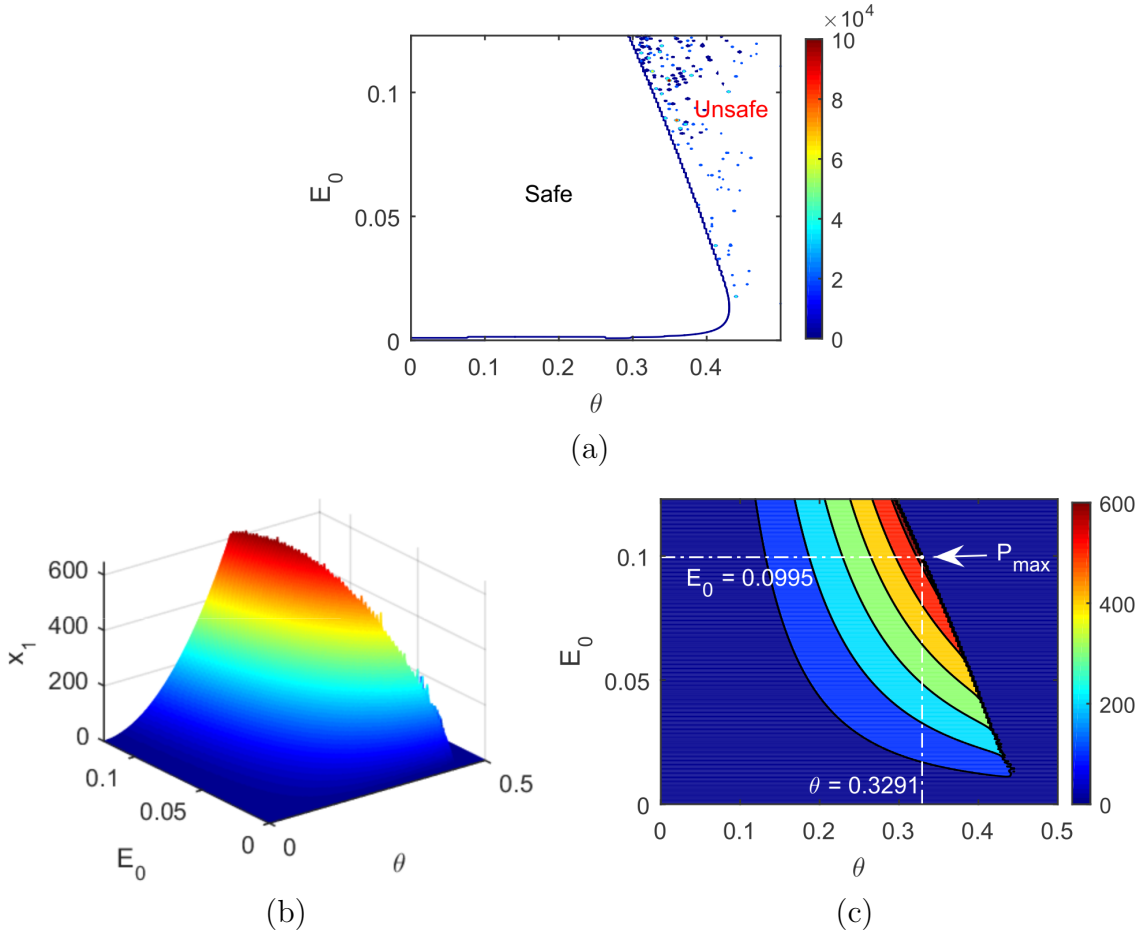

Figure 4.16: Piezoelectric linear case $\Theta = 0$ and initial condition $x_{01} = 0.3$ (a) Contour of the maximum displacement of the structure related to the amplitude E_0 versus θ; (b) surface of the harvested power related to the amplitude E_0 versus θ; (c) coloured contour of the harvested power related to the amplitude E_0 versus θ

The new initial condition is very important because it changes the unstable behaviour to a stable behaviour which provides a high amount of harvested power than with the first initial condition, as shown in in Tab. 4.7.

Table 4.7: Summary of Subsec. 4.4.1

Initial Condition x_{01}	Amplitude of the External Force E_0	Linear Piezoelectric Coefficient θ	Stability	Average Power
0.001	$0.0249 < E_0 \leq 0.0527$	$0 \leq \theta \leq 0.5$	Unstable	-
	$0 \leq E_0 \leq 0.0249$	$0 \leq \theta \leq 0.3266$	Stable	$0 \leq P_{avg} \leq 148.24$
0.300	$0 \leq E_0 \leq 0.1229$	$0.430 < \theta \leq 0.5$	Unstable	-
	$0 \leq E_0 \leq 0.1229$	$0 \leq \theta \leq 0.430$	Stable	$0 \leq P_{avg} \leq 645.00$
Max. Power 0.001	0.0249	0.3266	Stable	148.24
Max. Power 0.300	0.0995	0.3291	Stable	645.00

However, another important factor to be studied is the nonlinear contribution of the piezoelectric material. Thus, in the next subsection will be discussed the same analysis of the amplitude related to the linear piezoelectric coefficient considering $\Theta = 1$.

4.4.2 Amplitude *versus* Nonlinear Piezoelectric Coefficient Case

The contribution of the nonlinear piezoelectric coefficient is very important because it approximates the power numerical results to the experimental curve of the piezoelectric strain. Therefore, the next numerical simulations will show the various analysis of the linear piezoelectric coefficient *versus* the amplitude of the external force considering the contribution of the nonlinear piezoelectric coefficient, fixed at $\Theta = 1.0$. It is possible to observe the most real effect of the piezoelectric material with the increasing of the amplitude of the external force.

Figures 4.17a and 4.17c show the surface of the maximum horizontal displacement related to the amplitude *versus* initial conditions x_{01} and x'_{01}, respectively. With the contribution of the nonlinear piezoelectric coefficient, the peaks of the surfaces become very well defined, i.e., the coloured area (unstabilities) is higher than in the case of the sole linear piezoelectric contribution. Through the contour of the surfaces in Figs. 4.17b and 4.17d, it is possible to observe that the best initial condition continues to be $x_{01} = 0.3$, whose white area is the stable behaviour. However, the interval of variation of the amplitude decreases to $1 \leq F_0 \leq 362.9N$ ($0 \leq E_0 \leq 0.0637$), approximately, different of the sole linear case which was $1 \leq F_0 \leq 688N$ ($0 \leq E_0 \leq 0.1208$).

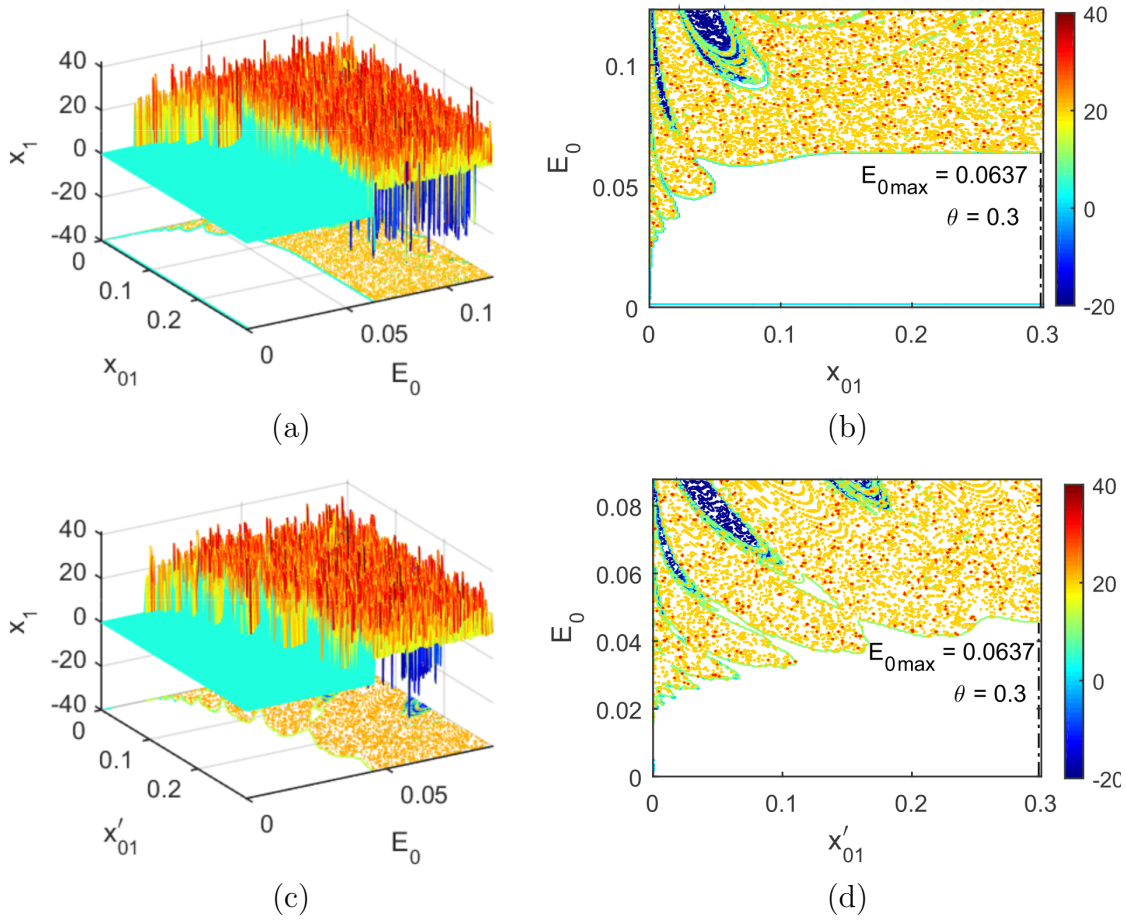

Figure 4.17: Piezoelectric nonlinear case $\Theta = 1$ to surfaces (a) and (c), Contour (b) and (d), of the maximum horizontal displacement of the structure related to the amplitude *versus* initial conditions x_{01} and x'_{01}

As the initial conditions continues to be important because it changes the stability of the system, the same analysis of stability and harvested power related to the amplitude *versus* the linear piezoelectric coefficient, however considering the contribution of the nonlinear piezoelectric coefficient, is carried out with $x_{01} = 0.001$ and $x_{01} = 0.300$.

Firstly, Figs. 4.18 show the analysis of stability and harvested power with $x_{01} = 0.001$.

Fig. 4.18a shows the contour of the maximum horizontal displacement of the structure related to the variation of the amplitude *versus* linear piezoelectric coefficient. Related to the linear case, the stable area decreases to $0 \leq F_0 \leq 140.2N$ $(0 \leq E_0 \leq 0.0246)$ and $0 \leq \theta \leq 0.2965$. Through Figs. 4.18b and 4.18c, which are the surface and contour of the harvested power related to the amplitude *versus* the linear piezoelectric coefficient, it is observed that the high level amount of power area decreases too, related to the system of linear case, however, even the amplitude and linear coefficient are of small values the maximum amount of power in the stable are higher with value of 157.82. Moreover, the isolated stable points among the unstable area are smaller.

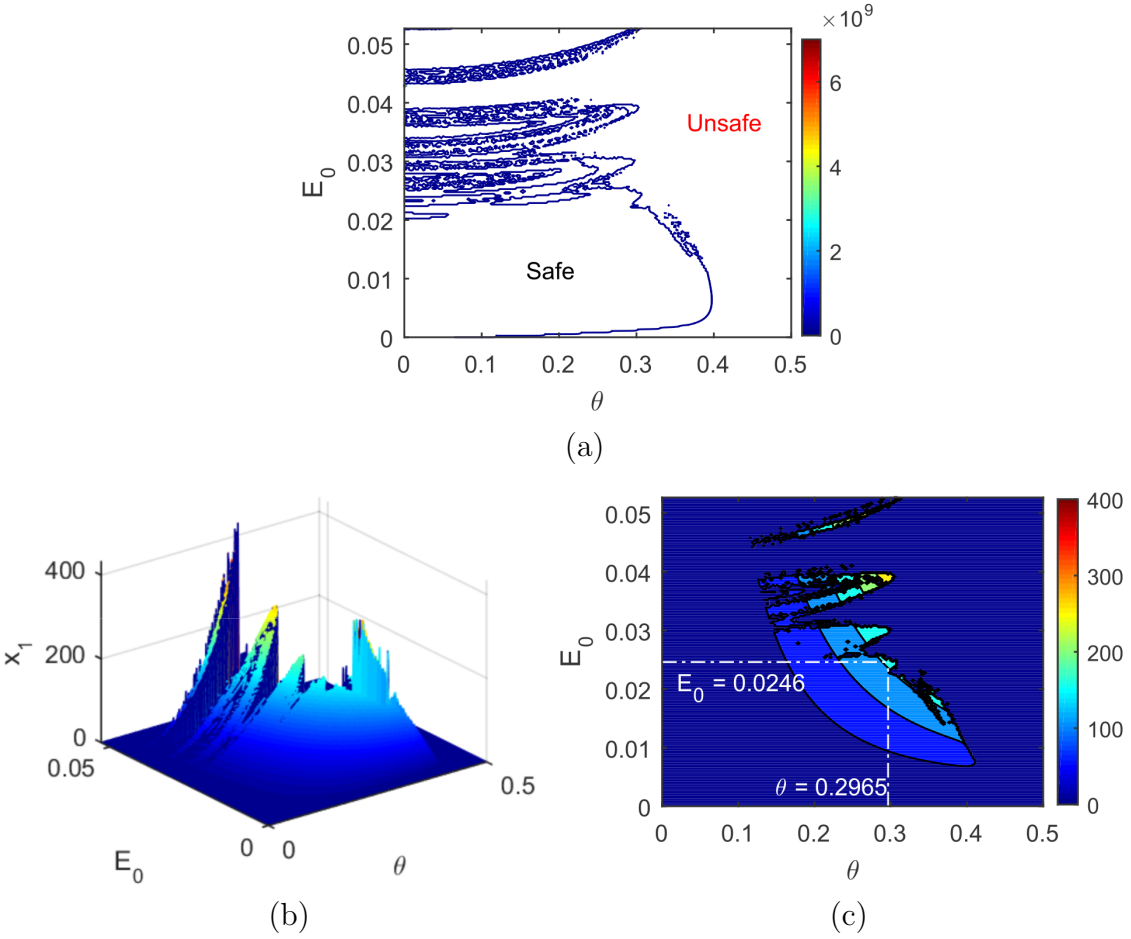

Figure 4.18: Piezoelectric nonlinear case $\Theta = 1$ and initial condition $x_{01} = 0.001$ (a) Contour of the maximum displacement of the structure related to the amplitude E_0 versus θ; (b) surface of the harvested power related to the amplitude E_0 versus θ; (c) coloured contour of the harvested power related to the amplitude E_0 versus θ

Next, considering the initial condition $x_{01} = 0.300$, Figs. 4.19 are presented.

Figure 4.19a shows the contour of the maximum horizontal displacement of the structure related to the variation of the amplitude *versus* linear piezoelectric coefficient. The same what it is observed in Fig. 4.16a happens in this case. However, the peaks are very better defined than the linear case, and the stable area is reduced related to the linear piezoelectric coefficient, which is $0 \leq \theta \leq 0.397$. Moreover again, the system obtains stable values with amplitude higher than $F_0 = 700N$ ($E_0 = 0.1229$), although the maximum power is obtained in $F_0 = 633.2$ ($E_0 = 0.1112$) and $\theta = 0.2362$ that is $P_{max} = 641.82$, as it can be seen in Fig. 4.19b and 4.19c, that represent a surface and a coloured contour of the harvested power related to the variation of the amplitude *versus* linear piezoelectric coefficient.

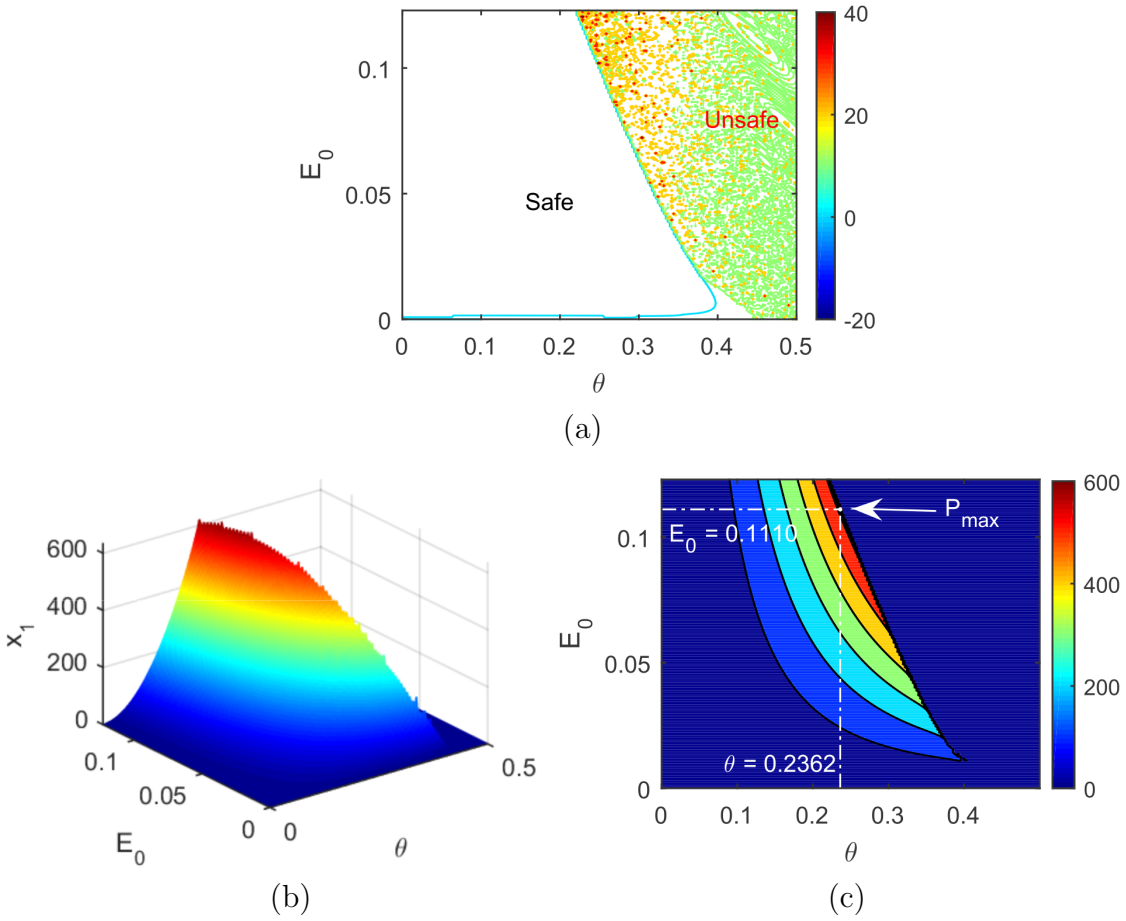

Figure 4.19: Piezoelectric nonlinear case $\Theta = 1$, and initial condition $x_{01} = 0.3$ (a) Contour of the maximum displacement of the structure related to the amplitude E_0 versus θ; (b) surface of the harvested power related to the amplitude E_0 versus θ; (c) coloured contour of the harvested power related to the amplitude E_0 versus θ

Therefore, in the nonlinear case, $\Theta = 1.0$, is observed that the unstable and stable areas becomes to be very better defined than in the linear case. The best initial condition continued to be $x_{01} = 0.3$ although there are many others similar to this one. The range of the linear piezoelectric coefficient reduced considerably, however, the maximum power keeps close in the linear case with a smaller value of the linear coefficient. All these results are related to the variation of the amplitude and are summarized in Tab. 4.8.

Table 4.8: Summary of Subsec. 4.4.2 in comparison to Subsec. 4.4.1

Piezoelectric Case	Initial Condition x_{01}	Amplitude of the External Force E_0	Linear Piezoelectric Coefficient θ	Stability	Average Power
$\Theta = 0$ Linear	0.001	$0.0249 < E_0 \leq 0.0527$	$0 \leq \theta \leq 0.5$	Unstable	-
	0.300	$0 \leq E_0 \leq 0.1229$	$0.3266 < \theta \leq 0.5$	Unstable	-
	0.001	$0 \leq E_0 \leq 0.0249$	$0 \leq \theta \leq 0.3266$	Stable	$0 \leq P_{avg} \leq 148.24$
	0.300	$0 \leq E_0 \leq 0.1229$	$0 \leq \theta \leq 0.430$	Stable	$0 \leq P_{avg} \leq 645.00$
$\Theta = 1$ Nonlinear	0.001	$0.0246 < E_0 \leq 0.0527$	$0 \leq \theta \leq 0.5$	Unstable	-
	0.300	$0 \leq E_0 \leq 0.1229$	$0.397 < \theta \leq 0.5$	Unstable	-
	0.001	$0 \leq E_0 \leq 0.0246$	$0 \leq \theta \leq 0.2965$	Stable	$0 \leq P_{avg} \leq 157.82$
	0.300	$0 \leq E_0 \leq 0.1229$	$0 \leq \theta \leq 0.397$	Stable	$0 \leq P_{avg} \leq 641.82$
$\Theta = 0$ Linear	Max. Power 0.001	0.0249	0.3266	Stable	148.24
	Max. Power 0.300	0.0995	0.3291	Stable	645.00
$\Theta = 1$ Nonlinear	Max. Power 0.001	0.0246	0.2965	Stable	157.82
	Max. Power 0.300	0.1112	0.2362	Stable	641.82

The PART I of this work, which was analyzed the portal frame with a nonlinear piezoelectric coupling base-excited by a harmonic force, ends here. In the following begins the PART II which considers the external excitation induced by an electro-dynamical shaker.

PART II

Global Analysis of the System with Electro-dynamical Shaker

Chapter 5

Full Portal Frame Foundation Mathematical Model

In this part of this work the electro-dynamical shaker will be considered in order to excite the base of the main structure. Same as in Chapter 3, the full model will be presented as illustrated in Fig. (3.1).

The usage of the electro-dynamical shaker is due to its possible usage in a future experiment to validate the system. In addition, the dynamics of the system, somehow, will change.

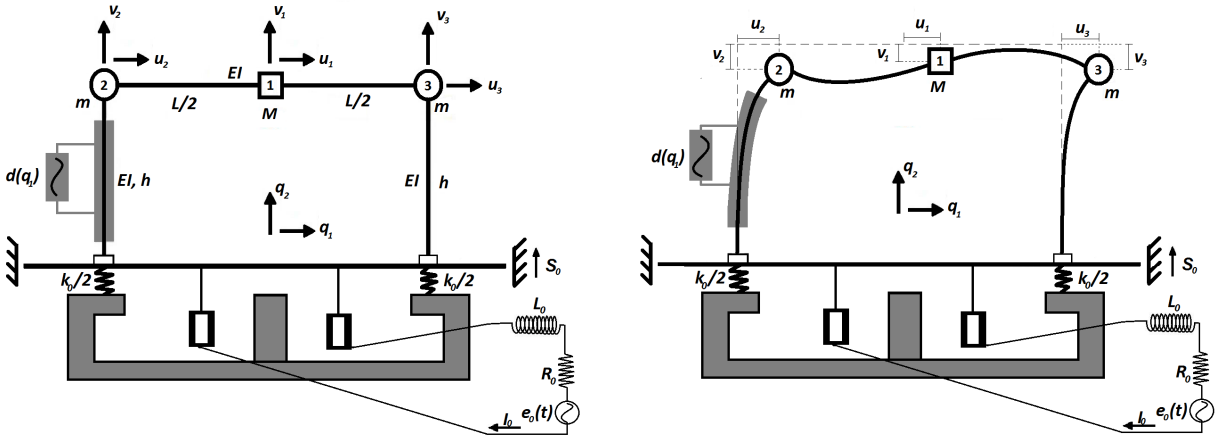

(a) (b)

Figure 5.1: Schematic model of a simple portal frame with a piezoelectric material coupled to one of its column and an electro-dynamical shaker coupled to its base, (a) non-deformed, (b) deformed

The two-degrees-of-freedom system, illustrated in Figs. 5.1, as in Chapter 3, the non-deformed schematic model of the simple portal frame is represented in Fig. 5.1a, and the deformed schematic model is represented in Fig. 5.1b. This system is constituted by:

- two columns clamped in their bases with length h,

• horizontal beam pinned to the columns at both ends with length L,

• both columns and beam have flexural stiffness EI, where E is the Young's modulus and I is the momentum of inertia of beam and columns,

• the mass at mid-span of the beam is M,

• the masses of each columns is represented by m,

• piezoelectric coupling given by $d(q_1)$,

however, there is:

• base with mass m_0

• base-excitation by an electro-dynamical shaker considering its electric and mechanic parts.

The excitation induced by the shaker is given by the bass with mass m_0, stiffness k_0, and damping c_0. Its electrical part is constituted by a RL circuit of resistance R_0, inductance L_0, voltage source $e_0(t)$ that is a cosine input, electric current I_0, and electric charge Q_{s0}, where $I_0 = \frac{dQ_{s0}}{dt}$.

The main structure is modelled as in Chapter 3. The form functions and the stiffness of the columns and beam are the same. However, the nodal displacements of the system becomes to be as in Eq. (5.1)

$$\begin{array}{lll} u_1 = q_1 & u_2 = u_1 + \dfrac{B}{4}v_1^2 & u_3 = u_1 - \dfrac{B}{4}v_1^2 \\ v_1 = S_0 + q_2 & v_2 = S_0 - \dfrac{A}{2}u_1^2 & v_3 = S_0 - \dfrac{A}{2}u_1^2 \end{array} \tag{5.1}$$

where $A = 6/5h$ and $B = 24/5L$ and S_0 is the base displacement.

The nonlinear piezoelectric material is coupled to the column as an electric RC circuit as in Eq. (3.6) in Chapter 3.

In the next Section, the mathematical modelling of the full system with the energy method where the Lagrange's formulation is used.

5.1 Mathematical Modelling of the Full Portal Frame

In this section will be discussed the mathematical modelling of the portal frame excited via an electro-dynamical shaker. To perform the equations of motion is used the Lagrange's function and Euler-Lagrange equation given by Eqs. (3.7) and (3.8), respectivelly.

The kinectic energy is given by the motion of the masses of the beam M, columns m and base m_0, and by the inductance of the shaker L_0, defined by Eq. (5.2).

$$T = \frac{1}{2}M(\dot{x_1}^2 + \dot{y_1}^2) + \frac{1}{2}m(\dot{x_2}^2 + \dot{x_3}^2 + \dot{y_2}^2 + \dot{y_3}^2) + \frac{1}{2}m_0\dot{S}_0^2 + \frac{1}{2}L_0\dot{Q}_{s0}^2 \tag{5.2}$$

Substituting the nodal displacements of Eq. (5.1), it is obtained the kinetic energy in

function of the generalized coordinates q_1, q_2, S_0 e Q_0, denoted by Eq. (5.3).

$$T = \frac{1}{2}M(\dot{q_1}^2 + \dot{q_2}^2 + 2\dot{q_2}\dot{S_0} + \dot{S_0^2}) + \frac{1}{2}m(2\dot{q_1}^2 + 2\dot{S_0^2} - 4A\dot{S_0}q_1\dot{q_1}) + \frac{1}{2}m_0\dot{S_0^2} + \frac{1}{2}L_0\dot{Q}_{s0}^2 \quad (5.3)$$

The potential energy is given by the stiffness of the columns, beam and base, the potential gravitational energy, the electric potential energy of the piezoelectric material, and the electromotive force of the shaker, obtaining the Eq. (5.4).

$$\begin{aligned} V = \frac{1}{2}k_c(x_2^2 + x_3^2) + \frac{1}{2}k_b\left(y_1 - \frac{y_2 + y_1}{2}\right)^2 + mg(y_2 + y_3) + Mgy_1 + ... \\ ...\frac{1}{2}k_0S_0^2 + K\dot{Q}_{s0}S_0 - \frac{d(q_1)}{C_p}Q_p(u_2 + v_2) + \frac{1}{2}\frac{Q_p^2}{C_p} \end{aligned} \quad (5.4)$$

Substituting in terms of Eq. (5.1), the potential energy is given in function of the coordinates q_1, q_2, S_0, Q_{s0} e Q_p, as given in Eq. (5.5).

$$\begin{aligned} V = (k_c - mgA)q_1^2 + \frac{1}{2}k_b(q_2^2 + Aq_2q_1^2) + (M + 2m)gS_0 + Mgq_2 + ... \\ \frac{1}{2}k_0S_0 + K\dot{Q}_{s0}S_0 - \frac{d(q_1)}{C_p}Q_p\left(q_1 + S_0 + \frac{B}{4}q_2^2\right) + \frac{1}{2}\frac{Q_p^2}{C_p} \end{aligned} \quad (5.5)$$

The Rayleigh dissipation energy function is obtained through the damping of the columns c_1, beam c_2 and base c_0, the electric resistance R_p of the piezoelectric material, and the electric resistance of the shaker R_0. Therefore, the dissipation energy function is given by Eq. (5.6).

$$D = \frac{1}{2}c_1\dot{q_1}^2 + \frac{1}{2}c_2\dot{q_2}^2 + \frac{1}{2}c_0\dot{S_0^2} + \frac{1}{2}R_0\dot{Q}_{s0}^2 + \frac{1}{2}R_p\dot{Q_p}^2 \quad (5.6)$$

Lastly, the applied external force under the base is induced by the harmonic voltage source of the electro-dynamical device, whose function is defined in Eq. (5.7).

$$F_{ext} = e_0 cos\omega_n t \quad (5.7)$$

Using the Lagrange's function and Euler-Lagrange equations denoted by Eqs. (3.7) and (3.8), respectivelly, the governing equations of motion of the full system, illustrated in Fig. 5.1, are presented by Eqs. (5.8), (5.9), (5.10), (5.11) and (5.12), which are related to the horizontal motion, vertical motion, base motion, electrical part of the shaker, and piezoelectric material, respectivelly.

$$(2m+M)\ddot{q_1} + 2(k_c - mgA)q_1 + Aq_1q_2 + c_1\dot{q_1} = 2Am\dot{q_1}\dot{S_0} + \frac{d(q_1)}{C_p}Q_p \tag{5.8}$$

$$M(\ddot{q_2} + \ddot{S_0}) + c_2\dot{q_2} + k_bq_2 + \frac{Ak_b}{2}q_1^2 + Mg = \frac{d(q_1)}{C_p}\frac{B}{2}Q_pq_2 \tag{5.9}$$

$$(M+2m+m_0)\ddot{S_0} + M\ddot{q_2} + (2m+M)g + k_0S_0 + KI_0 + c_0\dot{S_0} = ... \tag{5.10}$$

$$2Am\dot{q_1}^2 + \frac{d(q_1)}{C_p}Q_p$$

$$L_0\dot{I_0} + R_0I_0 - K\dot{S_0} = e_0 cos\omega_n t \tag{5.11}$$

$$R_p\dot{Q_p} - \frac{d(q_1)}{C_p}\left(q_1 + S_0 + \frac{B}{4}q_2^2\right) + \frac{Q_p}{C_p} = 0 \tag{5.12}$$

In the following, a dimensionless process is carried out to generalize the obtained results.

5.2 Dimensionless Process of the Governing Equations of Motion of the Full System

The dimensionless process in this case adopts the dimensionless variables such as in Eq. (5.13).

$$\begin{gathered} x_1 = \frac{q_1}{h} \quad x_2 = \frac{q_2}{l} \quad V_p = \frac{Q_p}{Q_0} \quad Y = \frac{S_0}{h} \\ \tau = \omega_1 t \quad \omega_1 = \sqrt{\frac{2(k_c - mgA)}{2m+M}} \quad U = \frac{I_0}{i_0} \quad \hat{d}(q_1) = \frac{Q_{s0}}{h}d(x_1) \end{gathered} \tag{5.13}$$

Substituting the dimensionless variables (5.13) in the equations of motion (5.8), (5.9), (5.10), (5.11) and (5.12), the dimensionless governing equations of motions are obtained given by the Eqs. (5.14), (5.15), (5.16), (5.17) and (5.18).

$$x_1'' + \mu_1x_1' + x_1 + \alpha_1x_1x_2 = \beta_1x_1'Y' + \theta(1+\Theta|x_1|)\delta_1V_p \tag{5.14}$$

$$x_2'' + \varepsilon Y'' + \omega_2^2x_2 + \mu_2x_2' + \alpha_2x_1^2 + G_0 = \theta(1+\Theta|x_1|)\delta_2V_px_2 \tag{5.15}$$

$$Y'' + \delta_m\varepsilon x_2'' + \omega_0^2Y + \mu_0Y' + \gamma_1U + G_1 = \beta_2x_1'^2 + \theta(1+\Theta|x_1|)\delta_1V_p \tag{5.16}$$

$$U' + \gamma_2U - \gamma_3Y' = E_0\cos\Omega\tau \tag{5.17}$$

$$V_p' - \theta(1+\Theta|x_1|)(\delta_3(x_1+Y) + \delta_4x_2^2) + \delta_3V_p = 0 \tag{5.18}$$

where the dimensionless parameters are denoted by Eq. (5.19).

$$
\begin{aligned}
&\mu_1 = \frac{c_1}{(2m+M)\omega_1} \quad \alpha_1 = \frac{Ak_b l}{(2m+M)\omega_1^2} \quad \beta_1 = \frac{2mAh}{(2m+M)} \quad \varepsilon = \frac{h}{l} \\
&\omega_2 = \frac{1}{\omega_1}\sqrt{\frac{k_b}{M}} \quad \mu_2 = \frac{c_2}{M\omega_1} \quad \alpha_2 = \frac{Ak_b h^2}{2M\omega_1 l} \quad G_0 = \frac{g}{\omega_1^2 l} \quad \delta_2 = \frac{BQ_0^2}{2MC_p\omega_1^2 h} \\
&\delta_1 = \frac{Q_0^2}{\omega_1^2(2m+M)C_p h^2} \quad \delta_m = \frac{M}{M_T} \quad \omega_0 = \frac{1}{\omega_1}\sqrt{\frac{k_0}{M_T}} \quad \mu_0 = \frac{c_0}{M_T\omega_1} \\
&G_1 = \frac{(2m+M)g}{M_T\omega_1^2 h} \quad \gamma_1 = \frac{KI_0}{M_T\omega_1 h} \quad \gamma_2 = \frac{R_s}{L_s\omega_1} \quad \gamma_3 = \frac{Kh}{L_s I_0} \quad E_0 = \frac{e_0}{L_s\omega_1 I_0} \\
&\Omega = \frac{\omega_n}{\omega_1} \quad \delta_3 = \frac{1}{R_p C_p \omega_1} \quad \delta_4 = \frac{Bl^2}{4R_p C_p \omega_1 h} \quad \beta_2 = \frac{2MAh}{M_T} \\
&M_T = (2m + M + m_0)
\end{aligned}
\tag{5.19}
$$

The dimensional, dimensionless and average harvested power through the piezoelectric material are given at the same Eqs. (3.23), (3.24) and (3.25), respectively.

The next Chapter will perform the numerical simulations of the dimensionless full system with several analysis as in the Part I of this work.

Chapter 6

Numerical Simulations of the Full Portal Frame System

In this chapter, several numerical simulations identically to Chap. 4 will be carried out. However, the difference is the presence of the electro-dynamical shaker to excite the base of the structure. At the end, some considerations will be exposed comparing the Part I with the Part II, i.e., the system with an harmonic force and the influence of the electro-dynamical shaker.

The method of performance of the numerical simulations was the same Runge-Kutta of 4th and 5th order, carried out in Part I of this work.

The parameters used in this chapter are in Tab. 6.1. Most of them are the same of Tab. 4.1, however, it is necessary to consider the shaker's parameter which are retrieved from Xu et al. (2005, 2007).

Again, the parameters of Tab. 6.1 will be considered as default to the next simulations, except when it is described, although the same parameters will be analyzed. The same initial condition of $x_{01} = 0.001$ is fixed.

The presence of 2:1 internal resonance and external resonance continue to be important because of the saturation phenomenon occurs, i.e., $\omega_2 = 147.8 rad/s$ and $\omega_1 = 74 rad/s$ ($\omega_2 \approx 2\omega_1$), and $\omega_2 \approx \omega_n$.

Table 6.1: Parameters of the Full Portal Frame Foundation

Parameters	Values	Means
$g[m/s^2]$	9.81	Gravity acceleration
$M[kg]$	2.00	Beam mass
$m[kg]$	0.50	Column mass
$m_0[kg]$	15.88	Base mass
$c_1[Ns/m]$	1.55	Column damping
$c_2[Ns/m]$	3.14	Beam damping
$c_0[Ns/m]$	534	Base damping
$EI[nm^2]$	128	Linear flexural stiffness
$k_0[kg/m]$	86176	Base stiffness
$L[m]$	0.52	Beam length
$h[m]$	0.36	Column length
$e_0[V]$	40	Amplitude of the shaker
$R_0[\Omega]$	0.3	Electric resistance of the shaker
$L_0[mH]$	2.626	Inductance of the shaker
$K[N/A]$	130	Electromagnetic force of the shaker
$\omega_n[rad/s]$	148	Frequency of the shaker
$R_0[\Omega]$	0.3	Electric resistance of the shaker
$R_p[k\Omega]$	100	Electric resistance of the piezoelectric
$C_p[\mu F]$	1	Capacitance of the piezoelectric
θ	0.3	Linear piezoelectric coefficient
Θ	0	Nonlinear piezoelectric coefficient

6.1 Energy transfer and saturation phenomenon

In this section, the energy transfer and saturation phenomenon of this system, considering the influence of the shaker will be carried out. The total vibrating energy (energy index) of the horizontal, vertical and the electrical part of the piezoelectric material are given the same of Eqs. (4.1), (4.2) and (4.3), however, related to the equations of motion (5.14), (5.15), (5.16), (5.17) and (5.18), that are related to the system coupled to the electro-dynamical vibrator.

To directly analyze the energy transfer, the energy percentage is considered as Eqs. (4.4), (4.5) and (4.6) to each coordinate of the full system.

Thus, considering the parameters of Tab. 6.1, it is presented the results of the energy transfer percentage in three parts: neglecting the use of piezoelectric material and external resonance, disregarding the material and considering the resonance, and considering both the piezoelectric and external resonance. These results are shown in Figs. 6.1 considering the main structure and the piezoelectric material.

Firstly, the system out of resonance with the shaker is adopted, i.e., $\omega_n = 100 rad/s$.

Figure 6.1a shows the time history of the energy percentage assuming out of resonance, and it is observed that there was no transference of energy between the coordinates of the portal frame, consequently there is no saturation phenomenon. It is due to the fact that the external resonance is one of the conditions to saturation phenomenon occurs.

Next, assuming that the system is in resonance with the vertical coordinate ($\omega_n = 148 rad/s$) and still disregarding the piezoelectric coupling, Fig. 6.1b presents the time history of the energy percentage with the system in resonance. It shows that almost the whole vibrating energy of the vertical coordinate was transferred to the horizontal keeping almost 100% at steady state, that is, saturation phenomenon occurred.

In Figs. 6.1a and 6.1b, the blue curve which represents the electric energy of the piezoelectric there was no variation due to the uncoupling of the material. However, in Fig. 6.1c shows the time history of the energy percentage considering the system in resonance and coupled to the piezoelectric material. In this case, there was variation in the blue curve because part of the horizontal coordinate's energy was transferred to the piezoelectric material, i.e., the piezoelectric harvested some vibration energy of the columns' vibration.

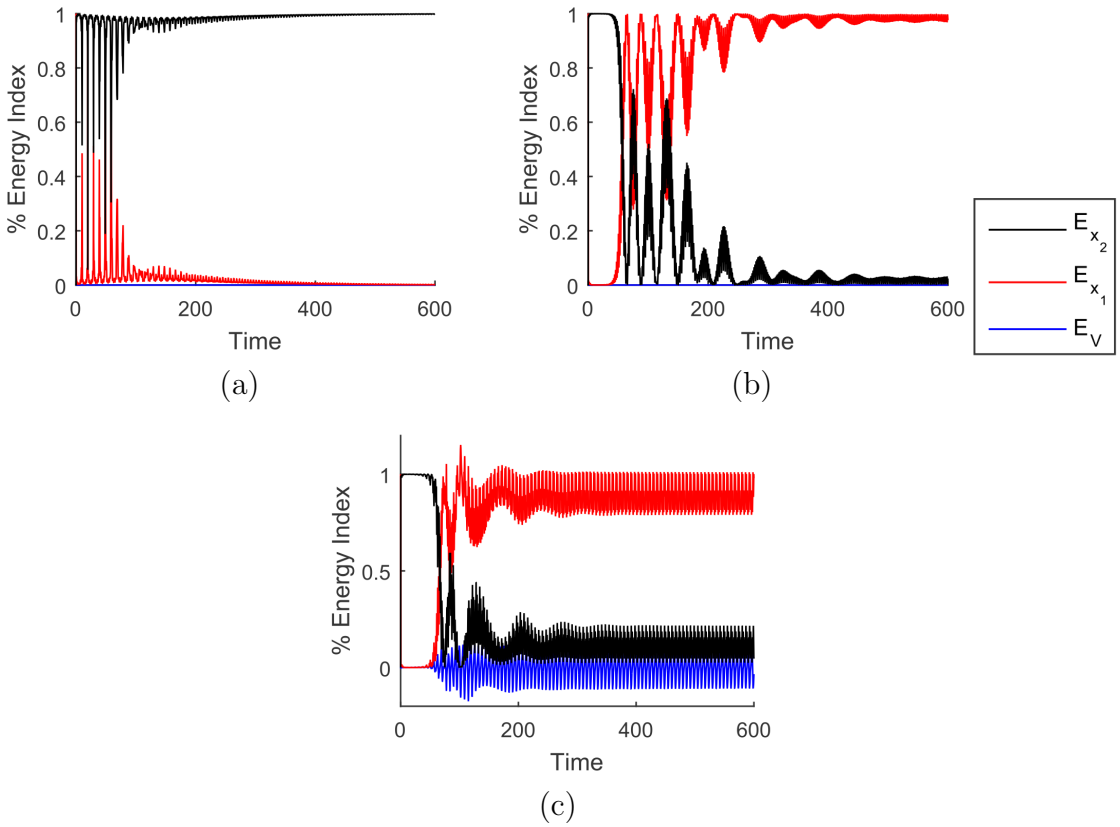

Figure 6.1: Energy percentage of the motion, considering the shaker, in horizontal direction (in red), vertical (in black), and the electric energy of the piezoelectric (in blue), (a) $\omega_n = 100 rad/s$ and $\theta = 0$, (b) $\omega_n = 148 rad/s$ and $\theta = 0$, (c) $\omega_n = 148 rad/s$ and $\theta = 0.3$

The results presented in this Part II of this work is very similar to the Part I, illustrated in Figs. 4.1. In addition, the energy transfer may be observed by time histories of the displacements, that are represented in Figs. 6.2, and directly related to Figs. 4.1.

Figure 6.2a shows the time history of the displacements with the system out of resonance and without the piezoelectric coupling. The amplitude of displacement of the horizontal coordinate tends to zero, while the vertical keeps constantly in motion. Unlike in Fig. 6.2b, that the horizontal coordinate becomes to be very higher than the vertical one, where the system is considered in resonance.

With the piezoelectric material coupled in the main structure, in Fig. 6.2c, the amplitude of horizontal motion decreased because the piezoelectric material is able to harvest vibration energy of the columns. The harvested power is shown in Fig. 6.2d that is, in average, 78.97.

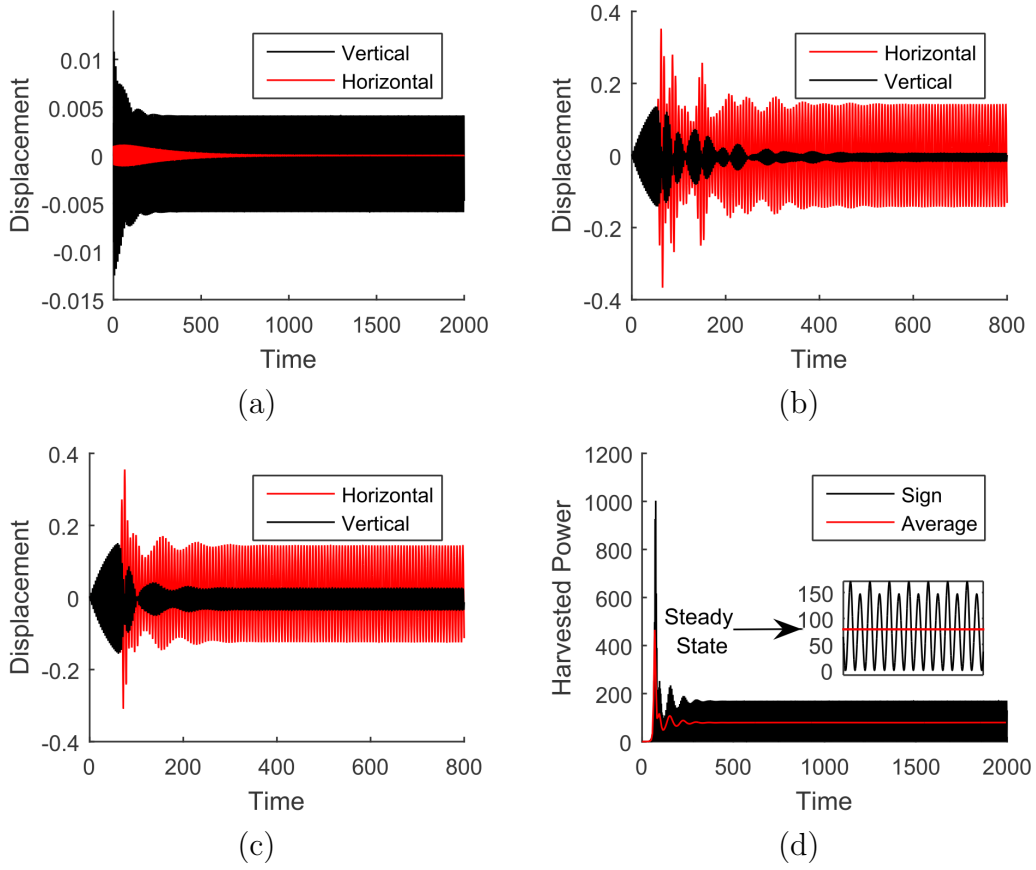

Figure 6.2: Time histories of the displacements, considering the shaker, of horizontal (in gray) and vertical (in black) motions. (a) $\omega_n = 100 rad/s$ and $\theta = 0$, (b) $\omega_n = 148 rad/s$ and $\theta = 0$, (c) $\omega_n = 148 rad/s$ and $\theta = 0.3$; (d) time history of the harvested power with $\omega_n = 148 rad/s$ and $\theta = 0.3$

In addition, the Poincare maps of Figs. 6.3, which is shown by the gray dots with the phase plane in black, show that the system is period-2 to the horizontal coordinate, in Fig.

6.3a, and period-2 to the vertical coordinate, in Fig. 6.3b.

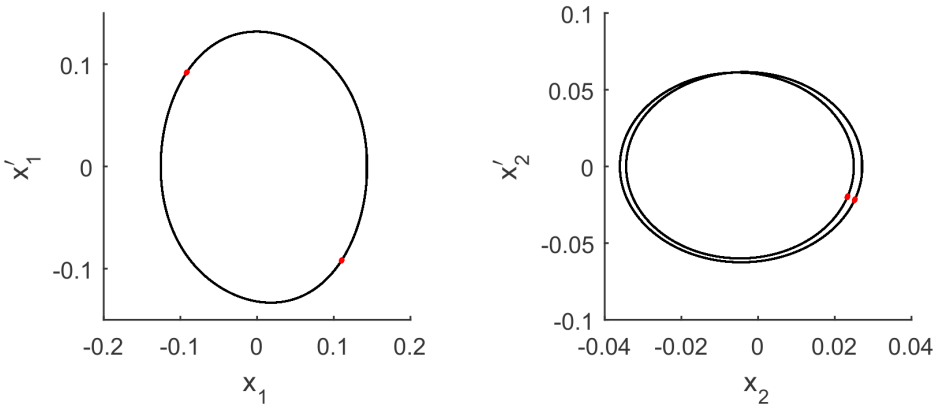

(a) (b)

Figure 6.3: Full portal frame phase plane (in black) and Poincaré map (gray dot) with $\omega_n = 148 rad/s$ and $\theta = 0.3$, (a) Horizontal, (b) Vertical

In the following, the Fast-Fourier Transform (FFT) illustrated in Fig. 6.4 shows that, even with the electro-dynamical shaker, the system continues to possess the 2:1 internal resonance.

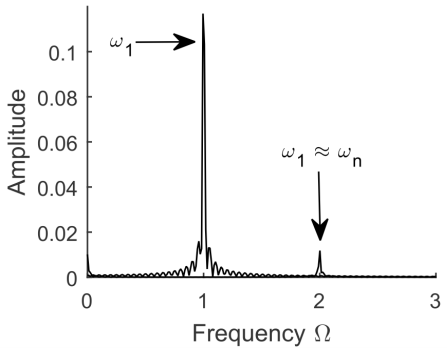

Figure 6.4: FFT with $\omega_n = 148 rad/s$ and $\theta = 0.3$

Therefore, knowing the importance of the frequency of the shaker, the next section will analyze its influence to the behaviour of the system and to the energy harvesting, and its influence considering the shaker.

6.2 Influence of the frequency of the shaker

In this section, the frequency of the electro-dynamical shaker will be analyzed making possible to observe the values of the frequency where the saturation phenomenon appears changing the energy harvesting of the system as in Sec. 4.2.

Firstly, the analysis of the harvested power related to the dimensional and dimensionless shaker's frequency is illustrated, respectively, in Figs. 6.5a and 6.5b. The range of dimensional frequency is $140 \leq \omega_n \leq 155[rad/s]$ while the dimensionless range is $1.9 \leq \Omega \leq 2.1$, which are the ranges used to the parametrical analysis. Therefore, the results of Fig. 6.5a shows that the energy harvesting is efficient when there is saturation phenomenon. As it is known, saturation occurs when $\omega_n \approx \omega_2 + \sigma$, where σ is a detuning factor which represents the interval of frequency that the amount of power is higher than the other values. Thus, the interval of high amount of power is when the dimensionless frequency is $141.2 \leq \omega_n \leq 154.0[rad/s]$ whose dimensionless range is $1.908 \leq \Omega \leq 2.081$. The harvested power in this interval of frequency is $70.61 \leq P_{avg} \leq 112.6$ where the maximum power is when $\omega_n = 152.1 rad/s$, in dimensionless $\Omega = 2.056$, whose amount of power is very higher than in Sec. 4.2.

Figures 6.6 shows the bifurcation diagrams constructed to analyze the behaviour of the system along the shaker's frequency variation. When the system is out of the saturation interval, both coordinates possess period-1 behaviour. When the system is in the saturation interval $1.908 \leq \Omega \leq 2.081$, it possesses period-2 to both coordinates.

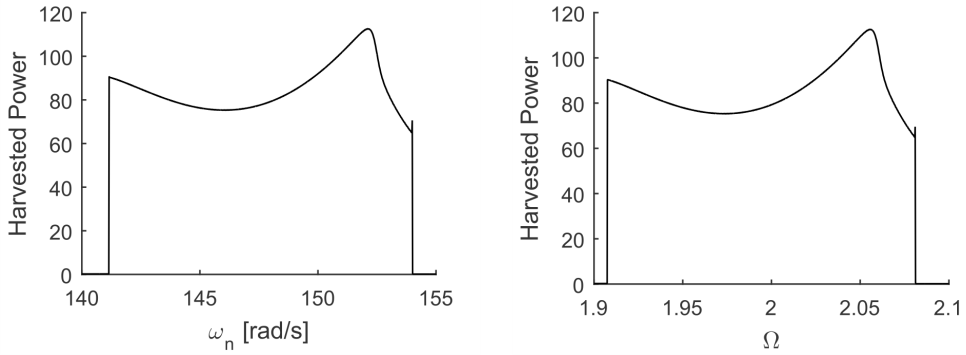

Figure 6.5: Parametrical analysis of the shaker's frequency related to the average power to (a) ω_n (dimensional), (b) Ω (dimensionless)

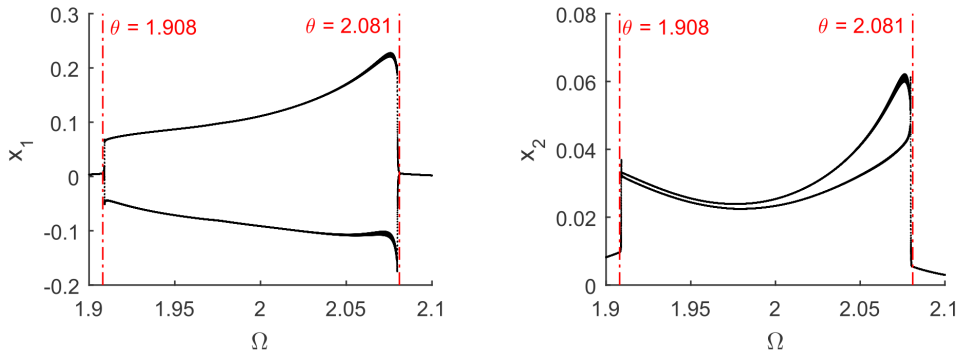

Figure 6.6: Bifurcation diagram of the dimensionless shaker's frequency Ω related to the (a) horizontal, (b) vertical coordinates

A deep analysis of the stability of the system considering the shaker was carried out in Figs. 6.7. The surface of Fig. 6.7a shows the peaks that are the instability points of the system, where the displacements tends to infinite. The countour in Fig. 6.7b shows a better description of the surface, which contains some coloured fullfilled areas, that are the instability behaviours and the white areas that are the stable area. A detailed description of these areas are separated in three regions in Tab. 6.2.

In region 3 the system is out of resonance, consequently out of saturation. Higher the amplitude of the shaker, no effect is given to the column. Hence, the column displacements is almost zero.

When system is approximating to resonance with the vertical coordinate, saturation begins to appear, and the column displacements increases, that is, part of the vertical vibration energy is transferred to the horizontal mode that is what region 1 shows in Fig. 6.7b. The column displacements are not zero anymore, growing significantly to keep the system stable. It is the best area to harvest energy.

However, there is a limit which the amplitude of the shaker has stable behaviour, that is approximately $e_0 = 73.6V$. It is shown by region 2 that the column displacements is higher than 5 in various locations. Therefore, it is possible to see that, with saturation, we have a significantly sensibility in some parameters, in special, the frequency of the shaker, because of the conditions to the phenomenon occurs.

Table 6.2: Studied regions of Fig. 6.7b

Regions	Color	Frequency $\omega_n[rad/s]$	Amplitude e_0 [V]
1	Blue	$120.1 \leq \omega_n \leq 174.6$	$0 \leq e_0 \leq 73.6[V]$
2	Red	$120.1 \leq \omega_n \leq 174.6$	$73.6 \leq e_0 \leq 500[V]$
3	Black	$\omega_n < 120.1$ and $\omega_n > 174.6$	$0 \leq e_0 \leq 500[V]$

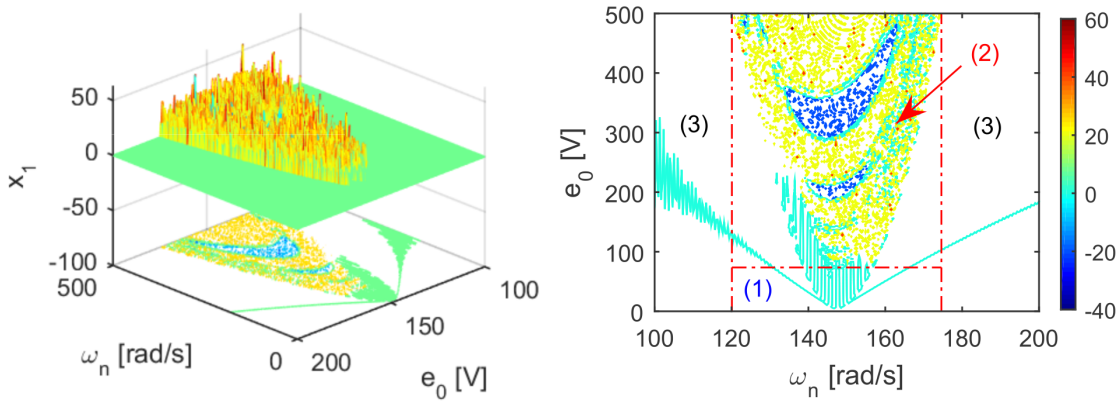

(a) (b)

Figure 6.7: (a) Surface (b) Contour; of the shaker's frequency $\omega_n[rad/s]$ related to the shaker's amplitude $e_0[V]$ and the maximum displacement of the structure

The summary of this section of the influence of the shaker's frequency is summarized in Tab. 6.3. As the frequency is an important parameter to the system behaviour's changing and the energy harvesting, in the next section, the analysis of the piezoelectric coefficients will be carried out because of its directly influence on the energy harvesting.

Table 6.3: Summary of Sec. 6.2

Frequency	Behaviour		Average Power
	Horizontal	Vertical	
$141.2rad/s \leq \omega_n \leq 154.0rad/s$ (Dimensional)	Periódic - 2	Periódic - 2	$70.61 \leq P_{avg} \leq 112.6$
$1.908 \leq \Omega \leq 2.081$ (Dimensionless)			

6.3 Influence of the piezoelectric material

As it is known, the piezoelectric material is coupled to the main structure in order to harvested energy from the vibration of the columns. This can change the behaviour of the system because the material transform such mechanical energy into electric energy. It will depend on its strain coefficient. In addition, the piezoelectric material is considered a nonlinear device because of the hysteresis. Thus, this section will be divided in two subsections, firstly analyzing the case of the sole linear piezoelectric coefficient, and, in the following, the case of the linear and nonlinear piezoelectric coefficient.

6.3.1 Case of the sole linear piezoelectric material $\Theta = 0$

Considering the linear piezoelectric material and the electro-dynamical shaker, in this section, the analysis of the sole linear piezoelectric coefficient will be analyzed related to the energy harvesting and the behaviour of the system.

Firstly, the parametrical analysis of the linear piezoelectric coefficient, in the interval $0 \leq \theta \leq 0.5$, related to the energy harvesting is carried out, where the results are shown in Fig. 6.8. The harvested amount of power is directly influenced by the linear coefficient, because until a certain value of the linear coefficient, higher its value higher is the harvested power, which has its maximum at $\theta = 0.3038$ with $P_{max} = 79.79$. However, after the maximum, the energy harvesting decreases tending to zero, fastly.

Figures 6.9a and 6.9b show the bifurcation diagram of the parametrical analysis of the linear coefficient related to the horizontal and vertical motions, respectively. When the energy harvesting increases, the system behave like a period-2. When the energy harvesting decreases, it is due to the fact of the system begins to become totally unstable. Therefore, there are two ranges of the coefficient's value to be considered, which is in Tab. 6.4.

Table 6.4: Numerical results to the linear piezoelectric coupling

Linear Piezoelectric Coefficient θ	General Behaviour	Average Power	Conclusion
$0 \leq \theta \leq 0.3038$	Periodic-2 (Stable)	$0 \leq P_{avg} \leq 79.79$	Gain of Energy
$0.3038 < \theta \leq 0.5$	- (Unstable)	P_{avg} tends to zero	Loss of Energy

In the following subsection will be performed the same analysis of the linear piezoelectric coefficient, however, considering the influence of the NONLINEAR coefficient fixed at $\Theta = 1$.

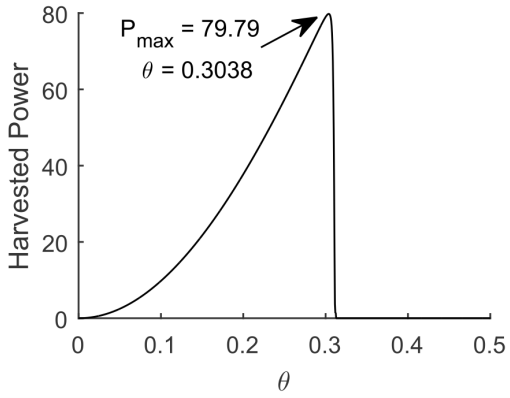

Figure 6.8: Parametrical variation of the linear piezoelectric coefficient θ related to the average harvested power, considering the shaker

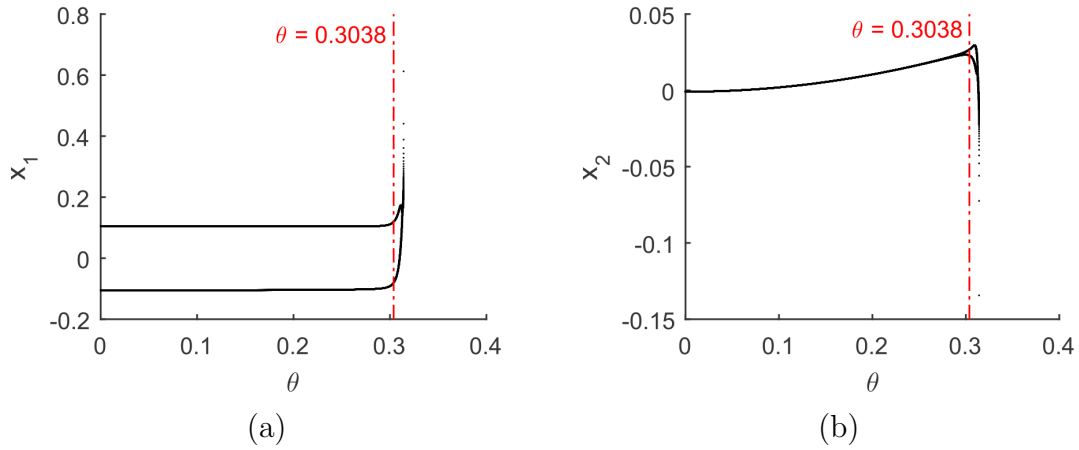

Figure 6.9: Bifurcation diagram, considering the shaker, of the linear piezoelectric coefficient θ related to the (a) horizontal, (b) vertical coordinates

6.3.2 Case of the nonlinear piezoelectric material $\Theta = 1$

As it was decribed in Subsec. 4.3.2, the piezoelectric material is considered as a nonlinear material. Thus, in this subsection, its nonlinear coefficient will be considered fixed $\Theta = 1$, and the same analysis of the linear coefficient will be carried out.

Thus, Fig. 6.10 shows the analysis of the linear piezoelectric coefficient to the interval $0 \leq \theta \leq 0.5$ considering the contribution of the nonlinear coefficient. In this case, the amount of power continues to increase until a different maximum of power at $\theta = 0.2763$ with $P_{max} = 83.85$. The maximum power is a little higher related to the linear case, also, the linear coefficient is smaller to reach the same value of power. When the system begins to decrease its amount of power until zero with $\theta > 0.2763$, with the nonlinear contribution.

The bifurcation diagrams of the linear piezoelectric coefficient variation related to the

horizontal and vertical motions are shown, respectively, in Fig. 6.11a and 6.11b. When the energy harvesting is increasing, the system continues to be Period-2. However, when the energy harvesting begin to decrease, the unstable behaviour appears more fastly than in the linear case, i.e., it appears after $\theta = 0.2763$. Table 6.5 shows a summary of this subsection.

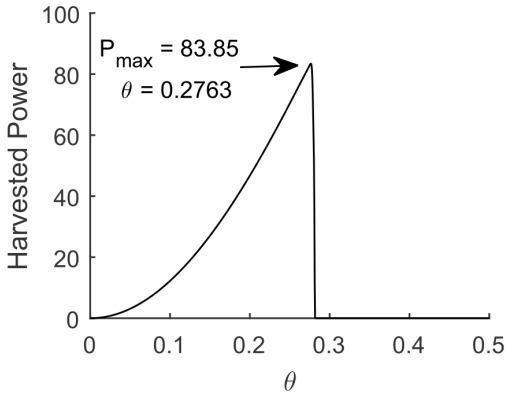

Figure 6.10: Parametrical variation of the linear piezoelectric coefficient θ related to the average harvested power, considering shaker and $\Theta = 1$

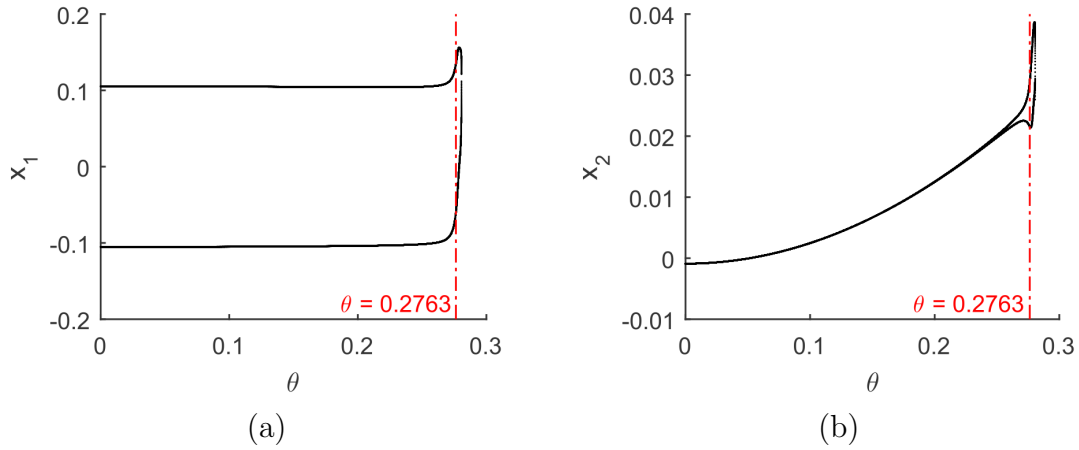

Figure 6.11: Bifurcation diagram, considering shaker and $\Theta = 1$, of the linear piezoelectric coefficient θ related to the (a) horizontal, (b) vertical coordinates

Other important factor to be studied is the initial conditions, because it may becomes from unstable behaviour to a stable behaviour. Therefore, considering the electro-dynamical shaker as a base excitation device, the analysis of the initial conditions related to the variation of the amplitude of the shaker will be carried out.

Table 6.5: Numerical results to the linear piezoelectric coefficient considering its nonlinearity and the electro-dynamical shaker

Linear Piezoelectric Coefficient θ	General Behaviour	Average Power	Conclusions
$0 \leq \theta \leq 0.2763$	Period-2 (Stable)	$0 \leq P_{avg} \leq 83.85$	Gain of Power
$0.2763 < \theta \leq 0.5$	- (Unstable)	P_{avg} tends to zero	Loss of Power

6.4 Influence of the Shaker's Amplitude *versus* Initial Conditions

In Sec. 4.4, the study of the initial conditions of the portal frame foundation *versus* the amplitude of the external excitation was carried out. The initial conditions showed to be a great influence to the stability of the system related to the increasing of the amplitude of the external excitation. Therefore, in this section, the analysis of the initial condition *versus* the shaker's amplitude will be performed to further comparison related to the results of Sec. 4.4.

Thus, firstly, considering the linear piezoelectric coefficient $\theta = 0.3$ and $\Theta = 0$, the parameters of Tab. 6.1, and the interval of the shaker's amplitude $1 \leq e_0 \leq 500[V]$ ($0 \leq E_0 \leq 2573$), the analysis of the interval of the initial conditions $0 \leq x_{0i} \leq 0.3$ *versus* shaker's amplitude related to the maximum horizontal displacement were carried out and illustrated in Fig. 6.12.

Figures 6.12a, 6.12b, 6.12c and 6.12d show surfaces of the maximum horizontal displacement of the structure related to the initial conditions of horizontal displacement (x_{01}), horizontal velocity (x'_{01}), vertical displacement (x_{02}), vertical velocity (x'_{02}), respectively. The peaks are considered as the unstable points of the system, that is, when the displacement tends to infinite. The planes are the stable behaviour. The surfaces which possess the bigger plane areas, i.e., more stable behaviour are Figs. 6.12a, 6.12b.

A deep analysis of the surfaces of Figs. 6.12a, 6.12b is shown in the contours of Figs. 6.13a and 6.13b, respectively. The best initial condition, which possesses the highest interval, $0 \leq e_0 \leq 250[V]$ ($0 \leq E_0 \leq 1286$), of varying the shaker's amplitude is the initial horizontal velocity condition of value $x'_{01} = 0.3015$. In addition, the best initial horizontal displacement condition $x_{01} = 0.1658$ possesses a big interval of the shaker's amplitude with $0 \leq e_0 \leq 244[V]$ ($0 \leq E_0 \leq 1255.6$), however, as x'_{01} has the higher interval.

However, in the new initial conditions, there is a region (Q) where there are many stable and unstable behaviours which is worth to study, because the behaviour of there is a change of the behaviour of the system.

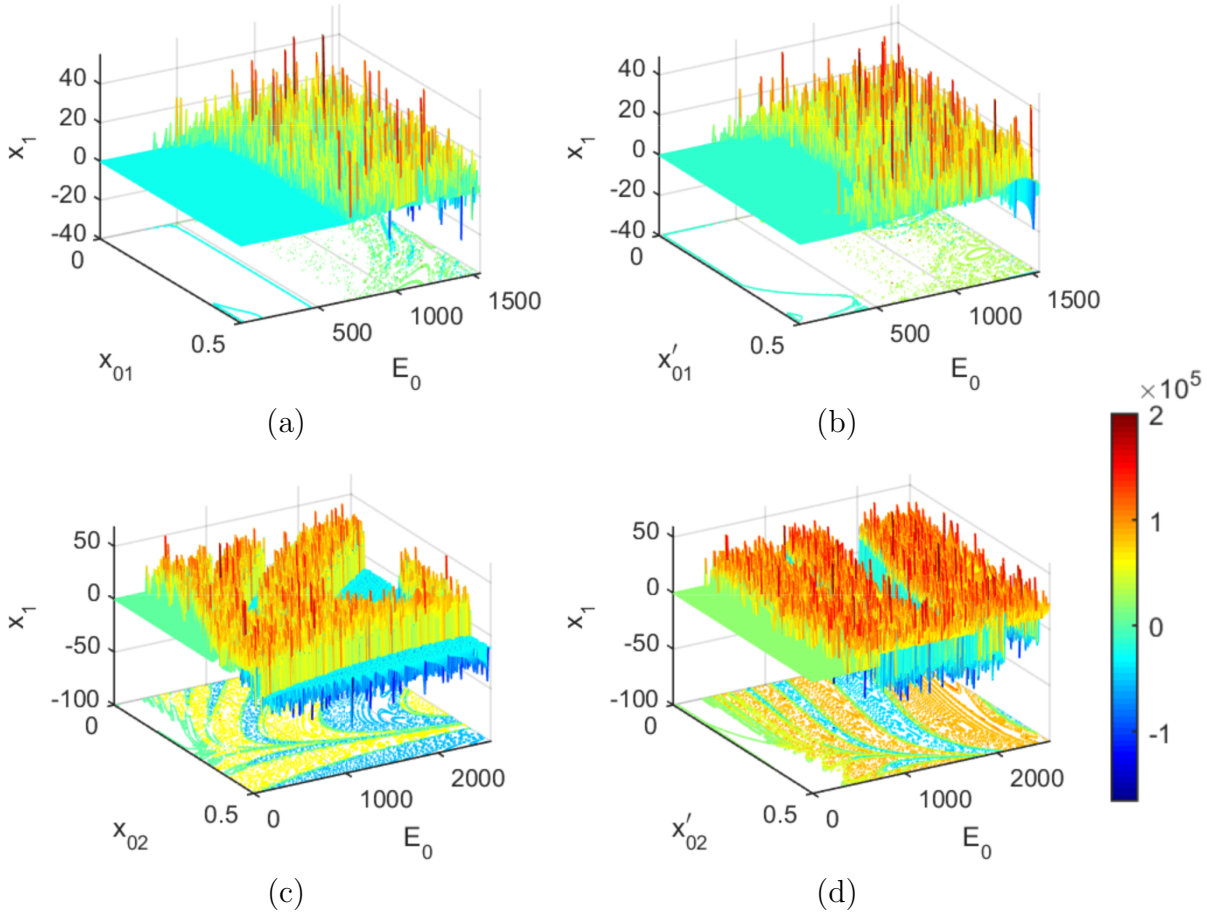

Figure 6.12: Surface of the maximum horizontal displacement related to the shaker's amplitude of the external excitation and initial conditions (a) x_{01}, (b) x'_{01}, (c) x_{02}, (d) x'_{02}

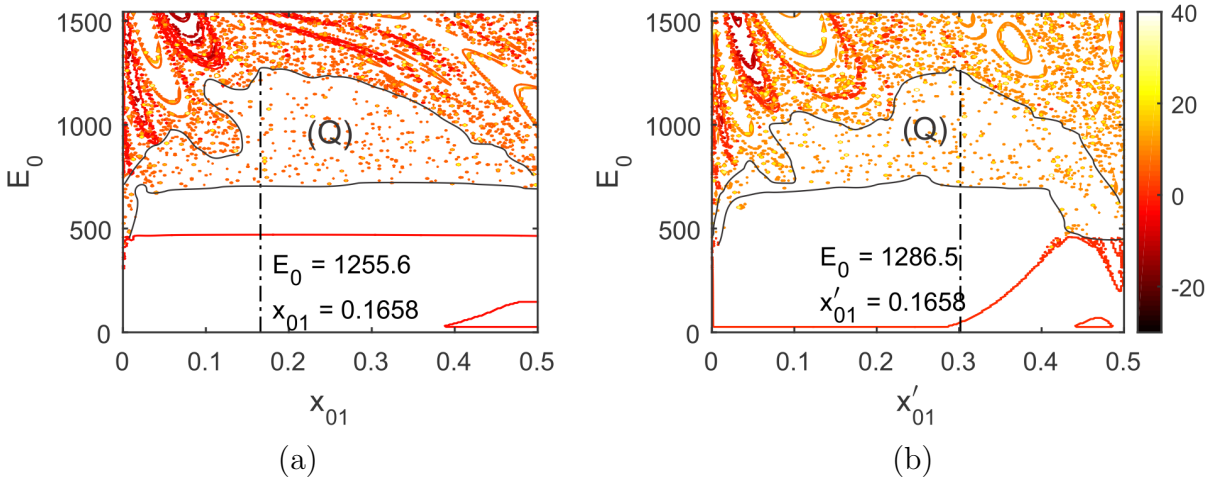

Figure 6.13: Contour of the maximum displacement of the structure related to the shaker's amplitude E_0 versus (a) x_{01}, (b) x'_{01}

Using the new initial condition $x'_{01} = 0.3015$, a variation of the electro-dynamical shaker's amplitude E_0 is carried out to the interval $0 \leq e_0 \leq 250[V]$ ($0 \leq E_0 \leq 1286.5$), related to the harvested power, as illustrated in Fig. 6.14. In this new case, the figure is divided in three regions. In region 1, the energy harvesting of the system increases linearly until the maximum in $e_0 = 69.1V$ ($E_0 = 355.59$) with $P_1 = 131.3$, After that, in region 2, the energy harvesting decays from the maximum to $P_2 = 76.9$ in $e_0 = 117.4V$ ($E_0 = 604.14$), and the system still has stable behaviour. However, in region 3, it is shown irregulars points. It is due to the fact that region 3 is in the region (Q) of Figs. 6.13a and 6.13b. In this region, the system has stables and unstable behaviours, however, it is not a periodic orbit.

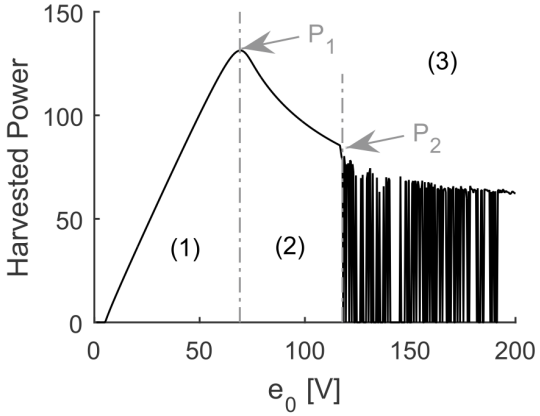

Figure 6.14: Parametrical variation of the shaker's amplitude $e_0[V]$ related to the average harvested power with $x'_{01} = 0.3015$

The bifurcation diagrams of the same interval of the electro-dynamical shaker's amplitude $0 \leq e_0 \leq 250[V]$ ($0 \leq E_0 \leq 1286$) is constructed in Figs. 6.15a, 6.15b in order to observe what happens in each region. In regions 1 and 2, the system keeps periodic-2. However, in region 3, the system presents an irregular motion, i.e., a quasiperiodic orbit or chaotic behaviour. Approximating region 3 in Fig. 6.15c and 6.15d, it is possible to conclude that the irregular motion is a quasiperiodic orbit.

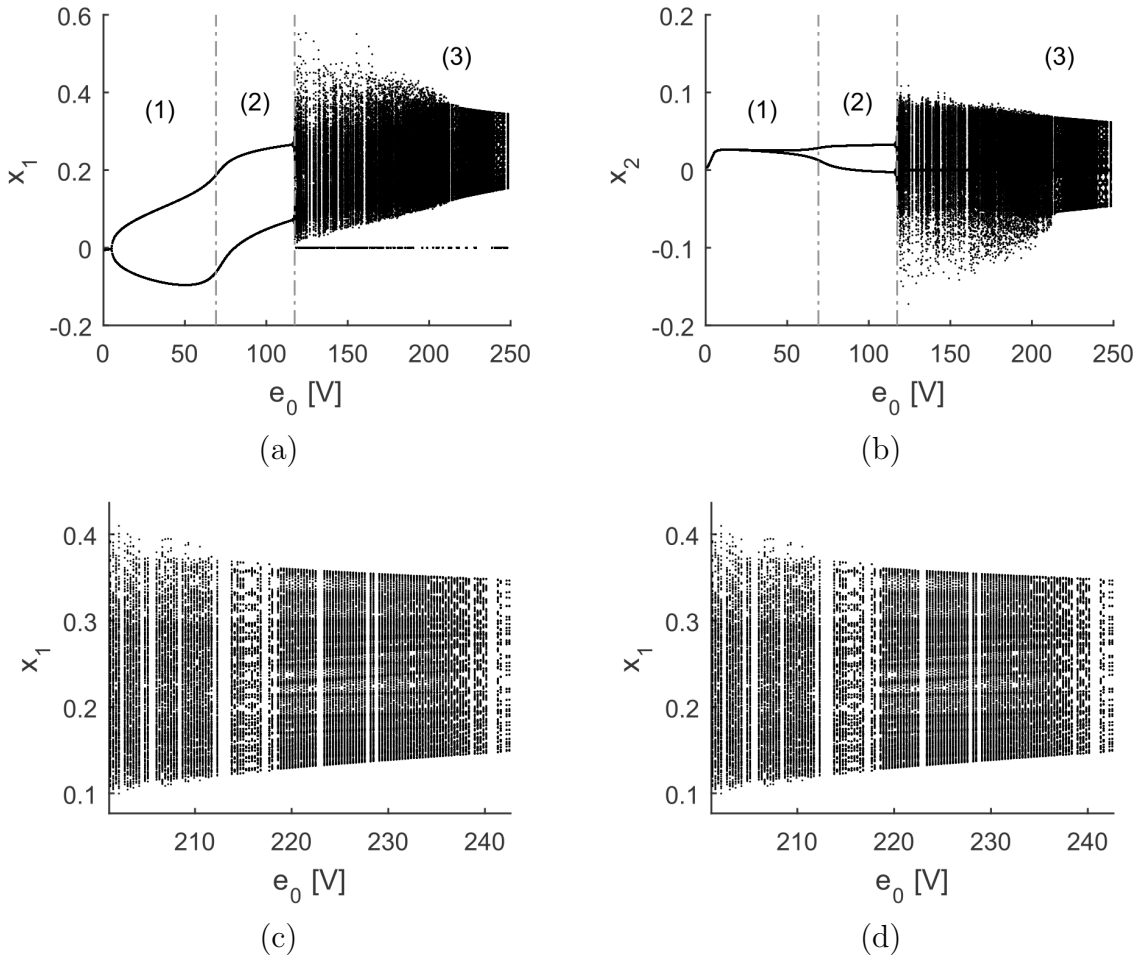

Figure 6.15: Bifurcation diagrams of the electro-dynamical shaker's amplitude $e_0[V]$ with $x'_{01} = 0.3015$

A deeply analysis of the irregular behaviour of the system in region 3, with $e_0 = 233V$ ($E_0 = 1199$) and still $x'_{01} = 0.3015$, is carried out in Figs. 6.16, that shows a Fast-Fouried Transform (FFT) and Poincaré maps of the portal frame.

Figure 6.16a shows the FFT of the portal frame with $e_0 = 233V$ ($E_0 = 1199$) and $x'_{01} = 0.3015$. There are many well defined peaks, different of a chaotic behaviour which would be almost a continuous spectrum and different of a periodic behaviour which would be very well defined unique peaks in resonance, as Fig. 4.4.

Moreover, Figs. 6.16b and 6.16c shows the phase planes (in black) and Poincare Maps (in gray) of the horizontal and vertical motions of the main structure, respectively. It is possible to observe that the poincare maps is shown as very well defined loops, which represents, and concluding, a quasiperiodic behaviour.

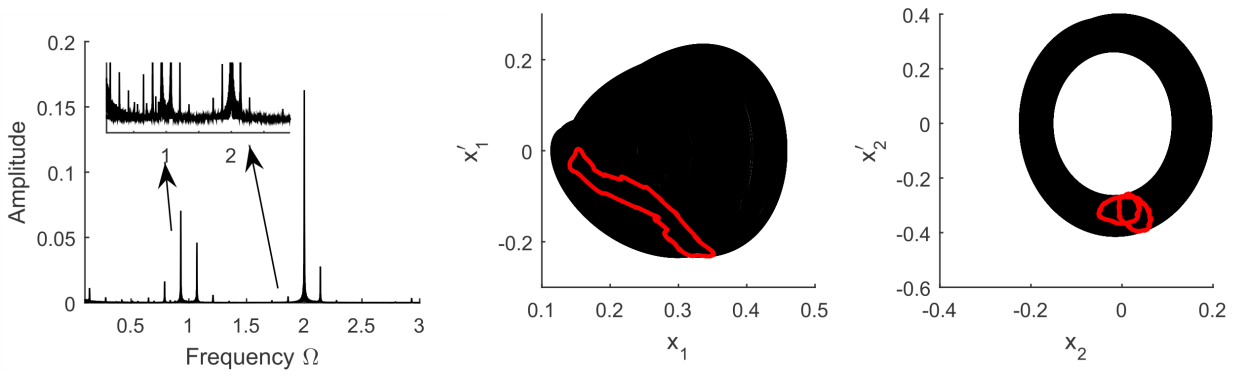

(a) (b) (c)

Figure 6.16: (a) FFT (b) Phane plane (in black) and Poincare Map (in gray) of the horizontal displacement of the portal frame (c) Phane plane (in black) and Poincare Map (in gray) of the vertical displacement of the portal frame; with $e_0 = 233V$ $(E_0 = 1199)$, $x'_{01} = 0.3015$

With the new initial condition was possible to increase the energy harvesting because of the higher interval of the electro-dynamical shaker's amplitude usage. In addition, a quasiperiodic behaviour was found, which is with many unstable behaviours. A summary of this section is presented in Tab. 6.6.

Table 6.6: Numerical results of the initial displacement condition x'_{01} variation related to the amplitude of the electro-dynamical shaker

Amplitude of the Electro-dynamical Shaker $e_0[V]$ (E_0)	Behaviour	Initial Displacement Condition x_{01}	Average Harvested Power	Stability
40 (205.84)	Periodic-2	0.001	78.97	Stable
69.1 (355.59)	Periodic-2	0.001	131.3	Stable
117.4(604.14)	-	0.001	-	Unstable
	Quasiperiodic	0.3015	76.92	Stable
233(1199)	-	0.001	-	Unstable
	Quasiperiodic	0.3015	61.92	Stable

As the amplitude and the new initial conditions showed to be very important, it is worth to study different combination of parameters with the previous ones. One of them is the piezoelectric coupling because of its directly influence on the energy harvesting. Therefore, an overview of combinations among the amplitude of the electro-dynamical shaker *versus* piezoelectric parameters related the harvested power will be carry out in the next Subsection.

6.4.1 Electro-Dynamical Shaker‘s Amplitude *versus* Sole Linear Piezoelectric Coefficient Case

Now, in this subsection, the piezoelectric coefficient will be evaluated related to the electro-dynamical shaker‘s amplitude comparing the first initial condition results $x_{01} = 0.001$ to the new initial condition results $x'_{01} = 0.3015$. As the piezoelectric coefficient is direclty linked to the energy harvesting, it is very important to study the initial condition influence to the material *versus* the device's amplitude.

Moreover, in order to compare the results obtained in this subsection to the Subsec. 4.3.1, the same analysis of stability and harvested power related to the electro-dynamical shaker's amplitude *versus* linear piezoelectric coefficient, i.e., $0 \leq e_0 \leq 500[V]$ ($0 \leq E_0 \leq 2573$) *vs* $0 \leq \theta \leq 0.5$, varying the initial condition between $x_{01} = 0.001$ and $x'_{01} = 0.3015$ is carried out.

The first analysis of this subsection is shown in Figs. 6.17, which considers the initial condition as $x_{01} = 0.001$.

Figure 6.17a shows the contour of the electro-dynamical shaker's amplitude *versus* linear piezoelectric coefficient related to the maximum horizontal displacement of the portal frame. The coloured area means the instability of the system, whose displacements tends to infinite. The white area means the stable behaviour which goes from $0 \leq \theta \leq 0.3038$, as shown in Subsec. 4.3.1. However, the best linear coefficient is $\theta = 0.2915$ because the shaker's amplitude has the maximum in $e_0 = 88.76V$ ($E_0 = 456.76$) (the maximum of the white area).

From Figs. 6.17b and 6.17c, which show the surface and contour of the harvested power related to the electro-dynamical shaker's amplitude *versus* linear piezoelectric coefficient, it is possible to observe that the best $\theta = 0.2915$ with $e_0 = 88.76V$ ($E_0 = 456.76$) has a maximum amount of power of $P_{max} = 174.1$.

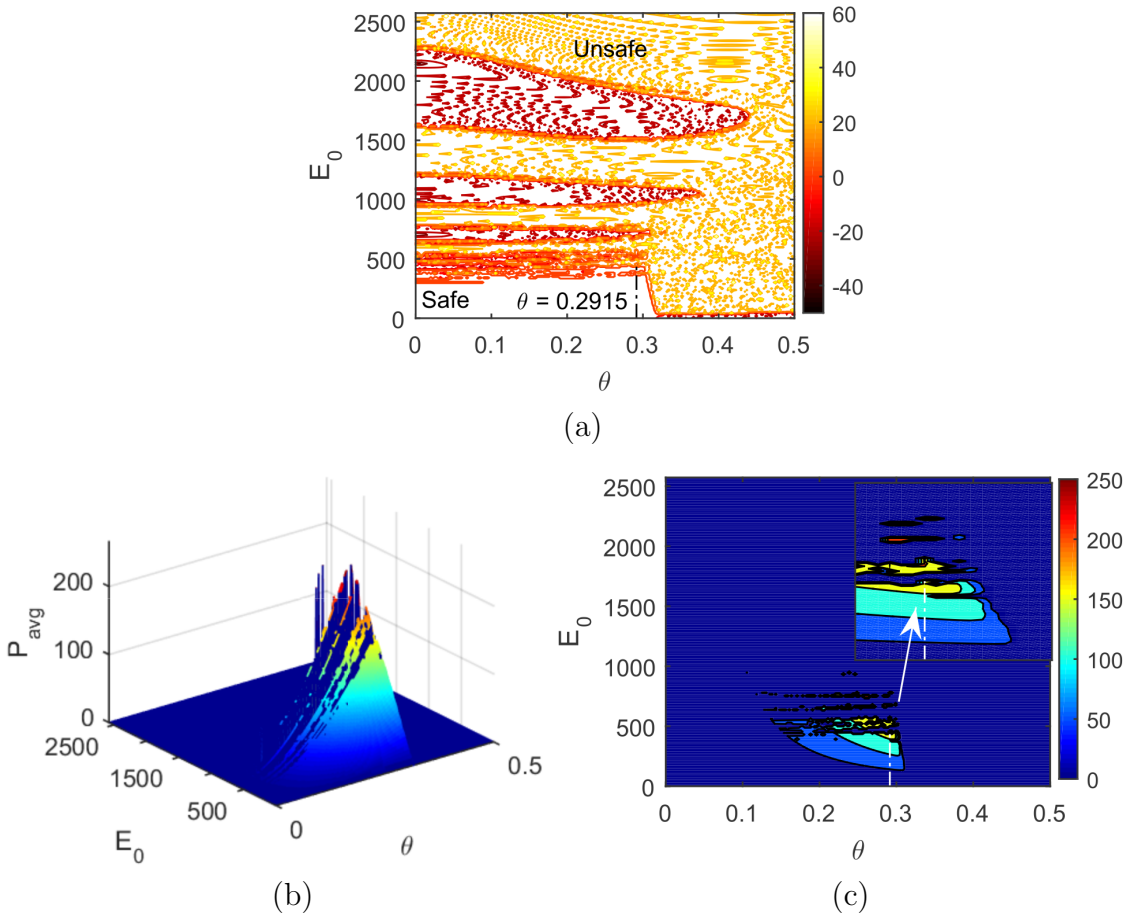

Figure 6.17: Piezoelectric linear case $\Theta = 0$ and initial condition $x_{01} = 0.001$ (a) Contour of the maximum displacement of the structure related to the amplitude E_0 versus θ; (b) surface of the harvested power related to the amplitude E_0 versus θ; (c) coloured contour of the harvested power related to the amplitude E_0 versus θ

In the case of the electro-dynamical shaker exciting the base of the portal frame, and the initial condition $x_{01} = 0.001$, the variation of the amplitude is very small, even in this linear piezoelectric case. However, with the new initial condition $x'_{01} = 0.3015$ the results are a little different.

Figure 6.18a shows the contour of the electro-dynamical shaker's amplitude *versus* linear piezoelectric coefficient related to the maximum horizontal displacement of the portal frame. The white area, of stable behaviour, increased related to the Fig. 6.17a, changing the value of best linear piezoelectric coefficient to $\theta = 0.2487$, with a maximum amplitude of $e_0 = 291V$ ($E_0 = 1497.5$), approximately, as represented by the red dotted line. In addition, the small magenta area (Q) represents where the system possesses quasiperiodic behaviour.

From Figs. 6.17b and 6.17c, which show the surface and contour of the harvested power related to the electro-dynamical shaker's amplitude *versus* linear piezoelectric coefficient,

it is possible to observe that the best $\theta = 0.2487$ with $e_0 = 291V$ ($E_0 = 1497.5$) has a maximum amount of power of $P_{max} = 403.3$, a very higher value than in the case of $x_{01} = 0.001$. In region Q, where there is a quasiperiodic behaviour, the amount of power does not overpass from $P_{quasi_{max}} \approx 100$.

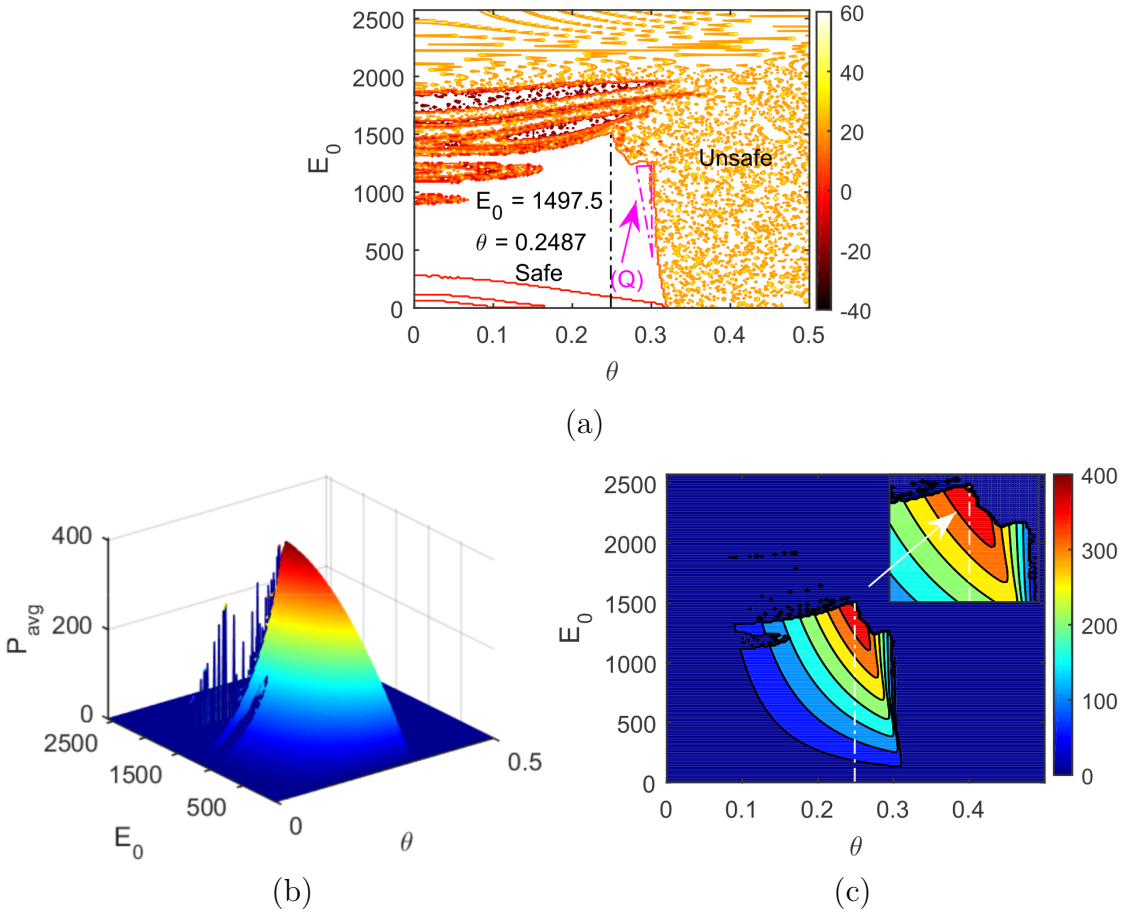

Figure 6.18: Piezoelectric linear case $\Theta = 0$ and initial condition $x'_{01} = 0.3015$ (a) Contour of the maximum displacement of the structure related to the amplitude E_0 versus θ; (b) surface of the harvested power related to the amplitude E_0 versus θ; (c) coloured contour of the harvested power related to the amplitude E_0 versus θ

Therefore, in the case of the sole linear piezoelectric material with the new initial condition, it was possible to increase the energy harvesting with higher values of the electro-dynamical shaker's amplitude keeping the periodic stable behaviour. A summary of the best configurations of this subsection is presented in Tab. 6.7.

Table 6.7: Summary of Subsec. 6.4.1

Initial Condition	Amplitude of the Electro-dynamical Shaker E_0	Linear Piezoelectric Coefficient θ	Stability	Average Power
x_{01} 0.001	$0 \leq E_0 \leq 2573$ $456.76 < E_0 \leq 2573$	$0.3038 < \theta \leq 0.5$ $0 \leq \theta \leq 0.5$	Unstable	-
	$0 \leq E_0 \leq 456.76$	$0 \leq \theta \leq 0.3038$	Stable	$0 \leq P_{avg} \leq 174.1$
x'_{01} 0.3015	$0 \leq E_0 \leq 2573$ $1497.5 < E_0 \leq 2573$	$0.32 < \theta \leq 0.5$ $0 \leq \theta \leq 0.32$	Unstable	-
	$0 \leq E_0 \leq 1497.5$	$0 \leq \theta \leq 0.32$	Stable	$0 \leq P_{avg} \leq 403.3$
Max. Power x_{01} 0.001	456.76	0.2915	Stable	174.1
Max. Power x'_{01} 0.3015	1497.5	0.2487	Stable	403.3

To conclude the whole analysis of the piezoelectric material, the nonlinear piezoelectric contribution is considered in the following due to its influence in the piezoelectric energy harvesting. Therefore, the next subsection will discuss the same analysis of the electro-dynamical shaker's amplitude *versus* linear piezoelectric coefficient considering the nonlinear piezoelectric coefficient fixed $\Theta = 1$.

6.4.2 Electro-Dynamical Shaker's Amplitude *versus* NONLINEAR Piezoelectric Case

As it is known previously, the contribution of the nonlinear piezoelectric coefficient is very important because the approximation to the experimental curve. Furthermore, in subsec. 4.4.2 was studied this influence varying the linear piezoelectric coefficient θ, the amplitude of the external force $E_0(F_0)$, and the initial conditions related to the energy harvesting and the maximum displacement of the system when the nonlinear coefficient is fixed in $\theta = 1.0$.

Therefore, in this subsection, the nonlinear piezoelectric coefficient will be considered fixed in $\Theta = 1.0$. The initial conditions will be varied between $x_{01} = 0.001$ and $x' = 0.3015$ in order to compare with the results of the linear piezoelectric case. The interval of the electro-dynamical shaker's amplitude $E_0(e_0)$ will be $0 \leq e_0 \leq 300[V]$ ($0 \leq E_0 \leq 1543.8$) and the linear piezoelectric coefficient is $0 \leq \theta \leq 0.5$. In the following, numerical simulations will be presented.

Firstly, considering the initial condition as $x_{01} = 0.001$, Figs. 6.19 are presented.

Figure 6.19a shows the contour of the electro-dynamical shaker's amplitude *versus* linear piezoelectric coefficient related to the maximum horizontal displacement of the portal frame. The coloured area and the white area on the right side of $\theta = 0.3$, approximately, the system is presented totally unstable in $0 \leq e_0 \leq 300V$ $(0 \leq E_0 \leq 1543.8)$. The small white area on the left side of $\theta = 0.3$ is stable until, approximately, $e_0 = 85.14V$ $(E_0 = 438.29)$. Moreover, the best linear piezoelectric coefficient is given by $\theta = 0.2538$ which has a maximum of stable behaviour in $e_0 = 85.14V$ $(E_0 = 438.29)$.

Looking at Figs. 6.19b and 6.19c, which show a surface and contour, respectively, of the electro-dynamical shaker's amplitude *versus* linear piezoelectric coefficient related to the average harvested power, it is possible to observe that the best $\theta = 0.2538$ with $e_0 = 85.14V$ $(E_0 = 438.29)$ has a maximum amount of power of $P_{max} = 177.4$.

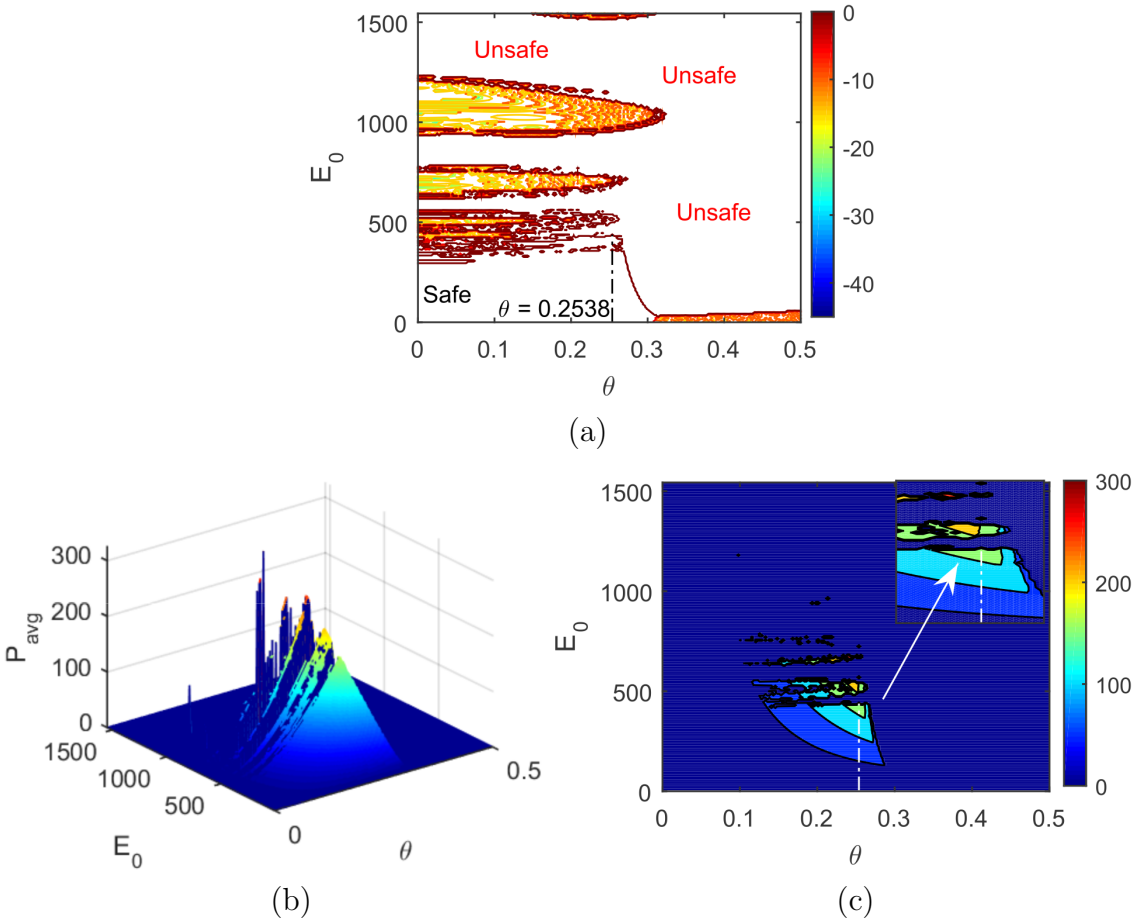

Figure 6.19: Piezoelectric nonlinear linear case $\Theta = 1$ and initial condition $x'_{01} = 0.001$ (a) Contour of the maximum displacement of the structure related to the amplitude E_0 versus θ; (b) surface of the harvested power related to the amplitude E_0 versus θ; (c) coloured contour of the harvested power related to the amplitude E_0 versus θ

With the initial condition $x_{01} = 0.001$ almost there was no difference between the nonlinear to the linear case. In the nonlinear case. the maximum amount of power is higher from $P_{lin_{max}} = 174.1$ to $P_{nonlin_{max}} = 177.4$. However, it was obtained a higher amount of power with a smaller linear piezoelectric coefficient which goes from $\theta_{lin} = 0.2915$ to $\theta_{nonlin} = 0.2538$, in addition, with a little smaller amplitude, which goes from $e_0 = 88.76V$ ($E_0 = 456.76$) to $e_0 = 85.14V$ ($E_0 = 438.29$). Here, it was possible to observe the influence of the nonlinear piezoelectric coefficient to the energy harvesting, because the amount of power may increase of decrease, it will depend on the value of the linear piezoelectric coefficient.

In the following, considering the initial condition as $x'_{01} = 0.3015$, Figs. 6.20 are presented.

Figure 6.20a shows the contour of the electro-dynamical shaker‘s amplitude *versus* linear piezoelectric coefficient related to the maximum horizontal displacement of the portal frame considering the new initial condition. In this case, the stable area increases, keeping $0 \leq \theta \leq 0.3$, approximately, with a stable area, however with the amplitude in $0 \leq e_0 \leq 283.5V$ ($0 \leq E_0 \leq 1458.9$). The coloured area near the maximum amplitude $e_0 = 283.5V$ ($E_0 = 1458.9$) and the white are of the right side of $0.3 < \theta \leq 0.5$ are unstable. furthermore in this case, the best linear piezoelectric coefficient is given by $\theta = 0.191$ which possesses a maximum of stable behaviour in $e_0 = 283.5V$ ($E_0 = 1458.9$).

Looking at Figs. 6.20b and 6.20c, which show a surface and contour, respectively, the electro-dynamical shaker‘s amplitude *versus* linear piezoelectric coefficient related to the average harvested power, it is possible to observe that the best $\theta = 0.191$ with $e_0 = 283.5V$ ($E_0 = 1458.9$) has a maximum amount of power of $P_{max} = 435.00$, approximately.

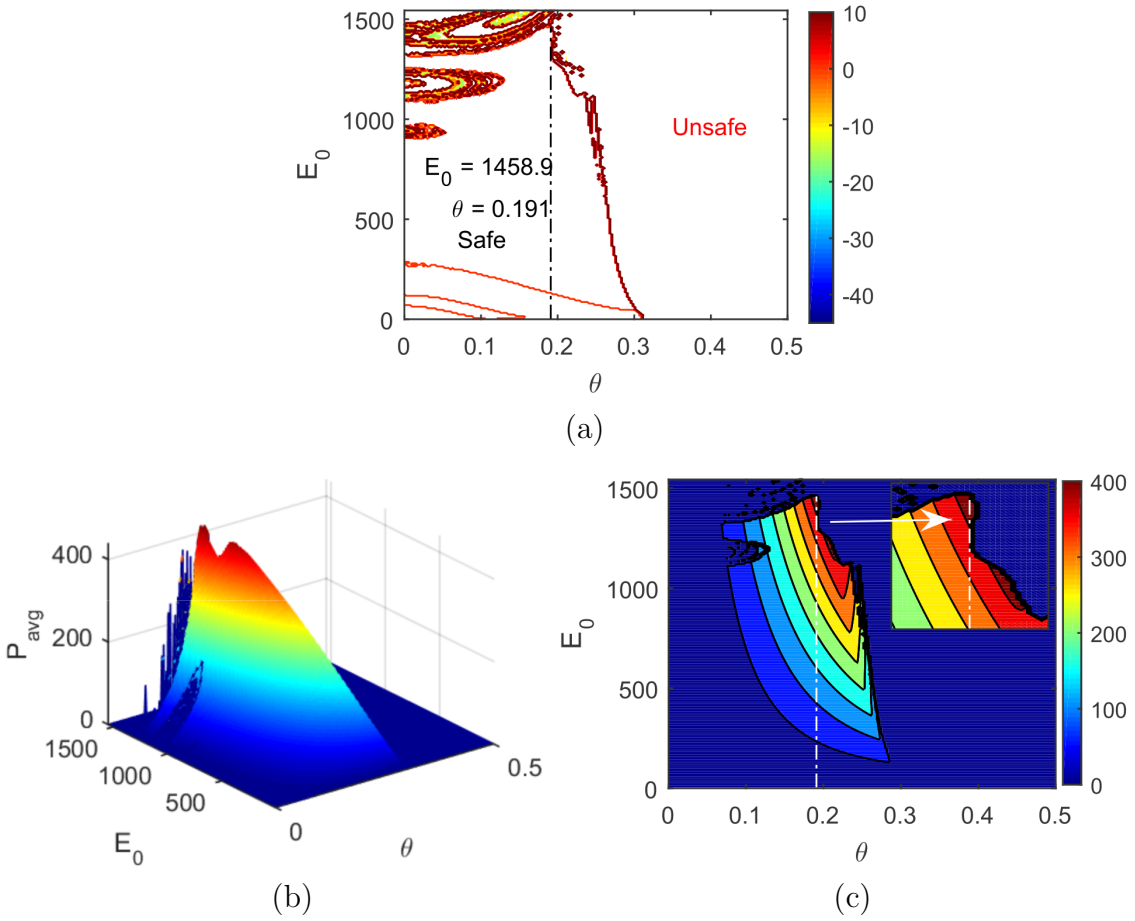

Figure 6.20: Piezoelectric nonlinear linear case $\Theta = 1$ and initial condition $x'_{01} = 0.3015$ (a) Contour of the maximum displacement of the structure related to the amplitude E_0 versus θ; (b) surface of the harvested power related to the amplitude E_0 versus θ; (c) coloured contour of the harvested power related to the amplitude E_0 versus θ

As in the case of the sole linear piezoelectric coefficient, with the new initial condition $x'_{01} = 0.3015$, the obtained results showed to be very different possessing better results of stability and energy harvesting in comparison to the case of the initial condition $x_{01} = 0.001$. There is a broad stable area with a higher maximum of harvested amount of power. Again, almost there was no difference between the nonlinear and linear case. In the nonlinear case, the maximum amount of power keeps almost the same of in the linear case, from $P_{lin_{max}} = 403.30$ to $P_{nonlin_{max}} = 403.00$. However, it was obtained with a smaller linear piezoelectric coefficient which goes from $\theta_{lin} = 0.2487$ to $\theta_{nonlin} = 0.191$. and a smaller electro-dynamical shaker's amplitude which goes from $e_{0_{lin}} = 291V$ ($E_0 = 1497.5$) to $e_{0nonlin} = 283.5V$ ($E_0 = 1458.9$).

The nonlinear piezoelectric contribution has a great influence to the energy harvesting and the behaviour of the system. When it is considered, most of time, the system is able to

harvest a high amount of power with a smaller value of the linear piezoelectric coefficient. Of course, it will depend on the value of the linear coefficient because the system may decrease the energy harvesting and becomes unstable more fastly. A summary of this subsection is presented in Tab. 6.8.

Table 6.8: Summary of Subsec. 6.4.1 in comparison to Subsec. 6.4.2

Piezoelectric Case	Initial Condition	Electro-Dynamical Shaker's Amplitude E_0	Linear Piezoelectric Coefficient θ	Stability	Average Power
$\Theta = 0$ Linear	x_{01} 0.001	$0 \leq E_0 \leq 2573$ $456.76 < E_0 \leq 2573$	$0.3038 < \theta \leq 0.5$ $0 \leq \theta \leq 0.5$	Unstable	-
	x'_{01} 0.3015	$0 \leq E_0 \leq 2573$ $1497.5 < E_0 \leq 2573$	$0.32 < \theta \leq 0.5$ $0 \leq \theta \leq 0.32$	Unstable	-
	x_{01} 0.001	$0 \leq E_0 \leq 456.76$	$0 \leq \theta \leq 0.3038$	Stable	$0 \leq P_{avg} \leq 174.1$
	x'_{01} 0.3015	$0 \leq E_0 \leq 1497.5$	$0 \leq \theta \leq 0.32$	Stable	$0 \leq P_{avg} \leq 403.3$
$\Theta = 1$ Nonlinear	x_{01} 0.001	$0 \leq E_0 \leq 1543.8$ $438.13 < E_0 \leq 1543.8$	$0.3 \leq \theta \leq 0.5$ $0 \leq \theta \leq 0.3$	Unstable	-
	x'_{01} 0.3015	$0 \leq E_0 \leq 1543.8$ $1458.9 < E_0 \leq 1543.8$	$0.3 < \theta \leq 0.5$ $0 \leq \theta \leq 0.3$	Unstable	-
	x_{01} 0.001	$0 \leq E_0 \leq 438.13$	$0 \leq \theta \leq 0.3$	Stable	$0 \leq P_{avg} \leq 177.4$
	x'_{01} 0.3015	$0 \leq E_0 \leq 1543.8$	$0 \leq \theta \leq 0.3$	Stable	$0 \leq P_{avg} \leq 435.00$
$\Theta = 0$ Linear	Max. Power x_{01} 0.001	456.76	0.2915	Stable	174.1
	Max. Power x'_{01} 0.3015	1497.5	0.2487	Stable	403.3
$\Theta = 1$ Nonlinear	Max. Power x_{01} 0.001	438.13	0.2538	Stable	177.4
	Max. Power x'_{01} 0.3015	1458.9	0.191	Stable	435.00

Therefore, PART II ends here with the analysis of the portal frame foundation excited by and electro-dynamical shaker. The next chapter will present the conclusions of this work comparing the results of the system excited by an harmonic force to the one excited by and electro-dynamical shaker.

Chapter 7

Conclusions

In this work, the energy harvesting of a portal frame foundation of two-degrees-of-freedom based on a nonlinear piezoelectric material considering a 2:1 internal resonance between the modes of vibration of the dynamical system with ideal and non-ideal excitations was studied. It was divided into two parts, which are PART I and PART II. The PART I consists of the study of the portal frame excited by a harmonic force. The PART II considers the portal frame excited by an electro-dynamical shaker. Therefore, the main purpose of this work is to compare the energy harvesting between both cases.

The first subject to be discussed is the saturation phenomenon. As explained along this work, saturation phenomenon is when the vibration energy of a coordinate in a two-degrees-of-freedom system is partially-transferred to the second coordinate. In addition, there are the conditions of 2:1 internal resonance, $\omega_2 \approx 2\omega_1 + \sigma$, and external resonance, $\omega_n \approx \omega_2 + \sigma$. In the studied portal frame foundation, the saturation phenomenon occurred and was of great importance to the energy harvesting. As the piezoelectric ceramics are coupled in a column, the vibration energy transferred from the vertical displacement, which is the excited direction, to the horizontal displacement makes the energy harvesting increase very much, even to both PARTs of the work.

Therefore, the frequency of excitation is a fundamental factor because the saturation phenomenon depends on the value of these parameter. A range of frequencies of the external force and the electro-dynamical shaker was analyzed related to the harvested power and to the displacement of the portal frame. When the dynamical system is on effect of saturation phenomenon, the system is periodic-2 most of time considering the parameter values of Tab. 4.1 and 6.1, and the harvested amount of power goes from near ZERO to a higher value. Moreover, depending on the value of the frequency, it is possible to improve the energy harvesting. Table 7.1 shows the values of the frequency when there is and there is not saturation phenomenon comparing the dynamical system excited by the external force and the electro-dynamical shaker. The most noted difference is the ranges

of frequency and average powers, whose electro-dynamical shaker possesses the higher range and higher amount of powers. Furthermore, when there is saturation phenomenon, the system becomes hardly unstable.

Table 7.1: Summary of the comparison between the frequencies of Sec. 4.2 and 6.2

PART	Frequency	Saturation Phen. +/-	Behaviour		Average Power
			Hor.	Vert.	
I	$\omega_n < 144$ and $\omega_n > 151.2[rad/s]$	-	Periodic-1		$P_{avg} \approx 7x10^{-7}$
	$144 \leq \omega_n \leq 151.2[rad/s]$ (Dimensional) $1.948 \leq \Omega \leq 2.042$ (Dimensionless)	+	Periodic-2		$26.56 \leq P_{avg} \leq 38.97$
	$\Omega_{P_{max}} = 2.042$				$P_{avg} = 38.97$
II	$\omega_n < 141.2$ and $\omega_n > 154.0[rad/s]$	-	Periodic-1		$0 \leq P_{avg} \leq 0.2269$
	$141.2 \leq \omega_n \leq 154.0[rad/s]$ (Dimensional) $1.908 \leq \Omega \leq 2.081$ (Dimensionless)	+	Periodic-2		$70.61 \leq P_{avg} \leq 112.6$
	$\Omega_{P_{max}} = 2.056$				$P_{avg} = 112.6$

Following the analysis of the frequencies, one the most important objectives of this work is the analysis of the nonlinear piezoelectric material because it is directly linked to the piezoelectric material which is the transduction mean of the vibration energy of the column. In the analysis of the sole linear piezoelectric case, higher the linear piezoelectric material higher will be the energy harvesting, however it will depend on its value. After a certain value, the dynamical system presents unstable behaviour. Considering the nonlinear piezoelectric case fixed at $\Theta = 1.0$, the variation of the linear piezoelectric coefficient until the dynamical system presents unstable behaviour decreased, however the maximum harvested amount of power increased. Next, considering the comparison between the results of PART I and PART II. When the electro-dynamical shaker excites de base of the portal frame, the interval of the linear piezoelectric coefficient decreased to both linear and nonlinear cases, related to the case of the excitation by a harmonic force. However, the harvested amount of power increased, i.e., the dynamical system becomes unstable more fastly. These results are shown in Tab. 7.2.

Table 7.2: Summary of the nonlinear piezoelectric material contribution with ideal and non-ideal excitations

PART	Piezoelectric Case	Linear Piezoelectric Coefficient θ	Stability	Average Power
I	Linear $\Theta = 0$	$0 \leq \theta \leq 0.423$	Stable	$0 \leq P_{avg} \leq 50.81$
		$0.423 < \theta \leq 0.456$	Unstable	$P_{avg} = 0$
	Nonlinear $\Theta = 1.0$	$0 \leq \theta \leq 0.399$	Stable	$0 \leq P_{avg} \leq 50.81$
		$0.399 < \theta \leq 0.420$	Unstable	$P_{avg} = 0$
II	Linear $\Theta = 0$	$0 \leq \theta \leq 0.3038$	Stable	$0 \leq P_{avg} \leq 79.79$
		$0.3038 < \theta \leq 0.5$	Unstable	$P_{avg} = 0$
	Nonlinear $\Theta = 1.0$	$0 \leq \theta \leq 0.2763$	Stable	$0 \leq P_{avg} \leq 83.85$
		$0.2763 < \theta \leq 0.5$	Unstable	$P_{avg} = 0$

The instabilities of the system may become stabilities depending on the initial conditions. Generally, the unstable behaviour appears when the amplitude of excitation is very high, letting the displacements of the system tending to infinite. Physically, it can mean a damage in the structure duo to the high amplitudes of motion. However, the amplitude of excitation is also directly linked to the energy harvesting, the higher the amplitude the higher will be the energy harvesting. Therefore, because of the extensive analysis of initial condition and the piezoelectric material *versus* the amplitude, it becomes the most important subject of this work.

The firsts performed analysis was the amplitude *versus* the initial conditions. The best initial condition of the PART I was different of the PART II. Moreover, the interval of amplitude was very higher in PART I than in the PART II, i.e., a greater harvested power. It is a different result of the other comparisons. In general, the results of the electro-dynamical shaker exciting the base showed that the energy harvesting is higher than considering the harmonic force. However, in the case of the amplitude, it does not happen.

Then, in the following, the piezoelectric material *versus* the amplitudes of excitation was analyzed related to the energy harvesting and stability of the system considering the old and new initial conditions. Considering the old initial condition, the electro-dynamical shaker had the best configurations to harvest energy, even considering the linear and nonlinear piezoelectric case. However, when it was considered the new initial conditions, the dynamical system with harmonic force had the best configuration to harvest energy, including that the best harvested amount of energy is very higher than in the case of the electro-dynamical shaker. A complete summary of the conclusion of this analysis of this work is up to compare 4.8 and 6.8.

Sometimes, the usage of the electro-dynamical shaker as an external exciter is less

efficient than using the harmonic force. However, the importance of considering the electro-dynamical device is that it can represents more realistic results, as it is observed the not so high values of the acceptable amplitudes of the portal frame. Moreover, the device possibilities a future experiment to comprove these results, including the energy harvesting, saturation phenomenon and the whole nonlinearities presented in this work.

Chapter 8

Future Works

To go further of the results of this work, the purposed future works to improve the understanding of this theme is listed above.

• Apply perturbation methods to find an approximated analytical solution of the modes of vibration of the system for an evaluation of the involved phenomena of the dynamical system;

• Carry out the basins of attraction to an overview of the equilibrium points and variations of the initial condition, moreover study the possible erosions in the basins of attraction;

• Apply the fractional-order in damping and stiffness;

• Study the uncertainties of the parameters of the adopted model;

• Perform a possible future experiment in order to comprove the nonlinearity of the piezoelectric material and the whole phenomena involved in the main structure.

Bibliography

Alevras, P., Yurchenko, D., and Naess, A. (2014). Stochastic synchronization of rotating parametric pendulums. *Meccanica*, 49(8):1945–1954.

Anton, S. R. and Sodano, H. A. (2007). A review of power harvesting using piezoelectric materials (2003–2006). *Smart materials and Structures*, 16(3):R1.

Arbex, H. C., Balthazar, J. M., de Pontes Junior, B. R., da Fonseca, R. M. L. R., Felix, J. L. P., Tusset, A. M., Bueno, Á. M., et al. (2015). On nonlinear dynamics behavior and control of a new model of a magnetically levitated vibrating system, excited by an unbalanced dc motor of limited power supply. *Journal of the Brazilian Society of Mechanical Sciences and Engineering*, 37(4):1139–1150.

Ashour, O. N. and Nayfeh, A. H. (2002). Adaptive control of flexible structures using a nonlinear vibration absorber. *Nonlinear Dynamics*, 28(3-4):309–322.

Avanço, R. H., Navarro, H. A., Brasil, R. M., Balthazar, J. M., Bueno, Á. M., and Tusset, A. M. (2015). Statements on nonlinear dynamics behavior of a pendulum, excited by a crank-shaft-slider mechanism. *Meccanica*, pages 1–20.

Balthazar, J., Rocha, R., Brasil, R., Tusset, A., de Pontes, B., and Silveira, M. (2014a). Mode saturation, mode coupling and energy harvesting from ambient vibration in a portal frame structure. In *ASME 2014 International Design Engineering Technical Conferences and Computers and Information in Engineering Conference*, pages V008T11A044–V008T11A044. American Society of Mechanical Engineers.

Balthazar, J. M., Brasil, R. M. L. R. d., Garzeri, F. J., et al. (2004). On non-ideal simple portal frame structural model: Experimental results under a non-ideal excitation. *Applied Mechanics and Materials*, 1:51–58.

Balthazar, J. M., Felix, J. L. P., Brasil, R. M. L. R. d., et al. (2003). On nonlinear dynamics and control of a particular portal frame foundation model, excited by a non-ideal motor. In *Materials science forum*, volume 440, pages 371–380. Trans Tech Publ.

Balthazar, J. M., Rocha, R. T., Tusset, A. M., Brasil, R. M. L. R. F., Pontes JR, B. R., Silveira, M., Bueno, A. M., and Felix, J. L. P. (2014b). On mode saturation phenomenon as an energy harvester generator. In *8th European nonlinear dynamics conference (ENOC 2014)*.

Brasil, R. M. L. R. F. (1990). Não-linearidade geométrica na dinâmica de estruturas aporticadas planas: um tratamento pelo método dos elementos finitos. *São Paulo. Tese (Doutorado)- Escola Politécnica, Universidade de São Paulo*.

Cottone, F. (2007). *Nonlinear Piezoelectric Generators for Vibration Energy Harvesting*. PhD thesis, Universita' Degli Studi Di Perugia.

Crawley, E. F. and Anderson, E. H. (1990). Detailed models of piezoceramic actuation of beams. *Journal of Intelligent Material Systems and Structures*, 1(1):4–25.

Daqaq, M. F., Masana, R., Erturk, A., and Quinn, D. D. (2014). On the role of nonlinearities in vibratory energy harvesting: A critical review and discussion. *Applied Mechanics Reviews*, 66(4):040801.

de Paula, A. S., Balthazar, J. M., and Felix, J. L. P. (2013). Some comments on the nonlinear dynamics of a portal frame under base excitation. *Shock and Vibration*, 20(6):1093–1101.

DuToit, N. E. and Wardle, B. L. (2007). Experimental verification of models for microfabricated piezoelectric vibration energy harvesters. *AIAA journal*, 45(5):1126–1137.

Erturk, A. (2009). *Electromechanical modeling of piezoelectric energy harvesters*. PhD thesis, Virginia Polytechnic Institute and State University.

Erturk, A., Hoffmann, J., and Inman, D. (2009). A piezomagnetoelastic structure for broadband vibration energy harvesting. *Applied Physics Letters*, 94(25):254102.

Erturk, A. and Inman, D. J. (2011). *Piezoelectric energy harvesting*. John Wiley & Sons.

Felix, J., Silva, E., Balthazar, J., Tusset, A., Bueno, A., Brasil, R., and Belhaq, M. (2014). On nonlinear dynamics and control of a robotic arm with chaos. In *Csndd 2014-International Conference On Structural Nonlinear Dynamics And Diagnosis*, pages 1–6. EDP Sciences.

Felix, J. L. P. (2002). *JL Teoria de Sistemas Vibratórios Aporticados Não Lineares e Não Ideais. 2002, 205 p.* PhD thesis, Tese (Doutorado em Engenharia Mecânica)-Universidade Estadual de Campinas-UNICAMP.

Felix, J. L. P., Balthazar, J. M., and Brasil, R. M. L. R. F. (2005). On saturation control of a non-ideal vibrating portal frame foundation type shear-building. *Journal of Vibration and Control*, 11(1):121–136.

Felix, J. L. P., Balthazar, J. M., da Fonseca, R. M. L. R., de Paula, A. S., et al. (2013). On an energy exchange process and appearance of chaos in a non-ideal portal frame dynamical system. *Differential Equations and Dynamical Systems*, 21(4):373–385.

Fujitsu, L. L. (2010). `http://www.fujitsu.com/global/about/resources/news/press-releases/2010/1209-01.html`. Accessed on: 10/05/2016.

Golnaraghi, M. F. (1991). Vibration suppression of flexible structures using internal resonance. *Mechanics Research Communications*, 18(2-3):135–143.

Gourdon, E., Lamarque, C.-H., and Pernot, S. (2007). Contribution to efficiency of irreversible passive energy pumping with a strong nonlinear attachment. *Nonlinear Dynamics*, 50(4):793–808.

Haddow, A. G., Barr, A. D. S., and Mook, D. T. (1984). Theoretical and experimental study of modal interaction in a two-degree-of-freedom structure. *Journal of Sound and Vibration*, 97(3):451–473.

Hall, B. D., Mook, D. T., Nayfeh, A. H., and Preidikman, S. (2001). Novel strategy for suppressing the flutter oscillations of aircraft wings. *AIAA journal*, 39(10):1843–1850.

Heywang, W., Lubitz, K., and Wersing, W. (2008). *Piezoelectricity: evolution and future of a technology*, volume 114. Springer.

Iliuk, I., Balthazar, J. M., Tusset, A. M., Piqueira, J. R. C., de Pontes, B. R., Felix, J. L. P., and Bueno, Á. M. (2013a). Application of passive control to energy harvester efficiency using a nonideal portal frame structural support system. *Journal of Intelligent Material Systems and Structures*, page 1045389X13500570.

Iliuk, I., Balthazar, J. M., Tusset, A. M., Piqueira, J. R. C., de Pontes, B. R., Felix, J. L. P., Bueno, Á. M., et al. (2013b). A non-ideal portal frame energy harvester controlled using a pendulum. *The European physical journal. Special topics*, 222(7):1575–1586.

Iliuk, I., Brasil, R. M. L. R. d. F., Balthazar, J. M., Tusset, A. M., Piccirillo, V., and Piqueira, J. R. C. (2014). Potential application in energy harvesting of intermodal energy exchange in a frame: Fem analysis. *International Journal of Structural Stability and Dynamics*.

Jalili, N. (2010). Piezoelectric-based vibration control. *From Macro to Micro/Nano Scale Systems Springer*.

Jiang, X., McFarland, D. M., Bergman, L. A., and Vakakis, A. F. (2003). Steady state passive nonlinear energy pumping in coupled oscillators: theoretical and experimental results. *Nonlinear Dynamics*, 33(1):87–102.

Kecik, K. (2013). Energy harvesting of a pendulum vibration absorber. *Przeglad Elektrotechniczny*, 89(7):169–172.

Lee, Y., Frank Pai, P., and Feng, Z. (2008). Nonlinear complex response of a parametrically excited tuning fork. *Mechanical Systems and Signal Processing*, 22(5):1146–1156.

Lenci, S., Brocchini, M., and Lorenzoni, C. (2012). Experimental rotations of a pendulum on water waves. *Journal of Computational and Nonlinear Dynamics*, 7(1):011007.

Lenci, S., Pavlovskaia, E., Rega, G., and Wiercigroch, M. (2008). Rotating solutions and stability of parametric pendulum by perturbation method. *Journal of sound and vibration*, 310(1):243–259.

Lenci, S. and Rega, G. (2011). Experimental versus theoretical robustness of rotating solutions in a parametrically excited pendulum: a dynamical integrity perspective. *Physica D: Nonlinear Phenomena*, 240(9):814–824.

Litak, G., Friswell, M. I., and Adhikari, S. (2015). Regular and chaotic vibration in a piezoelectric energy harvester. *Meccanica*, pages 1–9.

Litak, G., Friswell, M. I., Kwuimy, C. A. K., Adhikari, S., and Borowiec, M. (2012). Energy harvesting by two magnetopiezoelastic oscillators with mistuning. *Theoretical and Applied Mechanics Letters*, 2(4):043009.

Litak, G., Wiercigroch, M., Horton, B. W., and Xu, X. (2010). Transient chaotic behaviour versus periodic motion of a parametric pendulum by recurrence plots. *ZAMM-Journal of Applied Mathematics and Mechanics/Zeitschrift für Angewandte Mathematik und Mechanik*, 90(1):33–41.

Luongo, A. and Zulli, D. (2012). Dynamic analysis of externally excited nes-controlled systems via a mixed multiple scale/harmonic balance algorithm. *Nonlinear Dynamics*, 70(3):2049–2061.

Luongo, A. and Zulli, D. (2013). Aeroelastic instability analysis of nes-controlled systems via a mixed multiple scale/harmonic balance method. *Journal of Vibration and Control*, page 1077546313480542.

Malatkar, P. and Nayfeh, A. H. (2007). Steady-state dynamics of a linear structure weakly coupled to an essentially nonlinear oscillator. *Nonlinear Dynamics*, 47(1-3):167–179.

Manevitch, L. I., Musienko, A. I., and Lamarque, C.-H. (2007). New analytical approach to energy pumping problem in strongly nonhomogeneous 2dof systems. *Meccanica*, 42(1):77–83.

Mankala, R. and Quinn, D. D. (2004). Resonant dynamics and saturation in a coupled system with quadratic nonlinearities. In *Proceedings of the ASME-DETC Conference, Anaheim*.

Mook, D. T., Plaut, R. H., and HaQuang, N. (1985). The influence of an internal resonance on non-linear structural vibrations under subharmonic resonance conditions. *Journal of Sound and Vibration*, 102(4):473–492.

Musienko, A., Lamarque, C.-H., and Manevitch, L. I. (2006). Design of mechanical energy pumping devices. *Journal of vibration and control*, 12(4):355–371.

Nayfeh, A. H. (2000). *Nonlinear interactions*. Wiley.

Nayfeh, A. H. and Balachandran, B. (2008). *Applied nonlinear dynamics: analytical, computational and experimental methods*. John Wiley & Sons.

Nayfeh, A. H. and Mook, D. T. (2008). *Nonlinear oscillations*. John Wiley & Sons.

Nayfeh, A. H., Mook, D. T., and Marshall, L. R. (1973). Nonlinear coupling of pitch and roll modes in ship motions. *Journal of Hydronautics*, 7(4):145–152.

Oueini, S. S. (1999). Techniques for controlling structural vibrations.

Oueini, S. S., Nayfeh, A. H., and Golnaraghi, M. F. (1997). A theoretical and experimental implementation of a control method based on saturation. *Nonlinear Dynamics*, 13(2):189–202.

Pai, P. F. and Schulz, M. J. (2000). A refined nonlinear vibration absorber. *International Journal of Mechanical Sciences*, 42(3):537–560.

Pai, P. F., Wen, B., Naser, A. S., and Schulz, M. J. (1998). Structural vibration control using pzt patches and non-linear phenomena. *Journal of Sound and vibration*, 215(2):273–296.

Pique, E. (2013). Thin philm piezoelectric. `http://www.enginyeriapique.cat/es/kyocera-piezo-esp/`. Accessed on : 10/05/2016.

Pratt, J. R., Oueini, S. S., and Nayfeh, A. H. (1999). Terfenol-d nonlinear vibration absorber. *Journal of intelligent material systems and structures*, 10(1):29–35.

Preumont, A. (2006). *Mechatronics: dynamics of electromechanical and piezoelectric systems*, volume 136. Springer.

Priya, S. and Inman, D. J. (2009). *Energy harvesting technologies*, volume 21. Springer.

Quinn, D. D. (2007). Resonant dynamics in strongly nonlinear systems. *Nonlinear Dynamics*, 49(3):361–373.

Rocha, R. T. (2014). Comportamento dinâmico não linear em fenômenos de colheita de energia usando dispositivos baseados em materiais piezoelétricos em estruturas aporticadas. Master's thesis, Universidade Estadual Júlio de Mesquisa Filho (UNESP), Faculdade de Engenharia de Bauru (FEB).

Rocha, R. T., Balthazar, J. M., Tusset, A. M., Brasil, R. M. L. R. F., Pontes JR, B. R., Silveira, M., Bueno, A. M., and Felix, J. L. P. (2014). Comportamento não linear em fenômenos de saturação em colheita de energia usando plataformas aporticadas e controle passivo. In *VIII Congresso Nacional de Engenharia Mecânica (CONEM 2014)*.

Rocha, R. T., Balthazar, J. M., Tusset, A. M., Piccirillo, V., Brasil, R. M. L. R. F., and Palacios, F. J. L. (2015). Using saturation phenomenon to improve energy harvesting in a portal frame platform with passive control by a a pendulum. In *Dynamical Systems - Theory and Applications Conference (DSTA 2015). (ISBN:978-83-7283-708-0, pages 501-510).*

Shoeybi, M. and Ghorashi, M. (2005). Control of a nonlinear system using the saturation phenomenon. *Nonlinear Dynamics*, 42(2):113–136.

Stephen, N. (2006). On energy harvesting from ambient vibration. *Journal of sound and vibration*, 293(1):409–425.

Syta, A., Bowen, C., Kim, H., Rysak, A., and Litak, G. (2015). Experimental analysis of the dynamical response of energy harvesting devices based on bistable laminated plates. *Meccanica*, 50(8):1961–1970.

Triplett, A. and Quinn, D. D. (2009). The effect of non-linear piezoelectric coupling on vibration-based energy harvesting. *Journal of Intelligent Material Systems and Structures*, 20(16):1959–1967.

Tusset, A. M., Balthazar, J. M., and Felix, J. L. P. (2012). On elimination of chaotic behavior in a non-ideal portal frame structural system, using both passive and active controls. *Journal of Vibration and Control*, page 1077546311435518.

Tusset, A. M., Piccirillo, V., Bueno, A. M., Balthazar, J. M., Sado, D., Felix, J. L. P., da Fonseca, R. M. L. R., et al. (2015). Chaos control and sensitivity analysis of a double pendulum arm excited by an rlc circuit based nonlinear shaker. *Journal of Vibration and Control*, page 1077546314564782.

Twiefel, J., Richter, B., Sattel, T., and Wallaschek, J. (2008). Power output estimation and experimental validation for piezoelectric energy harvesting systems. *Journal of Electroceramics*, 20(3-4):203–208.

Vakakis, A. F. (2008). *Nonlinear targeted energy transfer in mechanical and structural systems*, volume 156. Springer.

Von Wagner, U. and Hagedorn, P. (2002). Piezo–beam systems subjected to weak electric field: experiments and modelling of non-linearities. *Journal of Sound and Vibration*, 256(5):861–872.

Wang, R. and Jing, Z. (2004). Chaos control of chaotic pendulum system. *Chaos, Solitons & Fractals*, 21(1):201–207.

Warminski, J., Cartmell, M., Mitura, A., and Bochenski, M. (2013). Active vibration control of a nonlinear beam with self-and external excitations. *Shock and Vibration*, 20(6):1033–1047.

Xu, X., Pavlovskaia, E., Wiercigroch, M., Romeo, F., and Lenci, S. (2007). Dynamic interactions between parametric pendulum and electro-dynamical shaker. *ZAMM-Journal of Applied Mathematics and Mechanics/Zeitschrift für Angewandte Mathematik und Mechanik*, 87(2):172–186.

Xu, X., Wiercigroch, M., and Cartmell, M. (2005). Rotating orbits of a parametrically-excited pendulum. *Chaos, Solitons & Fractals*, 23(5):1537–1548.

Yokoi, Y. and Hikihara, T. (2011). Tolerance of start-up control of rotation in parametric pendulum by delayed feedback. *Physics Letters A*, 375(17):1779–1783.

Zulli, D. and Luongo, A. (2015). Nonlinear energy sink to control vibrations of an internally nonresonant elastic string. *Meccanica*, 50(3):781–794.

Appendix A

Improvement of the Energy Harvesting using a Nonlinear Energy Sink

In addition to the phenomena presented in this paper, there are other ways to try to improve the energy harvesting. One of them and studied by many authors is the use of the NES device. Therefore, in this part of this work, we will explore the use of a NES device as a passive controller coupled to the portal frame foundation of two-degrees-of-freedom structure. We will show numerical simulations of some analysis of control and improvement of the energy harvesting of the system setting a control parameter of the NES.

A.1 The Structural Problem

The most complete structure of Fig. A.1d, consists of the portal frame foundation of two-degrees-of-freedom which has two columns clamped in their bases with height h and a horizontal beam pinned to the columns at both ends with length L. Both columns and beam have flexural stiffness EI. The mass at the mid-span of the beam is considered as M, and the mass of a column is represented as m. The dimensional generalized coordinates are considered, related to the mass of the beam, as q_1 and q_2 that are its horizontal and vertical displacements, with natural frequencies ω_1 and ω_2, respectively.

Moreover, considering the two first vibration modes of the portal frame, the means of vibration of the columns and beam can be approximated by mathematical functions, nominated form functions, given by the equations below.

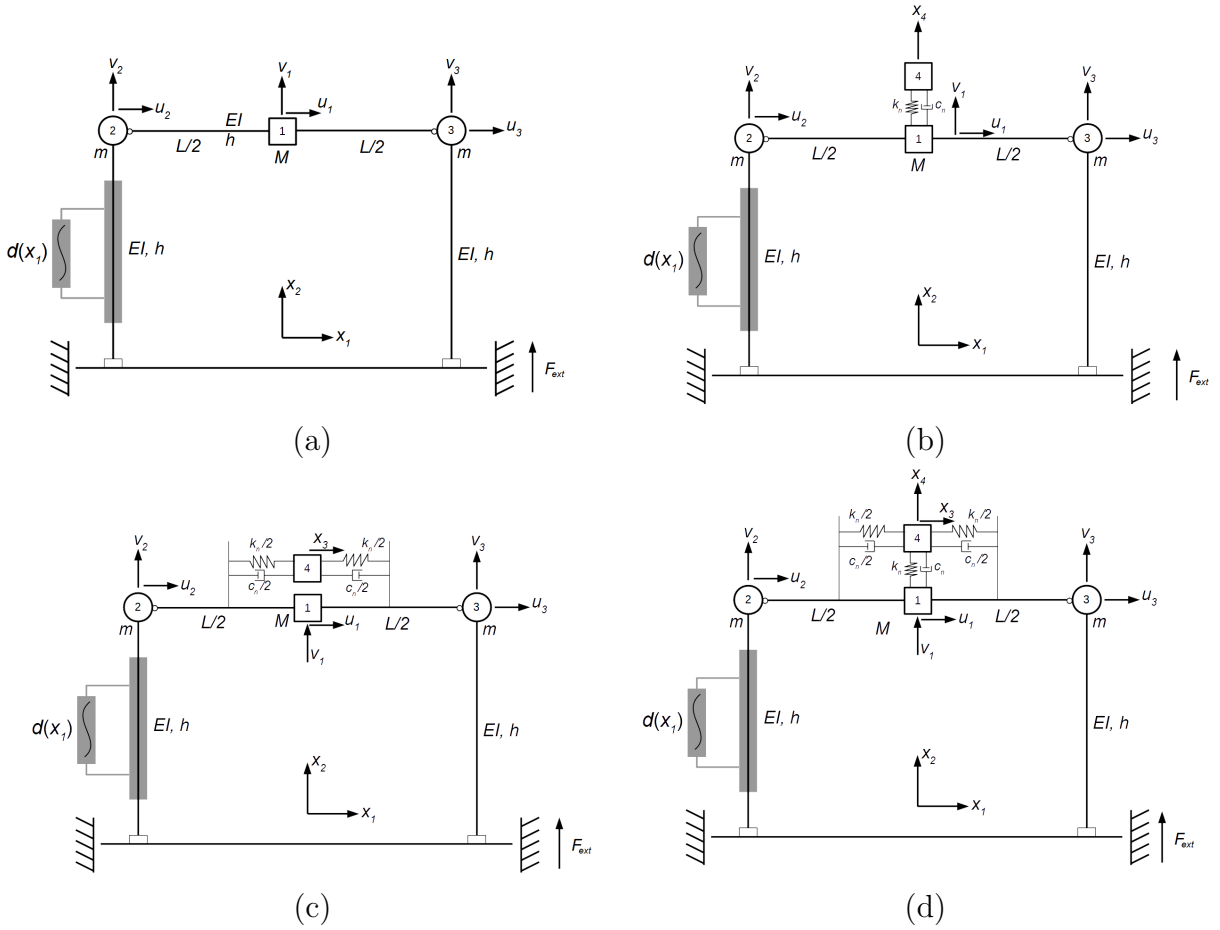

Figure A.1: Simple two-degrees-of-freedom portal frame foundation, (a) without NES, (b) With NES in vertical mode, (c) With NES in horizontal mode, (d) NES in both vertical and horizontal mode

The linear stiffness of the columns and beam, as shown before, can be evaluated by a Rayleigh-Ritz procedure using cubic trial functions, that are $k_c = 3EI/h^3$ and $k_b = 48EI/L^3$, respectively. Moreover, the support structure has a geometric nonlinearity introduced by considering the shortening due to bending of the columns and beam, given the nodal displacements, shown in Fig. A.1d, which are in Eq. (A.1).

$$\begin{aligned} u_1 &= q_1 & u_2 &= u_1 + \frac{B}{4}v_1^2 & u_3 &= u_1 - \frac{B}{4}v_1^2 \\ v_1 &= q_2 & v_2 &= -\frac{A}{2}u_1^2 & v_3 &= -\frac{A}{2}u_1^2 \end{aligned} \tag{A.1}$$

where $A = 6/5h$ and $B = 24/5L$.

The main structure possesses a nonlinear piezoelectric material coupled to a column which is considered as an electric RC circuit. This material is excited by an internal voltage (back-emf) proportional to the mechanical velocity, in order to harvest energy from the vibration of the column. Its circuit consists of an electric resistance R_p, a produced charge Q_p and a capacitance C_p of the piezoelectric‘s capacitor. The nonlinear contribution of the

material is given by the strain relation (2.2). Therefore, again, the piezoelectric material has an electric voltage given by Eq. (3.6).

The NES device of mass m_4 is coupled above the mid-span of the beam with damping c_n and stiffness k_n. It is considered as a two-degrees-of-freedom structure, which has x_3 as the horizontal movement and x_4 as the vertical movement.

The main structure is excited by a cosine harmonic force directly on its base, illustrated by F_{ext} in Fig. A.1d, whose force is given by an harmonic force as (3.14).

Hence, using the energy method of Lagrange's function and Euler-Lagrange equation, the modelling of the governing equations of motion of the most complete system, illustrated in Fig. A.1d, are given in Eqs. (A.2), (A.3), (A.4), (A.5), (A.6), whose equations represents the horizontal and vertical motion of the portal frame, the horizontal and vertical motion of the NES, and the piezoelectric material charge, respectively.

$$(2m+M)\ddot{q}_1 + 2(k_c - mgA)q_1 + Ak_b q_1 q_2 + c_1\dot{q}_1 + k_n(q_1 - q_3)^3 + ... \qquad \text{(A.2)}$$
$$c_n(\dot{q}_1 - \dot{q}_3) = \frac{d(q_1)}{C_p}Q_p$$

$$M\ddot{q}_2 + c_2\dot{q}_2 + k_b q_2 + \frac{Ak_b}{2}q_1^2 + Mg + k_n(q_2 - q_4)^3 + c_n(\dot{q}_2 - \dot{q}_4) = ... \qquad \text{(A.3)}$$
$$F_0\cos\omega_n t + \frac{d(q_1)}{C_p}\frac{B}{2}Q_p q_2$$

$$m_4\ddot{q}_3 - k_n(q_1 - q_3)^3 - c_n(\dot{q}_1 - \dot{q}_3) = 0 \qquad \text{(A.4)}$$

$$m_4\ddot{q}_4 - k_n(q_2 - q_4)^3 - c_n(\dot{q}_2 - \dot{q}_4) = 0 \qquad \text{(A.5)}$$

$$R_p\dot{Q}_p - \frac{d(q_1)}{C_p}\left(q_1 + \frac{B}{4}q_2^2\right) + \frac{Q_p}{C_p} = 0 \qquad \text{(A.6)}$$

Next, a dimensionless process was carried out, resulting the dimensionless equations of the dynamical system as follows in Eqs.(A.7), (A.8), (A.9), (A.10), (A.11).

$$x_1'' + \mu_1 x_1' + \alpha_1 x_1 x_2 + K_1(x_1 - x_3)^3 + \mu_{1n}(x_1' - x_3') = \theta(1 + \Theta|x_1|)\delta_1 V_p \qquad \text{(A.7)}$$

$$x_2'' + \mu_2 x_2' + \omega_2^2 x_2 + \alpha_2 x_1^2 + G_0 + K_2(x_2 - y_4)^3 + \mu_{2n}(x_2' - y_4') = ... \qquad \text{(A.8)}$$
$$E_0\cos\Omega\tau + \theta(1 + \Theta|x_1|)\delta_2 V x_2$$

$$x_3'' - K_3(x_1 - x_3)^3 - \mu_n(x_1' - x_3') = 0 \qquad \text{(A.9)}$$

$$x_4'' - K_4(x_2 - x_4)^3 - \mu_n(x_2' - x_4') = 0 \qquad \text{(A.10)}$$

$$V_p' - \theta(1 + \Theta|x_1|)(\delta_3 x_1 + \delta_4 x_2^2) + \delta_3 V_p = 0 \qquad \text{(A.11)}$$

where the dimensionless parameters are given in Eq. (A.12).

$$
\begin{aligned}
&x_1 = \frac{q_1}{h} \qquad x_2 = \frac{q_2}{L} \qquad x_3 = \frac{q_3}{h} \qquad x_2 = \frac{q_4}{L} \qquad V_p = \frac{Q_p}{Q_0} \\
&\tau = \omega_1 t \qquad \omega_1 = \sqrt{\frac{2(k_c - mgA)}{(2m+M)}} \qquad \hat{d}(x_1) = \frac{h}{Q_0} d(q_1) \\
&K_1 = \frac{k_n h^2}{(2m+M)\omega_1^2} \quad K_2 = \frac{k_n L^2}{M\omega_1^2} \quad K_3 = \frac{k_n h^2}{m_4\omega_1^2} \quad K_4 = \frac{k_n L^2}{m_4\omega_1^2} \\
&\mu_1 = \frac{c_1}{(2m+M)\omega_1} \quad \mu_2 = \frac{c_2}{M\omega_1} \quad \mu_{1n} = \frac{c_n}{(2m+M)\omega_1} \quad \mu_{2n} = \frac{c_n}{M\omega_1} \\
&\mu_n = \frac{c_n}{m_4\omega_1} \quad \omega_2 = \frac{1}{\omega_1}\sqrt{\frac{k_b}{M}} \quad \alpha_1 = \frac{Ak_bL}{(2m+M)\omega_1^2} \\
&\alpha_2 = \frac{Ak_bh^2}{2M\omega_1^2 L} \quad G_0 = \frac{g}{\omega_1^2 L} \quad \delta_1 = \frac{Q_0^2}{\omega_1^2 h^2 (2m+M) C_p} \quad \delta_2 = \frac{BQ_0^2}{2M\omega_1^2 h C_p} \\
&\delta_3 = \frac{1}{R_p C_p \omega_1} \quad \delta_4 = \frac{BL^2}{4R_p C_p \omega_1 h} \quad E_0 = \frac{F_0}{M\omega_1^2 L} \quad \Omega = \frac{\omega_n}{\omega_1}
\end{aligned}
\tag{A.12}
$$

The dimensional, dimensionless and average harvested power through the piezoelectric material are given at the same Eqs. (3.23), (3.24) and (3.25), respectively.

In the next section, numerical simulations will be discussed.

A.2 Numerical Simulations and Results

In this section, several numerical simulations were carried out in order to find an optimal configuration to improve de energy harvesting. To the simulations, the parameters of Tab. A.1 were used.

Moreover, a new control parameter was considered in order to analyze the optimal quantity of harvested power of the system, which is the most important purpose of this appendix. Equation (A.13) defines this new control parameter.

$$
e = \frac{1}{m_4} \tag{A.13}
$$

The new parameter "e" will be varied with the hypothesis that the ratio of the NES mass m_4 should not overpass the value of the mass of the mid span of the beam M. Therefore, the following restriction must be satisfied: $0.5 \leq e \leq 100$.

Table A.1: Parameters of the Portal Frame coupled to the NES

Parameters	Values	Means
$g[m/s^2]$	9.81	Gravity acceleration
$M[kg]$	2.00	Beam mass
$m[kg]$	0.50	Column mass
$m_4[kg]$	Vary	NES mass
$c_1[Ns/m]$	1.55	Column damping
$c_2[Ns/m]$	3.14	Beam damping
$c_n[Ns/m]$	100	NES damping
$EI[nm^2]$	128	Linear flexural stiffness
$k_n[N/m^3]$	74	Nonlinear NES Stiffness
$L[m]$	0.52	Beam length
$h[m]$	0.36	Column length
$F_0[N]$	40	Amplitude of the external force
$\omega_n[rad/s]$	148	Frequency of the external force
$R_p[k\Omega]$	100	Electric resistance of the piezoelectric
$C_p[\mu F]$	1	Capacitance of the piezoelectric
θ	0.3	Linear piezoelectric coefficient
Θ	0	Nonlinear piezoelectric coefficient

Next, we will discuss some results about the energy harvesting using the NES device in order to find the best configuration to each system, and the best way to use the NES device to this case of simple portal frame structure. All the numerical simulations were carried out considering the parameters of Tab. A.1.

A.2.1 Case 1 - Dynamical analysis of the simple portal frame foundation

In this subsection, we will show the energy harvesting of the system without the NES device to, afterwards, compare the effect of different NES devices on the portal frame systems. In Eq. (4) the third and fourth equations, that are x3 (horizontal movement of the NES) and x4 (vertical movement of the NES), and their dependent terms, are dismissed.

In Fig. A.2a we observe the time history of the vertical (in black) and horizontal (in red) displacements. Because of the saturation, as we explained before, there is energy exchange between the two vibratory coordinates keeping the highest amplitude at the horizontal coordinate so that the energy harvesting is more efficient at the columns.

In addition, as Figs. A.2c and A.2d illustrate, the vertical and horizontal movement are both periodic with period-2 and period-1, respectively. Hence, we can maintain the energy harvesting. Then, figure A.2b shows the time history of the harvested power (in black) and the average harvested power (in red). We conclude that the harvested power

to the case without the controller is 35.33.

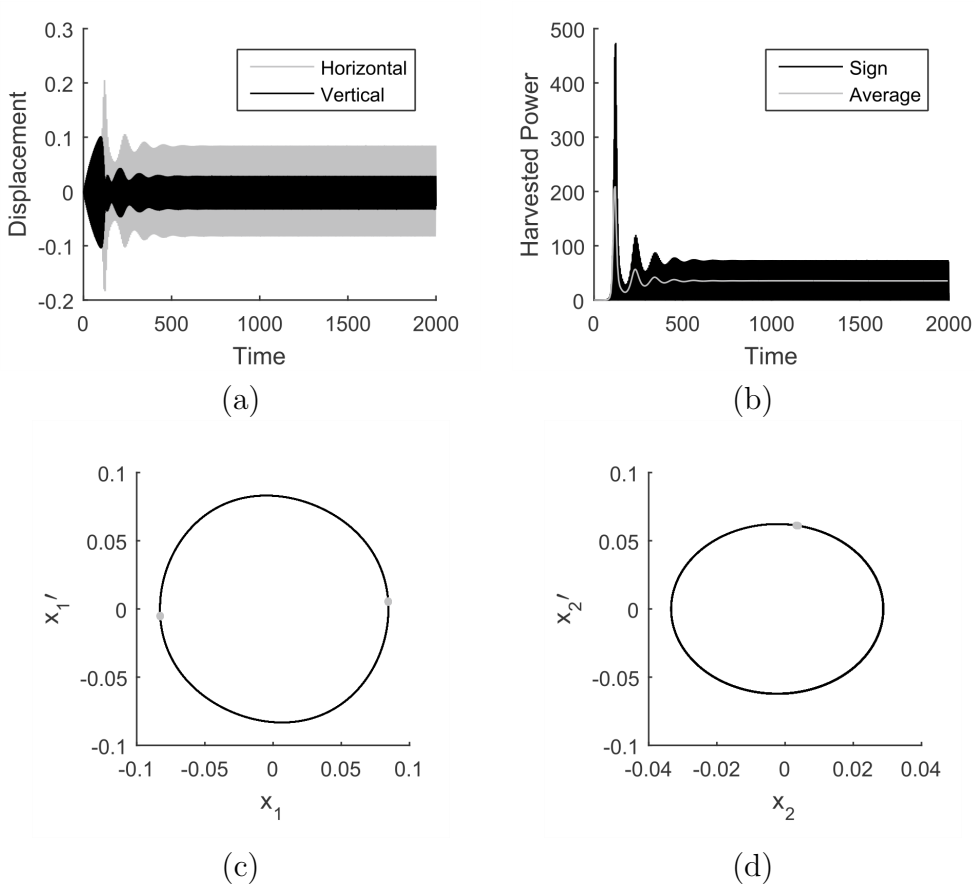

Figure A.2: Time histories of (a) displacements, (b) harvested power; and Phase planes (in black) and Poincaré Maps (red dot) of (a) horizontal displacement, (b) vertical displacement

The next step is to couple the passive controller NES to the structure and analyze its influence to the energy harvesting. That will be shown in the next subsections.

A.2.2 Case 2 - Influence of the NES in vertical mode

Starting from this subsection, it will be analyzed the influence of the NES device by three (3) different cases.

The first one is represented by Fig. A.1b, and will be analyzed in this subsection, which is the analysis of the NES in the vertical direction. The second one is illustrated in Fig. A.1c, which will analyze the case of the sole horizontal movement of the device. The last one is illustrated in Fig. A.1d, which will analyze the case of the NES at both vertical and horizontal coordinates.

Hence, neglecting Eq. (A.9), that is x_3 (horizontal movement of the NES) and its dependent terms, and also considering the parameters of Tab. A.1, a parametrical analysis and bifurcation diagrams were constructed.

Fig. A.3 shows the analysis of the parameter "e" versus the average harvested power. We can see that the average power increases in the interval of $0.5 \leq e \leq 64.5$, that is $2 \leq m_4 \leq 0.0155[kg]$. When $e = 64.5$, the average harvested power is maximum with the value of 35.98, higher than the system without the NES device. After the maximum power, it decreases along the increasing of "e" parameter until 100.

Figs. A.4 show the bifurcation diagrams of the control parameter variation related to the coordinates of the model, that are, horizontal movement, in Fig. A.4a, vertical movement, in Fig. A.4b, and NES movement, in Fig. A.4c. The system is periodic, however, there are two kinds of periodicity related to the value of the control parameter. The region 1 (left side of the red dotted division, in red), system is period-1, and in region 2 (right side of the red dotted division, in blue), system is period-2.

Hence, when the system is period-1, which represents a heavier mass, the energy harvesting is almost zero. When the system begins to be period-2, the amount of power increases quickly until stabilizes near $P_{avg} \approx 35.00$.

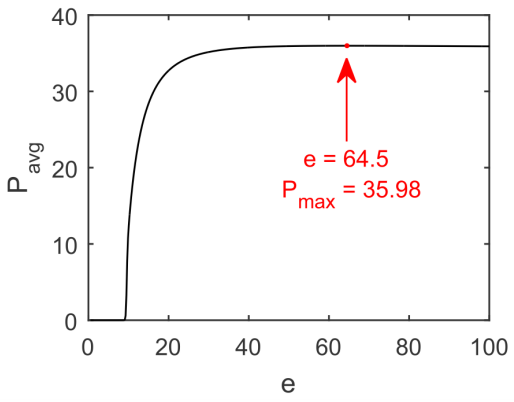

Figure A.3: Parametrical analysis of the control parameter "e" related to the average harvested power to the NES in vertical mode

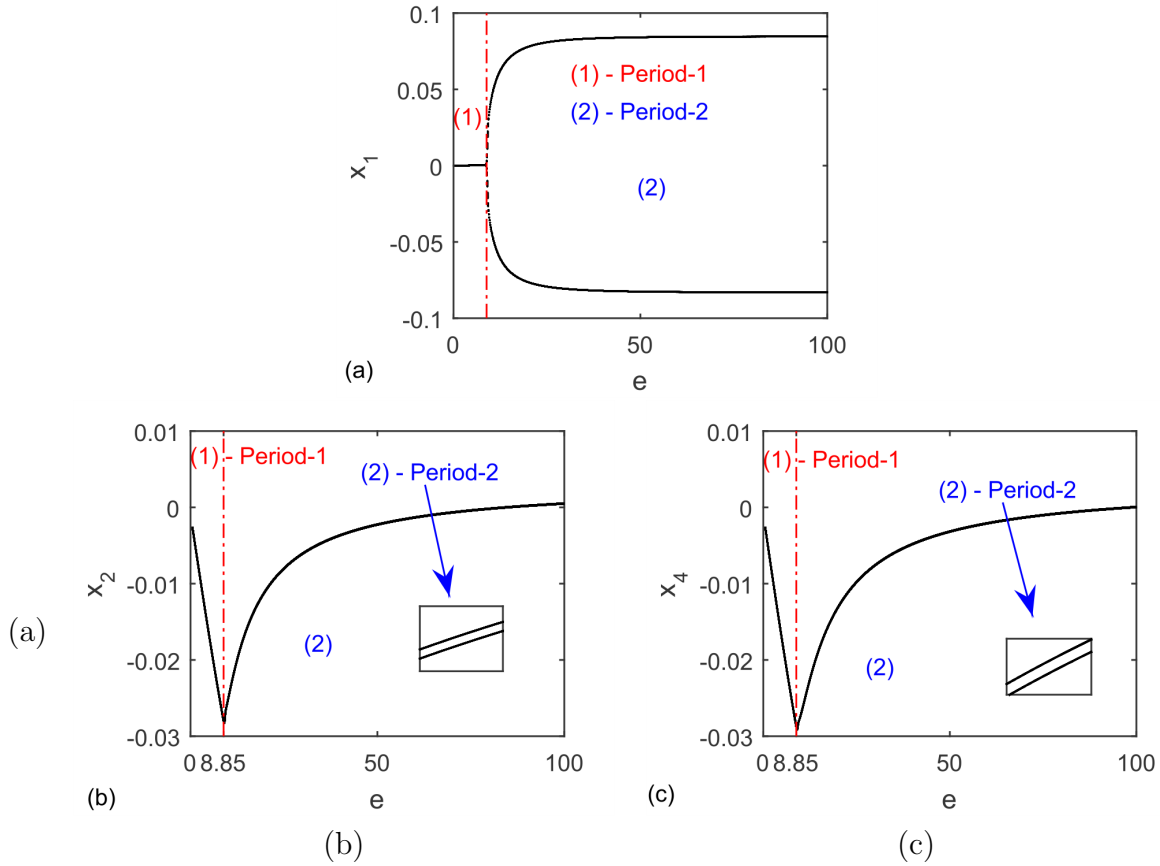

Figure A.4: Bifurcation diagrams of the control parameter "e", to the NES in vertical mode, related to (a) horizontal movement, (b) vertical movement, (c) NES movement

Therefore, depending on the value of the control parameter the system may present some gains or losses of energy. Now, in next section we will discuss the case of the sole horizontal NES movement.

A.2.3 Case 3 - Influence of the NES in horizontal mode

The influence of the horizontal movement of the NES device is another way to tune the energy harvesting of the system. Because of the piezoelectric material is coupled to a column, and it harvest energy through the horizontal movement of the structure, the NES device is able to change the amount of harvested power, just in the horizontal direction.

Therefore, neglecting the fourth equation Eq. (A.10), that is x_4 (vertical movement of the NES) and its dependent terms, in the following, parametrical analysis and bifurcation diagrams were presented.

Fig. A.5 shows the parametrical analysis of the control parameter "e" related to the average harvested power. It shows that with a small value of the parameter, the amount of harvested power is less than without the NES, however the amount of power increases quickly even with a low value of the control parameter until stabilizes near 35.58. The interval of "e" is $0.5 \leq e \leq 15.2$, that is approximately $2 \leq m_4 \leq 0.0657[kg]$. When $e = 15.2$, the power is maximum with its value of 35.58. After that, power decreases slowly until reach the original value of the case 1.

To obtain the behaviour of the system at those values of the control parameter, bifurcation diagram are constructed, as illustrated in Figs. A.6, which Fig. A.6a is related to the horizontal movement of the structure, Fig. A.6b is related to the vertical movement of the structure and Fig. A.6c is related to the horizontal movement of the NES. Those figures are divided in two regions, which are region 1 (left side of the curve, in red) and region 2 (right side of the curve, in blue). It is possible to observe that, again, in region 1, system is period-1 and power is very small, however, in region 2, system is period-2 and power increases quickly.

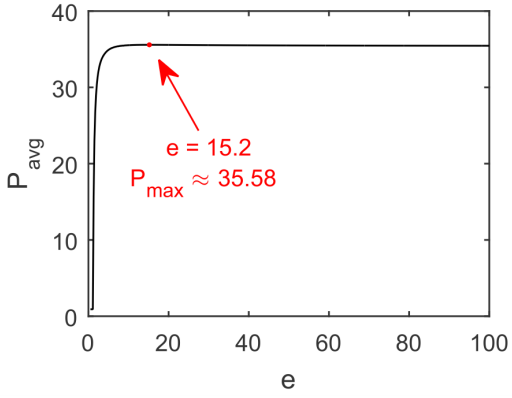

Figure A.5: Parametrical analysis of the control parameter "e" related to the average harvested power to the NES in horizontal motion

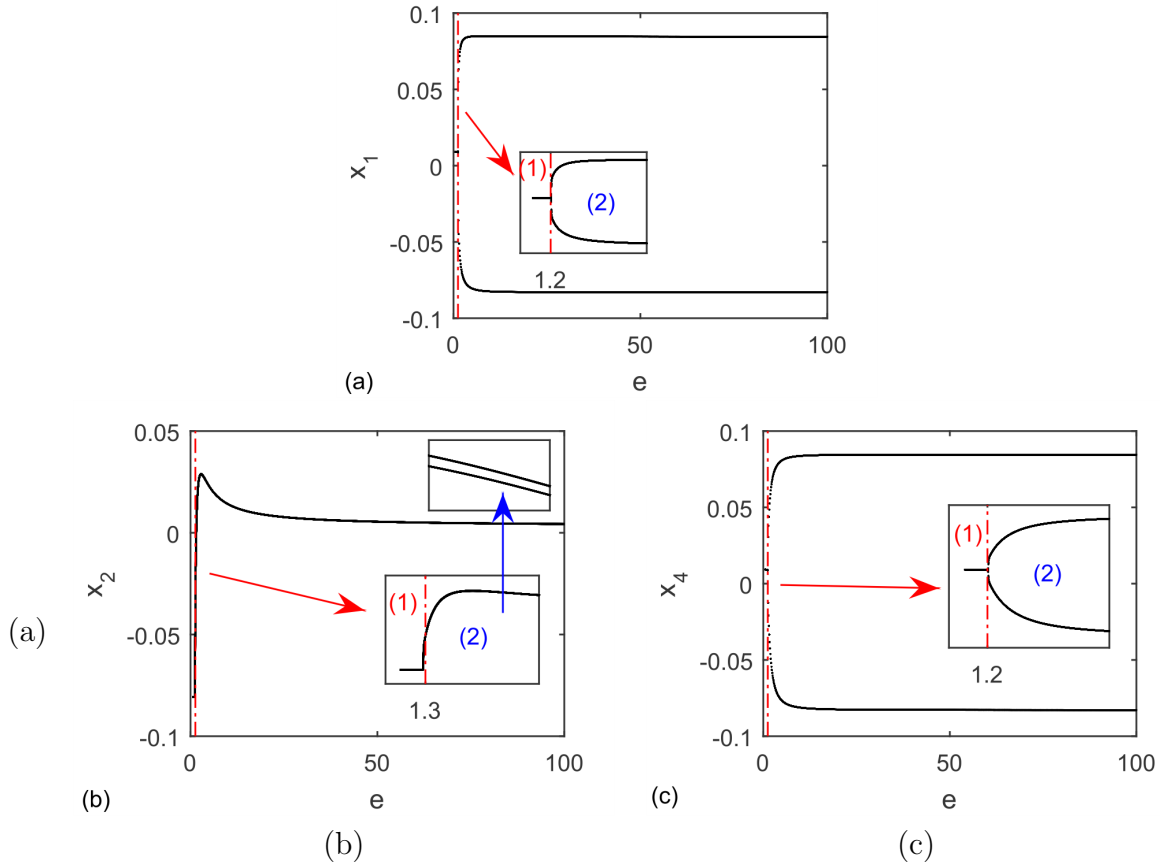

Figure A.6: Bifurcation diagrams of the control parameter "*e*", to the NES in horizontal movement, related to (a) horizontal movement, (b) vertical movement, (c) NES movement

In this case, the maximum amount of power occurs when the NES has a heavier considerably mass than in the case of its vertical movement. Therefore, in next section will be analyzed the system considering the two-degrees-of-freedom NES.

A.2.4 Case 4 - Influence of the NES in both vertical and horizontal modes

This last case 4, is when the NES actuates in both vertical and horizontal directions, i.e., considering all equations Eqs. (A.9) and (A.10). It can tune the vibration of the vertical movement, that is the excited direction, and the horizontal movement, at the same time. However, it is not necessarily that the influence of this 2DOFs will be both cases 2 and 3. It will be taken into account in the conclusions. Then, parametrical analysis and bifurcation diagrams are constructed.

Fig. A.7 shows a parametrical analysis of the control parameter "e" related to the average harvested power. In comparison to the case 2 and 3, the value of "e" of maximum power is 31, i.e., a value between the two other cases, but with a higher power, which is 36.87. We can see too that the first interval until system stabilizes is $0.5 \leq e \leq 31$, which is approximately $2 \leq m_4 \leq 0.032[kg]$. After that, power decreases until reach the original value without NES.

Bifurcation diagrams are constructed, as illustrated in Figs. A.8, in order to obtain the behaviour of the system in each value of "e". The system is totally periodic, but with different periodicities. Analyzing the regions 1 (left side of red dotted line, in red) and 2 (right side of red dotted line, in blue), it is possible to observe that the periodicity in each of the regions are period-1 and period-2, respectively. The low amount of power occurs when system is period-1 (region 1), and when it becomes period-2, power increased.

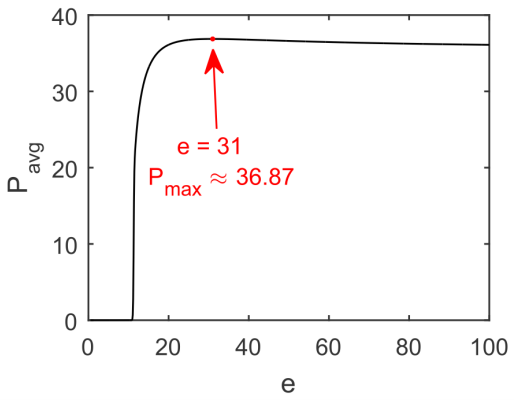

Figure A.7: Parametrical analysis of the control parameter "e" related to the average harvested power to the NES in both vertical and horizontal modes

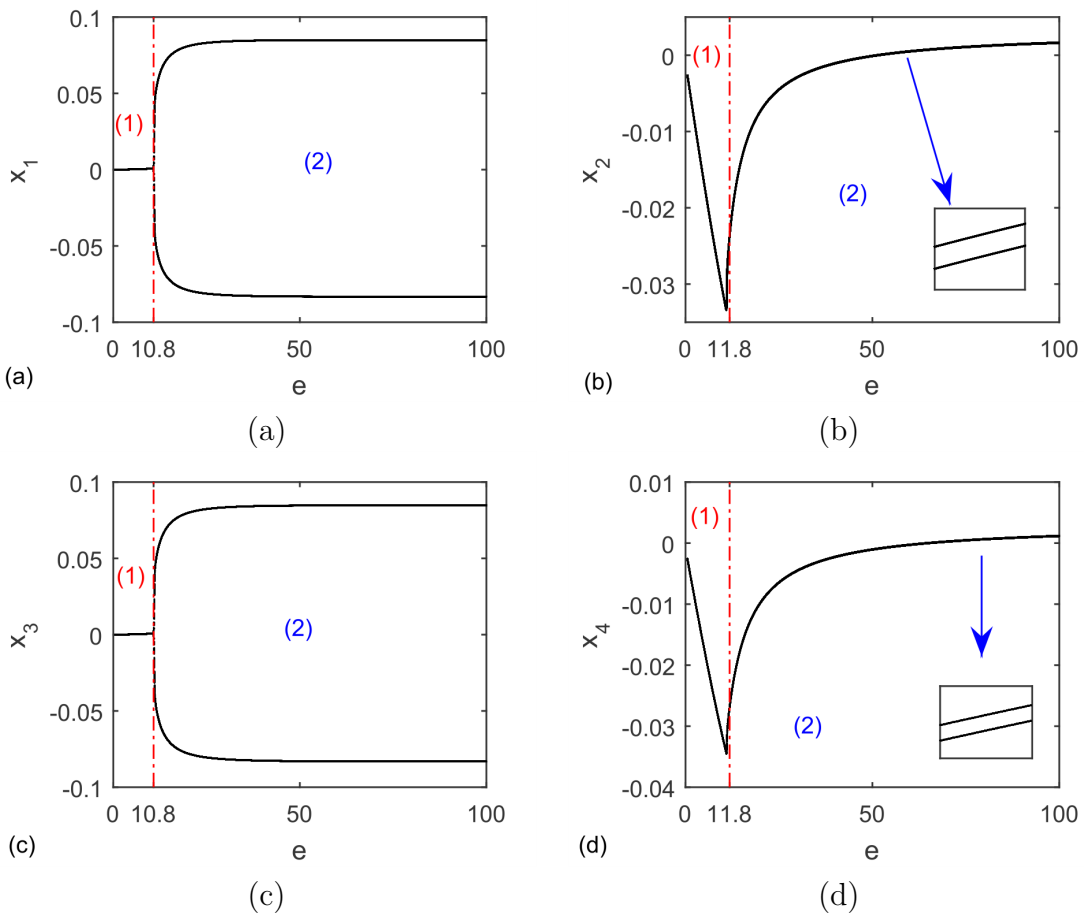

Figure A.8: Bifurcation diagrams of the control parameter "e", to NES in both vertical and horizontal directions, related to (a) horizontal movement, (b) vertical movement, (c) NES in horizontal movement, (d) NES in vertical movement

A.3 Short Conclusion of Appendix

In this work we presented an overview of the use of a passive controller in a two-degrees-of-freedom portal frame structure in order to harvest energy, considering saturation phenomenon and piezoelectric materials.

The NES device showed to be very useful to maintain the behaviour of the system, and even in the energy harvesting. With the device, we can guarantee that the system will be periodic every time, and then maintain the energy harvesting. In addition, NES proves to be very useful to tune the energy harvesting. Therefore, we presented three cases of using the NES.

The first case was considering just the NES in vertical movement, which presented the second best maximum harvested power, but with a very small mass. The second case was

considering just the NES in horizontal movement, which presented the worst maximum harvested power, but still being a gain of power. However, the device must present a considerably mass.

The third case, and the best of them, is considering the NES in both vertical and horizontal directions. It presented the maximum harvested power value. The device needs to have an intermediate mass between the other two cases, however, it optimized the two directions of movement of the structure, saturation was intensified at the same time with the horizontal movement of the NES.

Summarizing the results, Tabs. A.2 and A.3 were presented.

Table A.2: Summary of the Energy Harvesting VS. Control Parameter

Case	Region	Interval of Control parameter "e"	Internal of NES mass $m_4[kg]$	Average Harvested Power	*Gain*/**Loss**
1	0	0	0	35.32	To compare
2	1	$0.5 \leq e \leq 8.85$	$2.0 \leq m_4 \leq 0.113$	$0 \leq P_{avg} \leq$ **2.02**	**99.94 % Loss**
	2	$8.85 \leq e \leq$ ***64.5(max)***	$0.113 \leq m_4 \leq 0.155$	$2.02 \leq P_{avg} \leq$ *35.98*	*1.86 % Gain*
	2	***64.5 (max)*** $\leq e \leq 100$	$0.155 \leq m_4 \leq 0.010$	$35.98 \leq P_{avg} \leq$ *35.93*	*1.73% Gain*
3	1	$0.5 \leq e \leq 1.2$	$2.0 \leq m_4 \leq 0.833$	$0 \leq P_{avg} \leq$ **8.52**	**75.87 % Loss**
	2	$1.2 \leq e \leq$ ***15.2(max)***	$0.833 \leq m_4 \leq 0.657$	$8.52 \leq P_{avg} \leq$ *35.58*	*0.74 % Gain*
	2	***15.2(max)*** $\leq e \leq 100$	$0.657 \leq m_4 \leq 0.010$	$35.58 \leq P_{avg} \leq$ *35.45*	*0.37 % Gain*
4	1	$0.5 \leq e \leq 10.8$	$2.0 \leq m_4 \leq 0.0925$	$0 \leq P_{avg} \leq$ **9.42**	**73.33 % Loss**
	2	$10.8 \leq e \leq$ ***31.0(max)***	$0.0925 \leq m_4 \leq 0.032$	$9.42 \leq P_{avg} \leq$ *36.87*	*4.38 % Gain*
	2	***31.0(max)*** $\leq e \leq 100$	$0.032 \leq m_4 \leq 0.010$	$36.87 \leq P_{avg} \leq$ *36.10*	*2.21 % Gain*

Table A.3: Regions of the Behaviours

	Behaviour (Periodicity)			
	Horizontal	Vertical	NES in Horizontal Mode	NES in Vertical Mode
Region 0	Period-2	Period-1	-	-
Region 1	Period-1	Period-1	Period-1	Period-1
Region 2	Period-2	Period-2	Period-2	Period-2

Vita

Rodrigo Tumolin Rocha was born on 31th july, 1991, in Piracicaba, SP, Brazil. He earned his Bachelor's degree in Physics in Sao Paulo State University - Campus Rio Claro, Brazil, 2012. Moreover, he received his Master's degree in Mechanical Engineering in the Faculty of Mechanical Engineering of Bauru at Sao Paulo State University - Campus Bauru, Brazil, 1^{st} semester of 2014. He joined the Ph.D. program in Mechanical Engineering in the Faculty of Mechanica Engineering of Bauru at Sao Paulo State University - Campus Bauru, Brazil, in 2^{nd} semester of 2014. Since then, he has been working under the supervision of Full Professor José Manoel Balthazar in many problems of Nonlinear Dynamics and Energy Harvesting theme.

During his studies in the Ph.D course, he published many articles with his supervisor and co-authors that are listed above.

1) Published articles in international journals

· BALTHAZAR. J. M. ; BRASIL, R. M. L. R. F. ; FELIX, J. L. P. ; TUSSET, A. M. ; PICCIRILLO, V. ; ILIUK, I. ; **ROCHA, R. T.** ; NABARRETE, A. ; OLIVEIRA, C. . Dynamics behaviour of an elastic non-ideal (NIS) portal frame, including fractional nonlinearities. Journal of Physics. Conference Series (Online), v. 721, p. 012004, 2016.

· FELIX, J. L. P. ; BIANCHIN, R. P. ; ALMEIDA, A. ; BALTHAZAR. J. M. ; **ROCHA, R. T.** ; BRASIL, R. M. L. R. F. . On energy transfer between vibration modes under frequency-varying excitations for energy harvesting. Applied Mechanics and Materials, 2016.

· **ROCHA, R. T.** ; BALTHAZAR. J. M. ; TUSSET, A. M. ; PICCIRILLO, V. ; FELIX, J. L. P. . Comments on Energy Harvesting on a 2:1 Internal Resonance Portal Frame Support Structure, using a Nonlinear-Energy Sink as a Passive Controller. International Review of Mechanical Engineering (IREME), 2016.

2) Articles submitted in international journals

· **ROCHA, R. T.** ; BALTHAZAR. J. M. ; TUSSET, A. M. ; PICCIRILLO, V. ; FELIX, J. L. P. . Nonlinear piezoelectric vibration energy harvesting from a portal frame with two-to-one internal resonance. Meccanica, (10-June-2016).

· **ROCHA, R. T.** ; BALTHAZAR. J. M. ; TUSSET, A. M. . Using passive control by a pendulum in a portal frame platform with piezoelectric energy harvesting. Journal of Vibration and Control, (14-May-2016).

3) Articles published in international refereeing conferences

· **ROCHA, R. T.** ; BALTHAZAR. J. M. ; TUSSET, A. M. ; PICCIRILLO, V. ; BRASIL, R. M. L. R. F.; FELIX, J. L. P. Using saturation phenomenon to improve energy harvesting in a portal frame platform with passive control by a pendulum. In: 13th INTERNATIONAL CONFERENCE Dynamical Systems Theory and Applications, Łódź - Poland, December 7-10, 2015(DSTA'2015).

· **ROCHA, R. T.** ; BALTHAZAR. J. M. ; TUSSET, A. M. ; PICCIRILLO, V.. Using saturation phenomenon to improve energy harvesting in a portal frame platform with passive control by a pendulum. In: 23rd ABCM International Congress of Mechanical Engineering, Rio de Janeiro - Brazil, December 6-11, 2015 (COBEM 2015).

· FELIX, J.L.P ; BIANCHINR R.; ALMEIDA, A. ; BALTHAZAR, JOSÉ MANOEL ; **ROCHA R.T**.; BRASIL, R. M. L. R. F. . ON ENERGY TRANSFER BETWEEN VIBRATION MODES AND FREQUENCY-VARYING EXCITATIONS FOR ENERGY HARVESTING. In: the Biennial International Conference on Engineering Vibration (ICoEV-2015) to be held in Ljubljana, Slovenia, in September 7 - 10, 2015., 2015, Ljubljana, Slovenia. Proceedings of ICoEV 2015. Ljubljana,Slovenia: Department of Mechanical Engineering at the University of Ljubljana. v. 2015. p. 1.

· BALTHAZAR, JOSÉ MANOEL ; BRASIL, R. M. L. R. F. ; FELIX, J. L. P.; TUSSET, A. M. ;PICCIRILLIO, V. ; ILIUK, I.; **ROCHA, R.T.**; CONRAD, J. F. ; MARQUES, C. E. ; ARBEX, H.C.. TOUR OF NONLINEAR DYNAMIC ANALYSIS OF ELASTIC STRUCTURES. In: Symposium on the Mechanics of Slender Structures (MoSS2015). 21 - 22 September 2015, Northampton, UK, 2015, Northampton, UK. proceedings of MoSS2015. of Northampton, UK: University of Northampton, UK, 2015. v. 2015. p. 1

4) Articles accepted for publishing in international refereeing conferences

· **ROCHA, R. T.** ; BALTHAZAR, J. M. ; Quinn D. D. ; TUSSET, A. M. ; FELIX, J. L. P. . NON-IDEAL SYSTEM WITH QUADRATIC NONLINEARITIES CONTAINING A TWO-TO-ONE INTERNAL RESONANCE. In: ASME 2016 International Design Engineering Technical Conferences & Computers and Information in Engineering Conference (IDETC/CIE 2016), 2016, Charllote, North Carolina, USA.

· ALVES, A. C. ; BALTHAZAR, J. M. ; TUSSET, A. M. ; **ROCHA, R. T.** ; BUENO, A. M. . ON DYNAMIC MODELLING OF COMPRESSED AIR ENGINE WITH CONNECTING-ROD-CRANK TO CONTROL ANGULAR POSITION OF OSCILLATING ROTATION. In: ASME 2016 International Mechanical Engineering Congress and Exposition (IMECE - 2016), 2016, Phoenix, Arizona, USA.

· LIMA, J. J. ; **ROCHA, R. T.** ; JANZEN, F. C. ; TUSSET, A. M. ; BASSINELO, D. G. ; BALTHAZAR, J. M. . POSITION CONTROL OF A MANIPULATOR ROBOTIC ARM CONSIDERING FLEXIBLE JOINTS DRIVEN BY A DC MOTOR AND A CONTROLLED TORQUE BY A MR-BRAKE. In: ASME 2016 International Mechanical Engineering Congress and Exposition (IMECE - 2016), 2016, Phoenix, Arizona, USA.

5) Technical brief published in international refereeing conferences

· **ROCHA, R. T.** ; BALTHAZAR, J. M. ; TUSSET, A. M. ; PICCIRILLO, V. ; FELIX, J. L. P. ; BRASIL, R. M. L. R. F.. Energy Harvesting in a two degree of freedom portal frame model and the appearance of the saturation phenomenon. In: ASME 2015 International Design Engineering Technical Conferences & Computers and Information in Engineering Conference (IDETC/CIE 2015), 2015, Boston, Massachussets, EUA. Proceddings of ASME-IDETC/CIE 2015. NY, USA: ASME, 2015. v. 2015. p. 1.

· **ROCHA, R. T.** ; BALTHAZAR, J. M. ; TUSSET, A. M. ; PICCIRILLO, V. ; FELIX, J. L. P. ; BRASIL, R. M. L. R. F. . On energy harvesting of a flexible portal frame support exploitng the saturation phenomenon. In: ASME 2015 International Design Engineering Technical Conferences & Computers and Information in Engineering Conference (IDETC/CIE 2015),, 2015, Boston, Massachussets.. Proceddings of ASME-IDETC/CIE 2015.. NY, EUA: ASME, 2015. v. 2015. p. 1.

6) Book chapter published in international book

· TUSSET, A. M. ; PICCIRILLO, V. ; ILIUK, I. ; **ROCHA, R. T.** ; BALTHAZAR, J. M. ; FELIX, J. L. P. ; BRASIL, R. M. L. R. F. . Proposal of a Nonlinear Piezoelectric Coupling Term to Energy Harvesting Interactions. Structural Nonlinear Dynamics and Diagnosis. 1ed.: Springer International Publishing Switzerland, 2015, v. , p. 80-90.

7) Book chapter accepted for publishing in international book

· **ROCHA, R. T.** ; BALTHAZAR, J. M. ; TUSSET, A. M. ; PICCIRILLO, V. ; FELIX, J. L. P. . Using Saturation Phenomenon to improve Energy Harvesting in a Portal Frame Platform with Passive Control by a Pendulum. Springer Proceedings in Mathematics & Statistics, Vol 182, Awrejcewicz (Ed): Dynamical Systems: Theoretical and Experimental Analysis, 2016.